Tensile Fatigue Characterization of High Strength Hydrogels for Soft Tissue Applications

by

William Joseph Koshut

Department of Mechanical Engineering and Materials Science
Duke University

Date:_____

Approved:

_____
Kenneth Gall, Advisor

_____
Louis DeFrate

_____
Benjamin Wiley

_____
Stefan Zauscher

Dissertation submitted in partial fulfillment of
the requirements for the degree of Doctor
of Philosophy in the Department of Mechanical Engineering and
Materials Science in the Graduate School
of Duke University

2021

ABSTRACT

Tensile Fatigue Characterization of High Strength Hydrogels for Soft Tissue Applications

by

William Joseph Koshut

Department of Mechanical Engineering and Materials Science
Duke University

Date:_____

Approved:

_____
Kenneth Gall, Advisor

_____
Louis DeFrate

_____
Benjamin Wiley

_____
Stefan Zauscher

An abstract of a dissertation submitted in partial fulfillment of
the requirements for the degree of Doctor
of Philosophy in the Department of Mechanical Engineering and
Materials Science in the Graduate School
of Duke University

2021

Abstract

Synthetic cartilage implants have the potential to deeply transform the treatment of articular cartilage degeneration as well as the progression of osteoarthritis in load-bearing applications of various joints in the human body. To reduce patient morbidity and enhance range of motion, surgeons and material scientists alike are looking to synthetic alternatives re-establish articular cartilage function without introducing higher cost and health burdens. These implants are rigorously tested for their compressive and wear properties over longer timeframes, with the first instance of approved human use coming in the 1st metatarsophalangeal (MTP) joint with poly(vinyl alcohol) (PVA) being the predominant polymer in composition. Despite their promise of dissipating stress and providing smooth joint movement, these synthetic cartilage implants are not well-studied for their tensile fatigue properties which are extremely critical to *in vivo* performance and implant survival. As a synthetic substitute to match the properties of cartilage in human beings, hydrogels are extensively researched due to their potential biocompatibility. This research describes work dedicated to the advanced mechanical study of synthetic hydrogel systems for cartilage-based applications. The materials of interest are designed to have enhanced monotonic tensile properties for supplementary investigation via tensile fatigue testing. Superior mechanical behavior was achieved through the use of bio-friendly additives, freezing-thawing cyclic processing, and fiber

reinforcement. Lastly, the long-term failure mechanisms through flaw development for these synthetic hydrogel systems and biological tissue will be explored.

Dedication

I would like to dedicate my dissertation to my mother, father, sister, and brother-in-law Dan for the countless times of support and encouragement I received from them. Their guidance and ability to build me up during the rough times made this dream become a reality. I would not be where I am today without their example of working hard and tackling the roughest problems life can throw at you.

Contents

List of Tables

List of Figures

Acknowledgements

I would like to acknowledge Dr. Ken Gall for recruiting me to Duke to begin this journey. I would like to thank my remaining committee members: Dr. Benjamin J. Wiley, Dr. Stefan Zauscher, and Dr. Louis DeFrate for investing their time and energy in my success. I wish to thank Pat McGuire, John Goodfellow, Richard Nappi, and Bernie Jelinek for their patience and help in design reiterations for my project. I would like to thank Alina Kirillova for her mentorship and encouragement. I would like to thank Nick Kwon for helping make the finish line a reality toward the end of this journey. I send my deepest appreciation to Joey Rufo, Brittani Carroll, Dillon Huegen, Collin Katarski, and Sarah Kent for their incredible friendship. Lastly, I would also like to thank David Smoot, Caleb Rummel, Martha Byrket, Saige Sunier, and Ryan Gex, all of whom were amazing undergraduate students to work with.

Specific Aims and Timeline

The overarching goal of this dissertation is to study the advanced mechanical behavior of synthetic hydrogel systems through structure-property control. The three fundamental aims identified to achieve this goal include: 1) tensile fatigue characterization of poly(vinyl alcohol) hydrogels that are reinforced through bio-friendly toughening agents, (2) tensile fatigue study of a cartilage-like PVA hydrogel system reinforced with bacterial cellulose and poly(2-acrylamido-2-methyl-1-propanesulfonic acid), and (3) tensile fatigue characterization of controlled flaw types and sizes on poly(vinyl alcohol) hydrogels, composite hydrogels, and porcine cartilage. These three aims will be completed in **Table 1**, with further information provided in the entirety of this document.

Table 1: Work completed for the three aims of this dissertation

Aim	Start of Experiments	Anticipated Completion Date	Current Status
1	Yes	November 2019	Completed
2	Yes	August 2020	Completed
3	Yes	May 2021	Completed

Chapter 1. Introduction

1.1 Motivation

The progression of researching synthetic hydrogels has grown significantly in recent years, and the simultaneous development of the implantable biomaterials business has transformed from the pursuit of small market applications into a burgeoning industry. The ability to tune the mechanical properties of these elastic, synthetic hydrogels provides great promise for soft-tissue applications such as the 1st MTP joint. As orthopaedic applications continue to be presented for the use of hydrogels in the human body, a complete understanding of their mechanical behavior must be carried out. However, the capacity of studying these soft materials for long term mechanical behavior has presented a unique challenge to researchers. A number of synthetic hydrogels are not adequately understood for their fatigue behavior, which ultimately limits the scope of their usefulness. As such, a rare opportunity exists at the intersection of preparing mechanically robust hydrogels and characterizing them for load-bearing applications. This dissertation aims to unveil fundamental structure-property relationships of tough, synthetic hydrogels to be used as soft, implantable materials as well as to assess how the improvement of the monotonic properties of these materials translates to cyclic behavior.

1.2 Overview of Dissertation

The remainder of the document is organized in the following manner:

- Chapter 2: Literature review of major research relating to synthetic hydrogels, bio-friendly ways of improving the tensile properties of these hydrogels, and biomedical applications of relevant interest. Special attention is given to tough hydrogels made of PVA, bio-friendly additives used to enhance the mechanical properties of hydrogels, physical crosslinking in hydrogels obtained via freezing-thawing cyclic processing, and hydrogels for articular cartilage replacement.
- Chapter 3: My finished work in the areas investigated in the literature review of Chapter 2. Chapter 3 explores my work on PVA-based hydrogels for improvement of monotonic properties through bio-friendly additives and freezing-thawing cyclic processing. This work culminated with a study of the tensile fatigue life behavior of the top performing PVA-based double-network (DN) hydrogel compared to the control (no additive). The central hypothesis of this work was that a toughening additive could be used to improve both monotonic and fatigue mechanical behavior of the PVA hydrogel.
- Chapter 4: My finished work in the mechanical characterization of a double network hydrogel composite that matches the durability of

cartilage. Chapter 4 explores my work on this PVA-based composite hydrogel for improvement of monotonic tensile and compressive properties through a biomimetic design strategy. In re-creating the essential functions of cartilage, the central hypothesis of this work was examining the impact of modification to processing techniques and addition of tough composite additives to ultimately improve fatigue properties.

- Chapter 5: My finished work in the progression of differing flaw types and sizes as it relates to tensile fatigue behavior of poly(vinyl alcohol) hydrogels. This chapter examined the weakly explored field of fracture of materials as it relates to the tensile fatigue behavior of poly(vinyl alcohol) hydrogels. In understanding the impact of flaw type and dimension, the central hypothesis of this work was that flaw type (sharp, crack-like flaws vs. blunted, cylindrical hole-like flaws) was critical to monotonic and fatigue behavior.
- Chapter 6: My finished work in characterizing flaw impact on PVA-based composite hydrogels and a living tissue model of porcine costal cartilage. In studying the mechanical response to sharp cracks and cylindrical cavities for soft, high strain hydrogels, this work sought to examine a stronger hydrogel and a living tissue model. Similar to the previous

chapter, this work hypothesized that flaw type would once again be critical to fatigue performance. In addition, this chapter hypothesizes that the porcine costal cartilage and the stronger BC-PVA-PAMPS hydrogel composite will not be as flaw sensitive as the PVA-only hydrogel from Chapter 5.

- Chapter 7: The ultimate chapter will provide concluding remarks by drawing upon the investigations of Chapters 3-6. In addition, this chapter proposes future directions for this research based on inspiration of my own observation.

Chapter 2. Literature Review: Biocompatible Toughening Strategies for Synthetic Hydrogels

The following literature review was created with two primary reasons of consideration. The first explores research in the realm of improving mechanical behavior of synthetic hydrogels through bio-friendly additives and freezing-thawing cyclic processing. For the purposes of this review, the term "bio-friendly additive" refers to any material that has shown to be non-toxic, biocompatible, or has the potential to be proven non-toxic or biocompatible. The term freezing-thawing cyclic processing refers to continual freezing and subsequent thawing of a hydrogel in a cyclic fashion to induce physical crosslinking, thus improving the strength of a hydrogel. The goal of this portion of the review is to highlight basic structure-property relationships utilized through different processing techniques for synthetic hydrogels. These processing techniques will be viewed based on their ability to avoid toxic reagents, harsh acidic/basic conditions, or organic solvents.

The second surveys work in the area related to long-term tensile behavior (otherwise known as tensile fatigue behavior) of synthetic hydrogel systems as well as *in vivo* soft tissue systems. The state of the art in terms of analyzing the fatigue behavior of hydrogels will be considered. In the context of this literature review, tensile fatigue testing tracks the irreversible damage in a material from its native state, and this testing can be achieved in a cyclic fashion.[1] The hydrogel undergoes a cyclic strain of

amplitude *E*, and the test counts the numbers of cycles *N* of this applied strain until failure.[1] To merge these two main ideas of the literature review, specific focus is given to research where the fatigue properties of mechanically robust, biocompatible hydrogels was explored. Lastly, current work in the realm of improving poor fatigue properties of hydrogel systems will be contemplated.

2.1 Use of Synthetic Hydrogels in Biomedical Applications

As material scientists working with biomaterials, one of the greatest challenges we face comes in the form of replicating what nature has already provided to us through either: 1) a processing method that is easier to utilize or 2) with materials that are readily accessible. As daunting as that task may seem on the surface, its difficulty becomes magnified when trying to outperform the "natural" benchmark. Time and time again, the natural world has shown to be a better architect of soft materials for crucial physiological conditions and environments such as the ability of the epidermis to display anisotropy or the ability of collagen fibers to bundle.[2,3] These applications have demanding mechanical requirements that naturally occurring polymers are able to meet with no difficulty. On the other hand, synthetic materials such as hydrogels seem to lack the high-level cooperation needed to not only survive but thrive in the harsh settings of the human body. These materials hold the ultimate promise in biomedical applications due to their ability to mechanically maximize architecture and composition without

sacrificing key factors such as biocompatibility and non-toxicity.

Hydrogels are polymer networks of hydrophilic polymer chains that are capable of swelling extensively in water while maintaining a distinct three-dimensional (3D) structure.[4,5] As a synthetic alternative to mimic many of the naturally occurring tissue structures in human beings, hydrogels are comprehensively studied because of their biodegradability and biocompatibility in the fields of tissue engineering, drug delivery, and medical devices.[6–11] A brief view of hydrogel preparation for tissue engineering can be seen in Figure 1. These materials are of particular interest due to their ability to be co-cultured with cells to ultimately lead to cell proliferation.

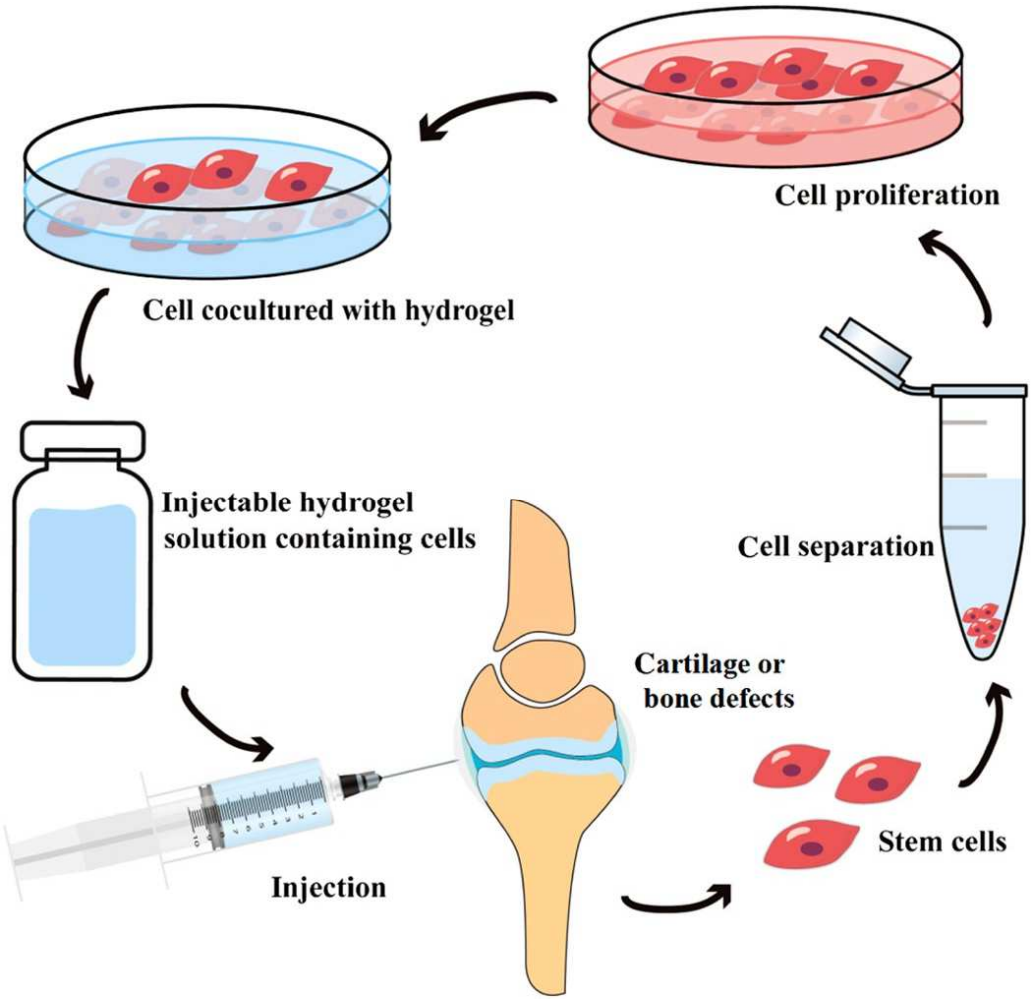

Figure 1: Schematic of injectable hydrogel prepared for tissue engineering.[12]

Hydrogels are particularly interesting for biomedical applications due to their favorable immunological response and the avoidance of toxic additives as part of their composition.[13] More specifically, the soft nature in terms of mechanical properties and hydrophilicity of hydrogels is promising for biomedical purposes,[14,15] and this interest is further compounded if the elasticity and mechanical properties of a hydrogel can be

tuned for a given application.

Advanced design of synthetic materials is no longer something interesting to pursue; it is completely obligatory for materials to have any practical applications. Hydrogels can be processed in ways to increase crosslinking, integrate other polymer networks or composite materials, or incorporate hydrogen bonding as an intermolecular force for smarter design of synthetic materials. These mechanisms will be explored in greater detail to reveal the current state-of-the-art techniques in making tougher hydrogels for biomedical applications.

2.1.1 Hydrogels as a Replacement for Articular Cartilage

With thoughts on a particularly promising use, hydrogels are considered to be an attractive class of soft materials for soft tissue replacement, in particular articular cartilage replacement.[16] As a surface of bones in all joints, articular cartilage leads to smooth movement and effective load-bearing by dissipating stress within a joint.[17] Articular cartilage is susceptible to degeneration (referred to as osteoarthritis), as sports-related injuries and natural aging are primary contributors to feelings of pain and stiffness in joints. For the knee alone, it is estimated that 14 million people in the United States have symptomatic knee osteoarthritis.[18,19] Expenditures to treat osteoarthritis have been expected around $16.5 billion at U.S. hospitals, accounting for roughly 4.3% of the combined costs for all hospitalizations.[20] Subsequently, there is increased need to

use a substitute material that re-establishes articular cartilage function without accelerating adjacent soft and hard tissue degeneration. For these load-bearing applications, high strength is needed along with elastic behavior in order to best mimic the function of articular cartilage.

Hydrogels are widely explored for their elastic nature, but they are not often considered for their strength in terms of being used as a substitute for articular cartilage. One example of hydrogel system with tunable elasticity, a key property for biomedical applications, includes the system based on polyethylene glycol dimethacrylate (PEGDMA).[21–23] With the ability to tailor the properties of PEGDMA hydrogels based on the balance between polymer molecular weight and water content,[24] a diverse range of biomedical applications has been pursued for further study.[25–28] However, PEGDMA hydrogels often lack sufficient strength for load-bearing applications. As such, these hydrogels often require reinforcement resulting in a moderate increase in mechanical behavior.[24,29–31] Given PEGDMA may be insufficient in terms of its strength for "permanent" replacement of articular cartilage, one such polymer that is both biocompatible and processable as a strong hydrogel for this particular application is poly(vinyl alcohol).[32]

Poly(vinyl alcohol) as a hydrogel holds great promise as a synthetic cartilage implant due to its mechanical, chemical, biodegradable, and swelling properties.[14,15,33–36] PVA hydrogels can be prepared with non-toxic reagents as well as under physiological

conditions that minimize harmful responses from cells and tissue alike.[37,38] PVA hydrogels have shown excellent lubrication in simulated synovial fluid.[39–41] In addition, PVA-based hydrogels are intrinsically non-adhesive toward cells and proteins, and this allows for the creation of cell-selective materials via incorporation with the hydrogel network.[37] The mechanical behavior of a hydrogel network based on PVA can be tuned appropriately for a given application based on the polymer concentration utilized. As such, the viscoelastic characteristics of a PVA-based hydrogel network can be adjusted to match soft tissue in humans.[42,43] This is also attributed to PVA's ability to form intramolecular as well as intermolecular hydrogen bonds. In this way, PVA can form an interpenetrating polymer network of improved mechanical behavior than the principal network of PVA by itself.[44] Once a compatible additive with PVA is selected, further study would be needed to understand the enhancement of the mechanical properties with regards to the hydrogel's lifetime for practical applications such as articular cartilage replacement.

2.2 Chemical and Physical Crosslinking in Synthetic Hydrogels

Hydrogels are typically prepared through synthetic processes known as chemical or physical crosslinking. The utilization of covalent bonds provides the basis of the 3D-network in chemically crosslinked hydrogels, while non-covalent interactions such as ionic interactions and hydrogen bonding act as the foundation of the 3D-network in

physically crosslinked hydrogels.[45] A graphical representation of the simple difference between physical and chemical crosslinking can be seen in Figure 2.

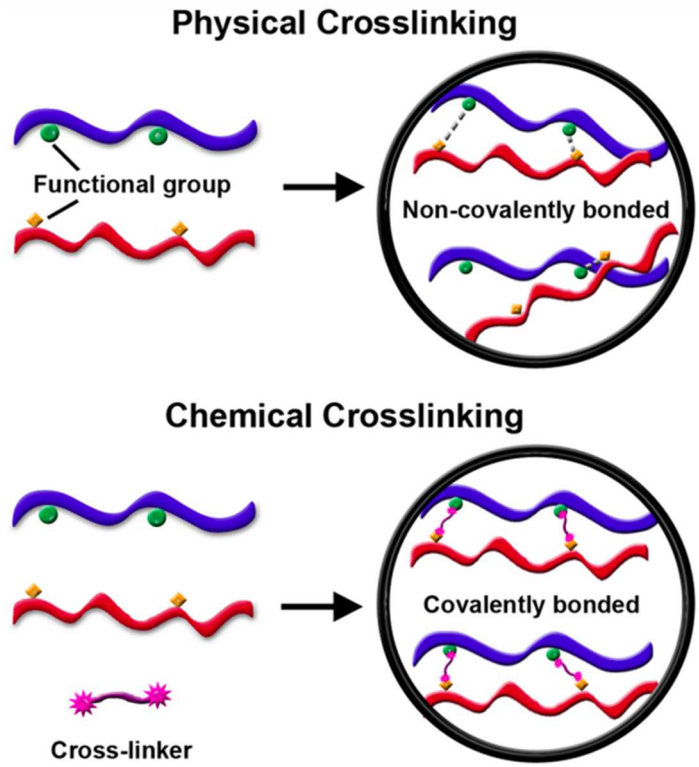

Figure 2: General graphical comparison of physical and chemical crosslinking.[46]

These non-covalent interactions may also include the use of hydrophobic interactions, chain entanglement, and development of crystalline domains within a hydrogel's network.[6] The decision to utilize either non-covalent or covalent interactions depends primarily on the application of interest.

With regards to selecting a synthetic pathway, chemical crosslinking methods

often provide suitable mechanical properties and stability in physiological conditions.[47] However, physical crosslinking provides the following benefits compared to chemical crosslinking: absence of sometimes toxic chemical crosslinkers, use of milder reaction conditions, enhanced biocompatibility without initiators and other chemically complex reagents.[48] Chemical crosslinking reactions can often leave behind unwanted bioactive materials that remain present in the hydrogel's matrix.[49] These compounds can be difficult to detect in terms of their presence or even harder to remove through subsequent purification steps. Physical crosslinking can avoid these potentially toxic materials, but hydrogels prepared through physical crosslinking often lack sufficient energy dissipation mechanisms for suitable strength and toughness. Thus, a battle exists between the mechanical stability provided by chemical crosslinking and the bio-friendliness of physical crosslinking.

As a result, an opportunity exists in either: 1) finding a chemical crosslinking pathway that is completely non-toxic or 2) a physical crosslinking pathway that maintains durability under physiological conditions. Physical crosslinking methods provide a greater number of "starting blocks" for potential mechanical improvement, while chemical crosslinking methods impose an even tougher restriction of keeping the material biocompatible. Ultimately, this restriction of biocompatibility has increased the need for improvement of a hydrogel's network structure through physical crosslinking methods. To widen the range of load-bearing applications for hydrogels in the human

body, physical crosslinking methods must address the weak resistance to polymer chain breakage that limits hydrogels.[50] Alternative methods for mechanical improvement must be pursued without impeding with the favorable properties of hydrogels such as elasticity and hydrophilicity.

One such physical crosslinking method that aids in the dissipation of mechanical energy is referred to as freezing-thawing cyclic processing. In this pathway, the polymer chains align to form small, highly ordered regions known as crystallites when subjected to freezing temperatures followed by a thawing step.[47] Molecular weight, polymer concentration in solution, temperature of each freezing step, amount of time of each freezing step, and number of freezing steps are all important considerations when analyzing a hydrogel system's capacity for improvement of strength. Hydrogel systems using PVA as a polymer component have taken advantage of crystallite formation for enhanced strength, as the crystallite regions are able to bear mechanical load.[51,52] In addition, hydrogel samples composed of PVA with freezing-thawing cyclic processing achieved improved stability during swelling tests at physiological temperatures.[53] Some downsides from freezing-thawing cyclic processing come in the translucent appearance of the hydrogels as well as a possible drop-off in stability against degradation.[54] Fortunately, these shortcomings are not as significant as the potentially toxic reagents used in chemical crosslinking pathways.

In terms of the synthetic pathway chosen, both physical and chemical crosslinking methods have advantages and disadvantages for preparing robust, tough hydrogels. The application of interest is critical to determining the best possible synthetic route. However, both chemical and physical crosslinking are primarily utilized for creation of hydrogels instead of mechanical improvement of them. Additional techniques may be compounded with these methods to attain the best possible mechanical properties. Though useful in terms of creating hydrogel, physical and chemical crosslinking need support from other reinforcement approaches for optimal mechanical performance. These methodologies will be considered in subsequent sections.

2.3 Reinforcement Strategies for Synthetic Hydrogels

In addition to using various crosslinking techniques for improved mechanical behavior, other reinforcement approaches have been pursued. These strategies include metal coordination, ionic interactions, plasma grafting to a hydrophobic substrate, and hydrophobic interactions in block copolymers.[55–59] An example of metal coordination in a hydrogel system can be found in that of Histine-Zn^{2+} for a self-healing hydrogel in Figure 3. In this work, researchers utilized the reversible (His)-metal coordination observed in mussel byssus to create a crosslinking mechanism for tuning the mechanical

properties.[60] This metal coordination concept served as a remarkable blueprint for the creation of a biomimetic hydrogel.

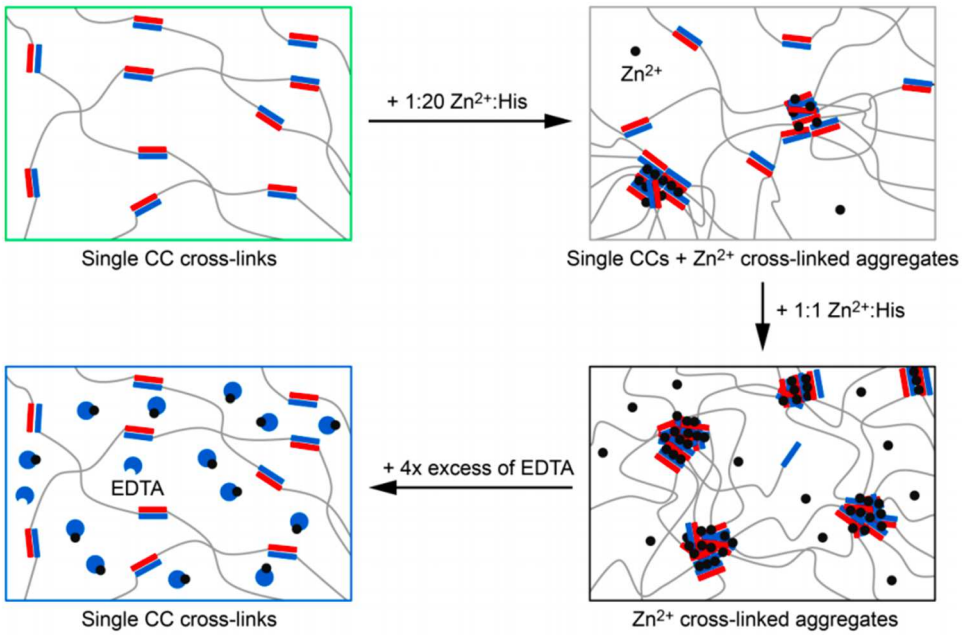

Figure 3: Histidine-Zn^{2+} coordination for the creation of a self-healing hydrogel.[60]

In addition to the use of metal coordination for improved properties in hydrogel systems, Yuan et al. capitalized on high density ionic interactions from copolymerization of negatively charged monomers in a positively charged solution.[59] In using electrostatics to their advantage with favorable ionic interactions, these researchers were able to obtain improved compressive and tensile properties. A schematic of the ionic interactions present in the network of the hydrogel can be seen in Figure 4.

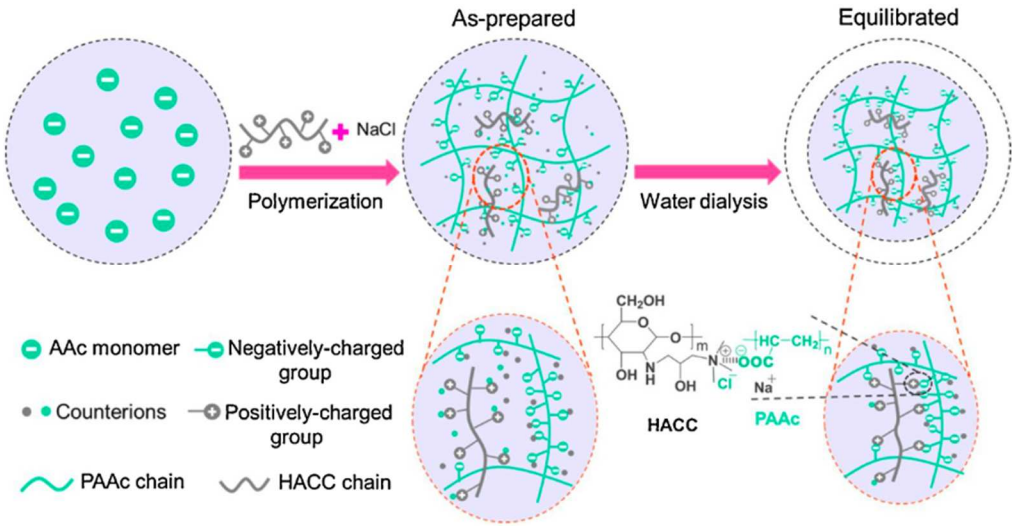

Figure 4: Hydrogel system using ionic interactions through copolymerization of negatively charged monomers in a positively charged solution for improved mechanical behavior[59]

Unfortunately, each of these techniques present unique challenges that are difficult to overcome if the overall goal for the soft material is implantation. The presence of metal ions, charged compounds, or hydrophobic compounds may restrict the possibility of hydrogel's biocompatibility and biodegradability being sufficient for human use, especially if implantation is at stake. These types of materials may also hinder the hydrophilicity of a hydrogel, which is one of its most promising aspects for intense study. On a similar note, the mechanical concerns created by poor interfacial adhesion of these hydrophobic materials only complicates matters further.[61] Due to these trepidations, the following sections of this dissertation will examine reinforcement approaches that maintain biocompatibility and can be termed "bio-friendly". At the same time, these bioinert reinforcement approaches seek to enhance mechanical

behavior to the same degree or better as metal coordination, ionic interactions, and hydrophobic interactions.

2.3.1 Bio-Friendly Reinforcements for the Creation of Hydrogel Composites

Apart from the strategies discussed above, reinforcement of a hydrogel's network with a biocompatible additive holds great promise for the improvement of a hydrogel's strength and toughness to match articular cartilage.[62,63] Calcium phosphate, silk fibroin, bacterial cellulose, hydroxyapatite, polydimethylsiloxane microspheres, and even PVA fibers themselves have all been utilized as biocompatible reinforcements for mechanical behavior of a hydrogel.[13,64–71] This approach is particularly reliant on ensuring one or some combination of the following concerns: 1) improving the mechanical properties of the hydrogel or 2) boosting ease of processing or 3) maintaining biocompatibility of the hydrogel for human use. A schematic of the process of creating a silk fibroin hydrogel composite for applications in auricular tissue engineering can be seen in Figure 5.

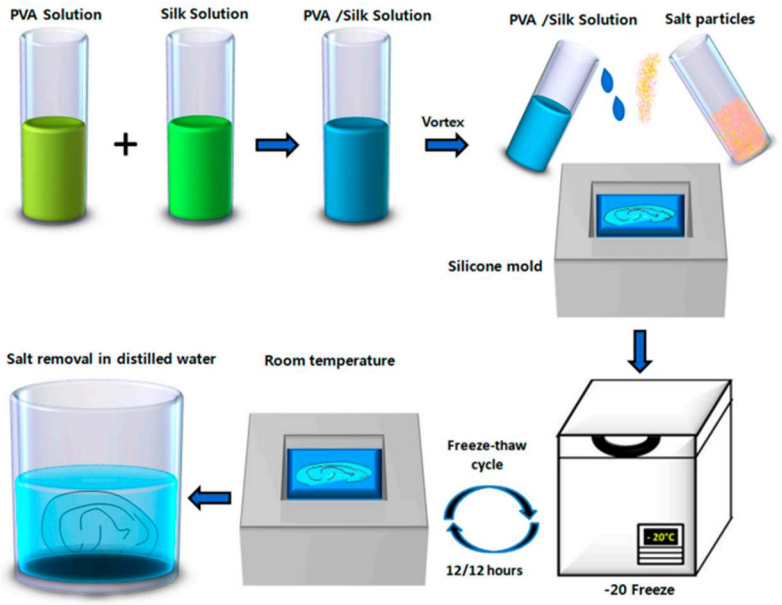

Figure 5: Hydrogel fabrication process using silk fibroin as a reinforcement for auricular cartilage applications[64]

Lee et al. were able to characterize different ratios of silk fibroin and poly(vinyl alcohol) hydrogel to obtain promising histological results *in vitro* and *in vivo*.[64] Additives of this nature are often used to improve the mechanical behavior without introducing harmful physiological effects or disrupting favorable network aspects of the base hydrogel.

Ideally, the material added to the hydrogel system can be utilized in such a way to selectively tune the mechanical properties. Material scientists often turn to fibrous materials such as stainless steel wool fibers, poly(ε-caprolactone) (PCL) fibers, and cellulose nanofibers to improve the strength and toughness of their hydrogel with the hope that the fibrous material will not hinder the main components of the hydrogel, leading to catastrophic failure.[72–74] In addition, the involvement of 3D-printing for

greater control of fiber alignment for mechanical reinforcement has been pursued in a process known as melt-electrospinning writing.[73,75] The usefulness of fibrous materials for clear improvement or tuning of tensile properties has been observed in the behavior of collagen, a material that is produced naturally in the body in cartilage.[76] The reinforcement materials are adept for load-bearing applications, but their use can often lead to challenging issues with the main hydrogel system. These problems may include degradation of the hydrogel for a given application or aggregation of drug-releasing agents to fibers.[77] As such, the range of applications for these composite hydrogels becomes restricted. Concerns of maintaining hydrophilicity, biocompatibility, and degradation are difficult to balance while seeking improvement in the mechanical properties of the hydrogel system through the addition of the fiber-based material. Pursuit of alternative reinforcement approaches is needed to ensure the fulfillment of both adequate mechanical and physiological behavior of the hydrogel.

2.3.2 Additions of Polymers and Small Molecules for Hydrogen Bonding in Hydrogels

In addition to composite approaches for creating reinforced hydrogels, scientists have turned to multifunctional crosslinkers and hydrogen bonding interactions as common solutions to improve the weak mechanical properties of hydrogels.[33,78–80] Dai et al. utilized a dual amide hydrogen bond domain to enhance the stability of their

supramolecular polymer hydrogel.[80] A schematic of this dual hydrogen bond concept can be seen in Figure 6.

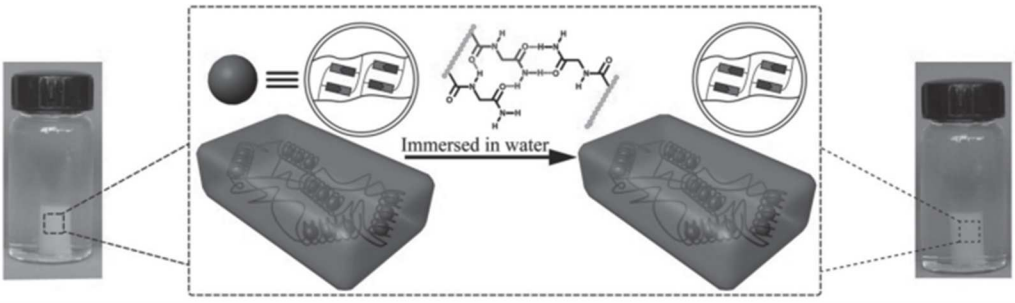

Figure 6: Supramolecular polymer hydrogel with enhanced stability from the use of a dual hydrogen bond domain[80]

Hydrogen bonding interactions are extensively studied in this area due to their lack of the adverse effects on cell behavior that can result from toxic chemical or photo-crosslinking agents as well as inclusion of a support structure that the human body may identify as a foreign target for inflammation and infection.[81] The ability of hydrogen bonding to improve tensile and compressive strengths of a given hydrogel suggests its usefulness as a strategy in further research.[82] As a result, the worlds of chemistry and materials science collide in finding compounds that are well-matched for extensive hydrogen bonding in a hydrogel. Unfortunately, this problem is further complicated with the restriction of ensuring that the compound is non-toxic and biocompatible for human use.

Researchers have often utilized materials such agarose, k-carrageenan, gelatin,

chitosan, poly(vinyl pyrrolidone), and starch to achieve biocompatible hydrogels with hydrogen bonding for improved mechanical properties.[83–87] Each of these additives was carefully selected for its ability to create a second network of favorable interactions without harming biocompatibility. Deng et al. employed κ-carrageenan to improve fracture tensile stress and toughness in their double-network hydrogel.[84] A schematic of their hydrogel system can be seen in Figure 7.

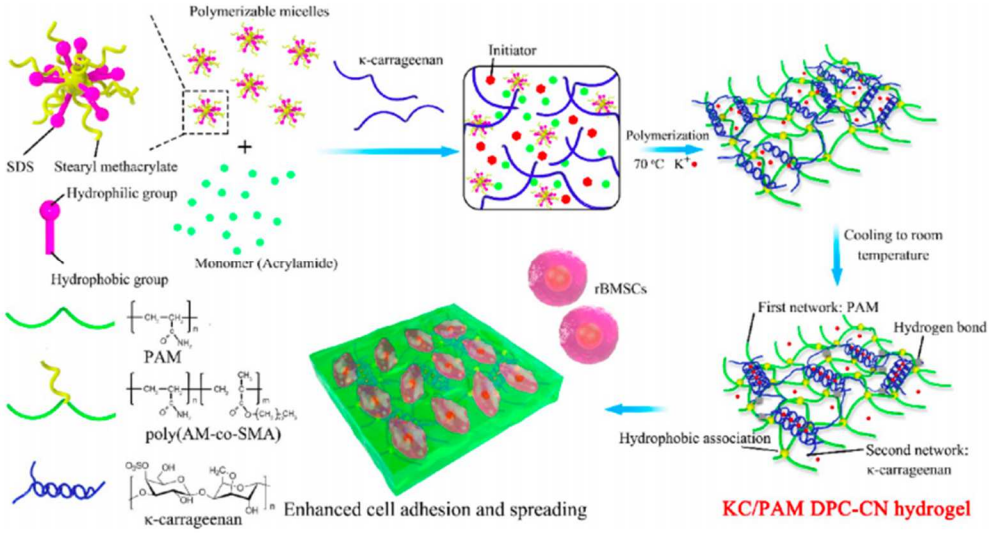

Figure 7: Double-network hydrogel comprising of κ-carrageenan and polyacrylamide for improved mechanical behavior and enhanced cell adhesion[84]

In addition to polymer-like materials, small molecule additives can be selected to form hydrogen-bonded intermolecular complexes (IMCs).[88] The improvement of mechanical properties by selecting small molecules must not stray away from maintenance of the hydrogel's bio-friendly nature. These small molecules can be better suited for

incorporation into a hydrogel's network structure due to their inability to disrupt favorable network interactions of the main component in the case of tannic acid with poly(vinyl alcohol).[89] Sadly, the reverse of this idea can also dominate when a larger polymer is preferred as an additive due to the impact that a small molecule may have on a network structure. In either case, both polymers and small molecules alike may be chosen for their ability to improve monotonic tensile strength and toughness.

2.4 Hydrogels Studied for Fatigue Behavior

Most often, synthetic implants are rigorously tested for their compressive and wear properties over longer timeframes. One area lacking sufficient pursuit in understanding the true lifetime of a hydrogel includes its tensile fatigue life behavior. Unfortunately, testing under compressive conditions is arbitrary in determining failure in a sample due to the enhanced ability of hydrogels and articular cartilage to recover shape and resist deformation when compressed.[35,90,91] The start of fracture within a sample tested in compression is much more difficult to observe in that it may occur internal to the sample in lieu of the outside portion of it. On the other hand, the start of fracture in tensile testing is much easier to observe in that it commonly begins at the outside of the sample. Researchers generally agree that more mechanically robust hydrogels that resist crack propagation are needed for increased interest in biomedical applications and their further study.[92–94] However, the tensile lifetime of these materials

is not well understood for non-catastrophic testing conditions.

For hydrogels that show promise in dissipating mechanical energy, many researchers have pursued insufficient study of their material through very low-cycle tensile testing conditions (10 to 1,000 cycles) with no systematic varying of the stress or strain the material experiences to determine a material's inherent resistance to fatigue.[6,58,95] It is impossible to extract information on a hydrogel's fatigue resistance from single stress amplitude tests, stopped at arbitrary cycle numbers, though many studies have focused on this analysis.[96–101] For deeper insight into this matter, Hu et al. provided an analysis of the monotonic tensile properties of their nanocomposite hydrogels as seen in Figure 8A.[101] However, they provided only five cycles of loading and unloading their nanocomposite hydrogel for a study of its cyclical mechanical behavior in Figure 8B.[101] As such, this testing complicates valuable insight on the long-term mechanical behavior of the hydrogel in question.

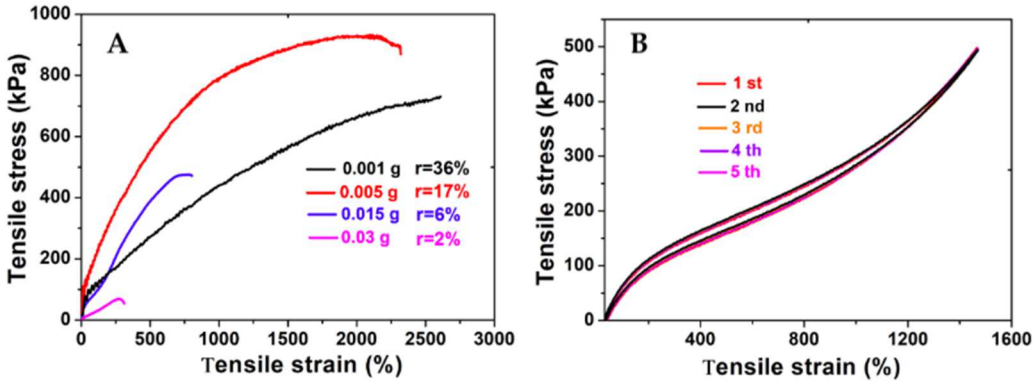

Figure 8: (A) Monotonic tensile stress-strain behavior of nanocomposite hydrogels. (B) Five cycles of loading and unloading the top-performing nanocomposite hydrogel.[101]

In conducting these low cycle tensile tests, material scientists are often faced with using a low strain rate for achieving damage accumulation and failure in samples. Strain rate is essentially how fast the sample deforms with respect to time. Higher cyclic strain rates can often lead to decreased hysteresis which ultimately brings about reduced energy dissipation.[102,103] Though promising at being able to test samples at a much faster rate for shorter overall testing times, one caveat comes in the form of how the sample behaves under much higher strain rates. Samples often fail to experience prolonged tensile loads at these high strain rates, as buckling and ratcheting become concerns. As such, there exists a tradeoff between causing a sample to experience sustained tensile loads and the selected strain rate for a given test. Ideally, the highest possible strain rate could be obtained to ensure adequate damage accumulation in a sample without the test taking an exorbitant amount of time. The ultimate goal of finalizing a PVA-based hydrogel would be understanding the strain-life curve (*E-N* curve) with regards to the presence of a selected additive, whether this contribution be negative or positive in its impact.

Chapter 3. Tensile Fatigue of Poly(Vinyl Alcohol) Hydrogels with Bio-Friendly Toughening Agents

3.1 Aims and Summary of Completed Work on Poly(Vinyl Alcohol) Hydrogels

Robust hydrogels have been continually pursued as soft biomaterials for implantation in the human body.[104–107] However, the applications of these materials are extremely limited by their inability to uphold long-term mechanical durability. In this work, we prepared double-network hydrogels of poly(vinyl alcohol) with the use of bio-friendly additives and freezing-thawing cyclic processing as a means to increase monotonic tensile toughness and explore fatigue behavior. The central hypothesis of this work was that a toughening additive could be used to improve both monotonic and fatigue mechanical behavior of the PVA hydrogel. Hydrogen bonding interactions were employed between these bio-friendly additives and PVA to improve the monotonic mechanical properties of the resulting hydrogel. Once a selected additive was deemed sufficient for its processing and improvement of mechanical properties, a deeper understanding of the magnitude of the additive's impact was pursued in terms of monotonic toughness and ultimate tensile strength. This study also sought to examine the tensile fatigue life behavior of the top performing hydrogel compared to the control hydrogel (no additive) with the goal of establishing a comparison between samples. As a

result of this testing, the top performing additive was shown to decisively improve monotonic properties but not fatigue properties. This study represents the first analysis of tensile fatigue properties of a synthetic hydrogel, and it can serve as an example of how improved monotonic toughness often cited in the literature does not necessarily translate to improved fatigue properties, which are most relevant to *in vivo* performance and implant survival.

To the author's knowledge, no such study focusing on full load spectrum cyclic, tensile testing has been published for a high-strength synthetic hydrogel. The difficulty of testing hydrogels like these in a cyclic tensile fashion has created a divide between high-level design of these materials and realizing their full mechanical behavior. This study aimed to bridge the divide using simple processability strategies and a more complete mechanical understanding of a PVA-based hydrogel. With the taxing physiological stresses applied to articular cartilage, it comes as no surprise that their mechanical properties must be substantial for cyclic tensile testing.[108–110] This presents a unique challenge to material scientists to create hydrogels that are able to bear physiological stresses, ultimately attaining a similar toughness to articular cartilage. Nevertheless, these hydrogels must maintain non-toxicity and biocompatibility due to their implantation in the human body. It is necessary for these hydrogels to be simple in terms of processability to keep a broad view of potential applications.

3.2 Results of PVA-based Hydrogel Investigations

3.2.1 Comparison to Typical PEGDMA System

As a starting block in this study, we set out to examine the mechanical properties of our raw PVA-based hydrogel against a hydrogel system composed of PEGDMA. We prepared PVA hydrogels via dissolving of the polymer in deionized water followed by using a freezing-thawing method to physically crosslink the polymer network through crystalline domains.[53,111] Researchers are often attracted to working with PEGDMA due to its tunable mechanical stiffness and bioinert components for biomedical applications.[21,25,29] PEGDMA samples of equal polymer composition compared to the PVA control sample were crosslinked with UV light with a range of molecular weights. The goal of the PEGDMA trials was to find a molecular weight of PEGDMA for which the crosslinked samples approximately matched the stiffness of the PVA control sample while also comparing the ultimate tensile strength and strain-to-failure of PVA vs. PEGDMA. The results of these tests can be seen in Figure 9A for representative stress vs. strain curves for the PEGDMA samples of differing molecular weights. The PVA control sample was included in this plot for reference, and a magnified version of the stress vs. strain curves at low strain values can also be seen for easier comparison in Figure 9B.

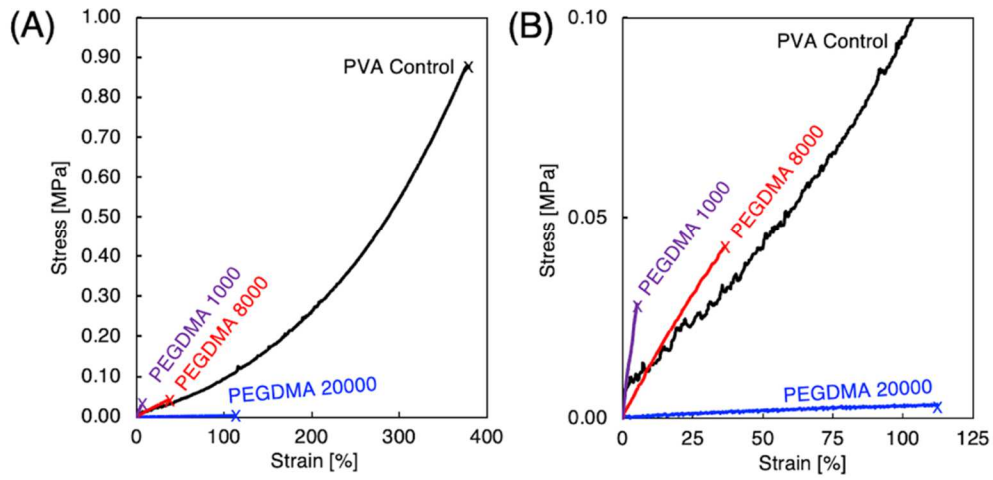

Figure 9: (A) Tensile stress-strain behavior of PEGDMA 1,000, PEGDMA 8,000, and PEGDMA 20,000 g mol^{-1} against PVA control sample. (B) Magnified portion of (A). The PVA control sample was prepared in a mold based on the ASTM D638-14 Type V shape, while the PEGDMA samples were prepared in Teflon molds that matched the dimensions of the customized fatigue shape for easier sample removal.

As shown in Figure 9, PEGDMA 8,000 g mol^{-1} provided the closest match to the stiffness of the PVA control sample, while PEGDMA 1,000 g mol^{-1} was stiffer and PEGDMA 20,000 g mol^{-1} was significantly softer due to changes in crosslink spacing of the PEGDMA networks. The PEGDMA samples were vastly weaker than the PVA control sample, showing lower strength and strain to failure.

3.2.2 Chemistry and Structure

Homogenous solutions with 16 wt% PVA (based off the weight of deionized water combined with PVA) were obtained with great processability for wt% ranges of 1 wt% to 6 wt% for a variety of bio-friendly additives (based off the weight of PVA). As noted previously, this pathway of improving non-covalent interactions through crystalline domain development can potentially enhance the mechanical properties of a PVA-based hydrogel further. Once refined, this mechanism can also work in unison with the previously mentioned non-covalent pathway of hydrogen bonding through bio-friendly additives to increase both the strength and toughness of the PVA hydrogel. In tandem, freeze-thaw cycles to enhance crystalline domains and additive reinforcement to promote hydrogen bonding combine to form a double-network hydrogel of PVA.[7,8,112,113] Each additive was selected for its ability to act as both a hydrogen bond acceptor and hydrogen bond donor. Furthermore, these additives were selected for their ability to mix with PVA at a molecular level for simple solution blending and processability.[8] The synthetic approach ultimately selected in this study can be seen in Figure 10 with starch being used as the example additive.

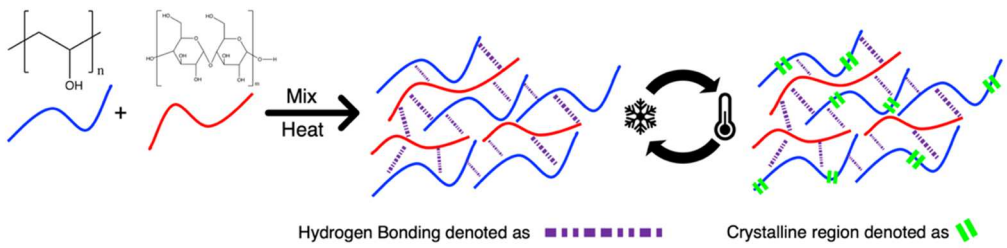

Figure 10: Schematic representation of the PVA-based tough hydrogel preparation strategy using a bio-friendly additive (starch used as an example) and freeze-thawing cyclic processing. PVA control samples had no additive present. A given amount of PVA was combined with a given amount of a bio-friendly additive. Deionized water was then added to the mixture which was held at 95°C until PVA had fully dissolved for pouring the solution into the stainless-steel molds. Freezing and subsequent thawing of the samples took place to create a double-network hydrogel. Hydrogen bonding could occur between PVA with itself and PVA with an additive. However, development of crystalline regions was solely attributed to PVA interacting with itself.

Representative pictures of typical monotonic tension samples after final preparation can be seen in Figure 11A, while typical fatigue tension samples can be seen in Figure 11B. ASTM D638-14 Type V shape could be successfully used for all monotonic tensile testing of the bio-friendly additives, as seen in Figure 11A. Adjustment of the shape of the sample was necessary due to the tendency of the Type V samples buckling when tested cyclically in strain controlled tension. In addition, ASTM D638-14 Type V samples had issues with failure near the grip section instead of the gauge section when stretched in a cyclic fashion. As a result, a shorter and thicker gauge section was designed. The ratio of the width of the grip section to the width of the gauge section was

controlled at 2:1 (ratio described as grip:gauge). The resulting shape of the cyclic tensile specimen can be seen in Figure 11B.

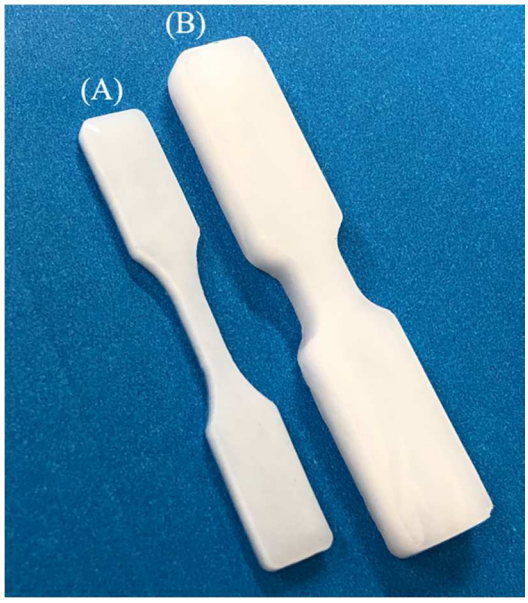

Figure 11: Representative optical images of (A) ASTM D638-14 Type V shape for monotonic tension and (B) customized fatigue tension samples.

3.2.3 Bio-Friendly Additive Screening Process

For improved tensile testing of the PVA-based hydrogel system, many non-toxic additives were pursued as possible materials that would improve the mechanical properties of a simple PVA-based hydrogel. We finalized the selection of 11 additives that formed homogenous, processable solutions when PVA was mixed with the selected additive and materials dissolved in water. In addition, we chose two additives

(hydroxyapatite and cotton flock) that would knowingly reinforce the PVA-based hydrogel even though these additives did not form a homogenous solution with PVA. All additives were used at 4 wt% with regards to the weight of PVA, and their testing samples were prepared according to the procedure described in the Material Preparation section in the same manner as the Agar example. The samples were then tested for their monotonic tension properties with the ASTM D638-14 Type V shape to obtain the top performing additives based solely on inherent toughness, which is defined as the area under the stress vs. strain curve. Toughness was selected as the key metric for screening additives due to its practical applications in the realm of articular cartilage when considering the ability of a hydrogel to dissipate energy, which is a direct relationship to toughness.[84,114–116] The results can be seen in Figure 12A in which toughness is shown for each additive. With these results in view, the top four performing additives on toughness enhancement alone were agar, xanthan gum, starch, and cotton flock. The representative stress vs. strain curves for these top additives as well as the control sample can be seen in Figure 12B.

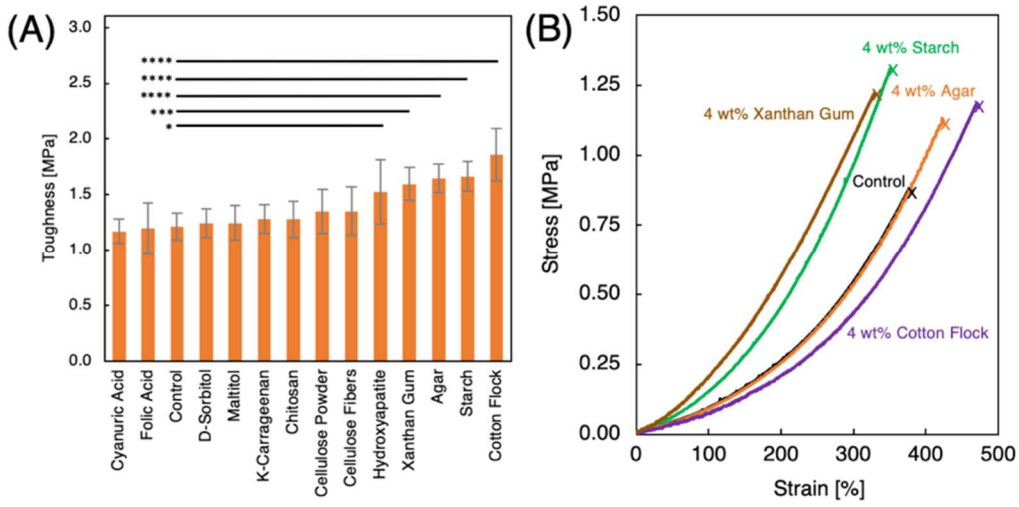

Figure 12: (A) Average toughness values for control samples and samples with all additives obtained from monotonic tensile stress-strain behavior with ASTM D638-14 Type V shape. Minimum of n=9; data depict mean toughness value ± standard deviation; compared with control by one-way analysis of variance (ANOVA); α=5%; * depicts statistical significance in the following manner: * p<0.05; ** p<0.01, *** p<0.001, **** p<0.0001. (B) Tensile stress-strain behavior of top performing additives (xanthan gum, agar, starch, and cotton flock) obtained from ASTM D638-14 Type V shape.

In a purely mechanical sense, the addition of fibers in the case of cotton flock helps with dissipation of mechanical energy compared to all other additives. Some theories may be proposed to explain the behavior observed from agar, xanthan gum, and starch with regards to the remaining additives. These three additives in particular had chemical structures with increased opportunities for hydrogen bonding solely based on the number of sites that can act as either hydrogen bond donors or hydrogen bond acceptors. The ability of the additive's molecular chains to act favorably with the

molecular chains of PVA greatly influenced the hydrogel's ability to dissipate mechanical energy when stretched. In addition, a major consideration of these additives came down to plasticizing effects on the network structure of PVA. If a selected additive will act as a plasticizer toward PVA, the resulting hydrogel would be mechanically weaker even if it were easily processable in terms of making the sample. Xanthan gum, agar powder, and starch had a delicate balance of favorable hydrogen bonding with PVA at 4 wt% while refraining from weakening plasticization effects.

To understand the impact of these additives on the functional properties of the PVA hydrogels, a swelling ratio comparison study was performed. Understanding hydrogel swelling is critical for drug release applications or stress dissipation mechanisms in articular cartilage.[117–119] Figure 13 shows the minimal impact that each of the top performing additives had on the ability of the hydrogel to swell in deionized water at room temperature according to the procedure described in 3.4.3 PVA-based Hydrogel Swelling Study.

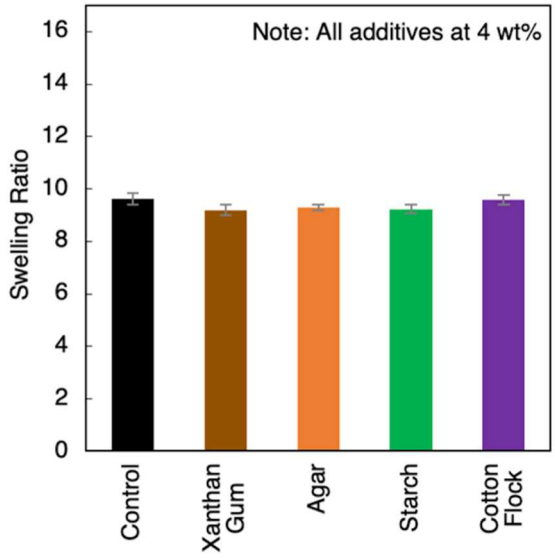

Figure 13: Swelling ratio comparison of top performing additives prepared via ASTM D638-14 Type V shape.

The average swelling ratios were 9.62, 9.58, 9.28, 9.23, and 9.19 for control, cotton flock, agar, starch, and xanthan gum, respectively. The swelling ratios of the additives differed from the control by 3.5%, 4.1%, and 4.5% for agar, starch, and xanthan gum, respectively. Cotton flock had the smallest percent difference from the control at 0.42% as a purely mechanical reinforcement. In terms of ease-of-processing in a qualitative sense, starch was the easiest sample to prepare followed by cotton flock, agar, and xanthan gum in increasing order of processing difficulty. This ranking was based on the following concerns: 1) the ability to easily mix the two additives, 2) pouring the resulting solution for freezing-thawing cyclic processing, and 3) removing the resulting hydrogels from the mold once freezing-thawing cyclic processing was completed. As shown in

Figure 13, these additives were successful in their ability to not significantly impact swelling capabilities. With this insight in mind, the decision to study a specific additive was based solely on the three ease-of-processing concerns addressed above. In reflection of the three main concerns, starch was selected as the top additive of choice.

3.2.4 Monotonic Mechanical Characterization of Starch Presence

Using starch as a building block, we set out to establish the limits of how much starch could be added to the system while still maintaining improved toughness, enhanced tensile strength, and ease-of-processing. The amount of starch was incrementally added in terms of percent by weight, starting from 1 wt% to 6 wt%, above which processing became tedious. Tensile properties were studied with increased starch using the same Type V dogbone and mechanical testing methods. The representative stress vs. strain curves for these samples can be seen in Figure 14A.

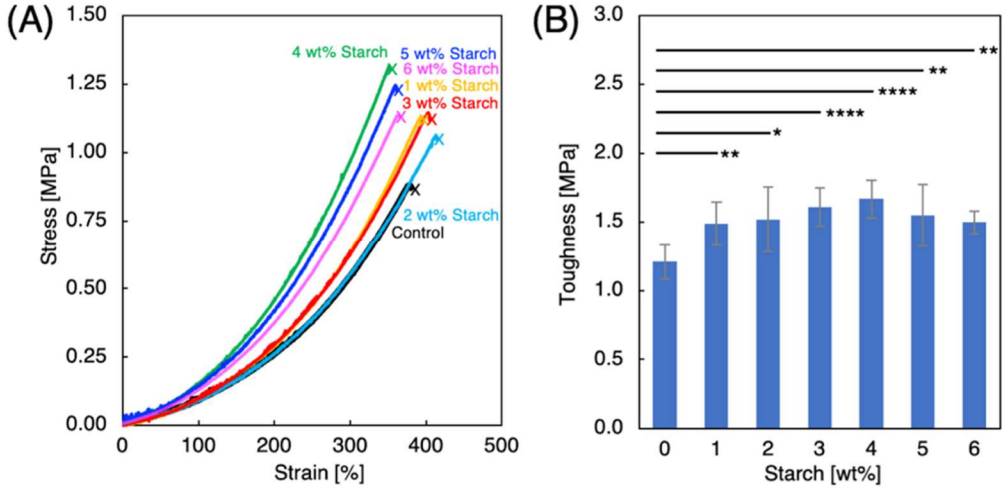

Figure 14: (A) Tensile stress-strain behavior and (B) comparison of average toughness values of all starch samples obtained from ASTM D638-14 Type V shape. Minimum of n=9; data depict mean toughness value ± standard deviation; compared with control by one-way analysis of variance (ANOVA); α=5%; * depicts statistical significance in the following manner: * p<0.05; ** p<0.01, *** p<0.001, **** p<0.0001.

As shown in Figure 14A, initial additions of starch help with increasing the strain at failure for the hydrogel samples. As the amount of starch increases, the samples shift to lower failure strains and higher values of ultimate tensile strength. There is a stiffening effect of steeper slopes in the stress vs. strain curves that is noticeable in the 4 to 6 wt% starch samples and unclear with 1 to 3 wt% starch. In addition to observing a change in the stress vs. strain curves for the presence of more starch, a similar trend was realized in the toughness values for these samples (Figure 14B). Minor additions of starch improved the toughness values for all samples compared to the control samples, with average values ranging from 1.21, 1.49, 1.52, 1.61, 1.67, 1.55, and 1.50 for control, 1,

2, 3, 4, 5, and 6 wt% starch, respectively. The slight drops in toughness after 4 wt% can be attributed to starch introducing plasticizing effects on the network structure of PVA. A deterioration of strength was observed with increasing presence of starch instead of bringing about continual improvement. This effect has been observed in hydrogel studies previously,[8] as plasticization effects ultimately lead to a loss of mechanical strength.

3.2.5 Crystallinity Analysis of Starch Presence

While characterizing the mechanical behavior of the addition of starch was critical, it was also deemed necessary to understand the chemical impact of starch's presence on the network structure of the hydrogel in terms of crystallinity and molecular interactions. Aside from the physical crosslinking attained via the freezing-thawing cyclic processing steps, hydrogen bonding was identified as a key interaction between PVA and starch. The ability to capitalize on hydrogen bonding in the hydrogel was critical for the sake of avoiding toxic crosslinking reagents or additional harsh treatments to the hydrogel. As such, it became critical to investigate the role of hydrogen bonding in the mechanical performance of the hydrogel. Both intramolecular (with PVA itself) and intermolecular (between PVA and starch) hydrogen bonding strongly influenced the toughness trend as seen in Figure 14B, but the role of these types of

hydrogen bonding were not well-characterized for the impact on the crystallinity degree of the hydrogel.

The next aim of this study was to determine if a connection existed between the presence of starch and the degree of crystallinity. However, the ability to analyze the samples in their as-prepared state was challenging. In drying out the hydrogel samples or instituting a freeze-drying process, the crystalline structure would be altered from its as-prepared state. Prior work has noted the change in the apparent dimensions of PVA crystallites or overall crystallinity of samples from as-prepared hydrogels as compared to dried out and aged ones.[120,121] An aging process or multiple freezing-thawing cycles were needed to obtain hydrogels with the stability of consistent crystallite dimensions.[120] Air drying and freeze-drying of hydrogels can often to lead to changes in the swelling, mechanical, or thermal behavior.[122,123] In addition, crystallinity of a swollen gel is not always proportional to that of a dried gel.[124] As a result, any change in the crystallinity degree could not be appropriately assigned to the presence of starch, as it would be unclear what role a particular drying process may have played. X-Ray Diffraction was then pursued to study the crystalline nature of the hydrogel samples in their as-prepared state, as seen in Figure 15A.

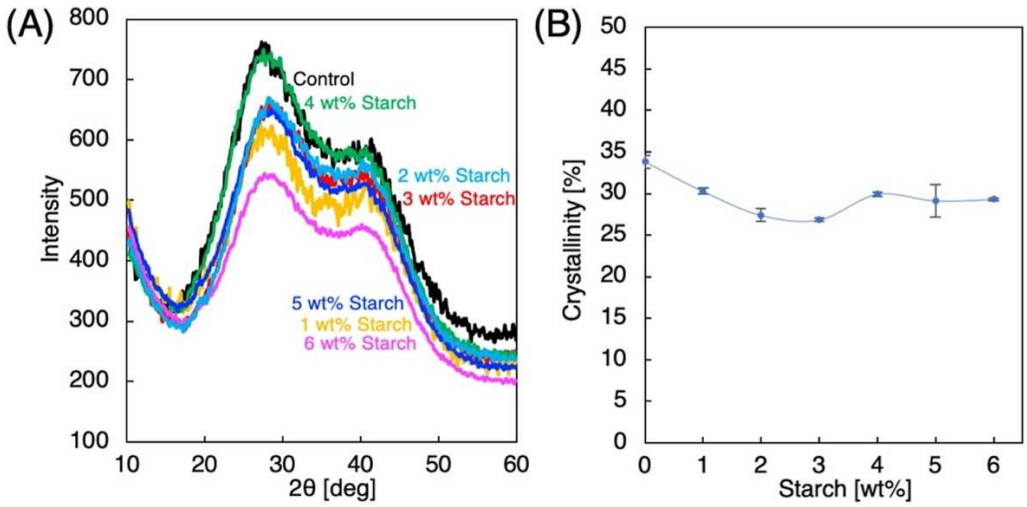

Figure 15: (A) XRD scans of PVA-starch samples. (B) Crystallinity of PVA-starch samples obtained from DSC measurements. Samples were initially prepared via ASTM D638-14 Type V shape before being cut up for XRD and DSC analysis; data depict mean crystallinity value ± standard deviation

The intensity of the diffraction pattern for the samples can be correlated to the presence of microcrystalline domains that formed in the network structure.[125] Dried out PVA gives way to sharp diffraction peak that can occur anywhere from 18-21° for a $10\bar{1}$ reflection of a typical PVA crystalline domain even though this peak was difficult to isolate from Figure 15A.[114] Prior work has shown the importance of the freezing-thawing process in forming enhanced microcrystalline domains.[53,120,126] However, XRD measurements were used in this study in a qualitative manner due to the highly amorphous nature of the hydrogels.[127] From Figure 15A, the peak area of the control sample and 4 wt% starch sample were similar, but the broad nature of all spectra from XRD measurements made quantitative analysis difficult. For the purposes of using the

diffraction patterns in Figure 15A, the free water in the network structure complicated the reliability of diffraction measurements.[128] An overwhelming majority of the hydrogel was free water in the network structure instead of polymer. Scanning Electron Microscopy (SEM) and Atomic Force Microscopy (AFM) were also not considered due to the risk of samples drying out over the course of a test, which would impact morphology and structure of the hydrogel. These concerns led to the pursuit of a complementary technique that would quantify the crystallinity of the PVA-based hydrogel in its native state.

As established before, the goal of a different quantitative technique would be to analyze the hydrogels in their as-prepared, swollen state. Differential Scanning Calorimetry (DSC) was utilized to analyze the samples in this native state. The PVA-based hydrogels consist of a swollen, amorphous network of PVA molecular chains that are physically crosslinked together with small, highly ordered pockets of PVA known as microcrystallites.[124] These microcrystallite regions develop from the freezing of water at very cold temperatures, giving way to small regions of minimal molecular motion that are highly concentrated with PVA.[129] With the PVA molecular chains in close proximity to one another, crystallite formation begins and it continues to progress during subsequent freezing cyles.[53,126,130] The crystallinity of the hydrogels can be calculated

from the endothermic melting of the PVA crystallites during the heating of a DSC scan.[121] The crystallinity degree ($\chi_{\%}$) of the hydrogels was calculated in Equation 1

$$\chi_{\%} = \frac{\Delta H}{\Delta H^{\circ} \times W_{PVA}} \times 100 \quad (1)$$

where ΔH was calculated as the area under the melting peak, ΔH° is the heat needed to melt a 100% crystalline PVA (138.6 J g^{-1}) , and W_{PVA} is weight fraction of the PVA polymer in the hydrogel sample with respect to deionized water.[38,131,132] Figure 15B provides a view of the trend of crystallinity degree with increasing starch.

The crystallinity degree for the control hydrogel sample was 33.8% in Figure 15B, and it decreased for 1, 2, and 3 wt% starch. This can be attributed to the molecular chains of starch disrupting PVA's ability to pack its molecular chains, which ultimately hinders the process of PVA crystallite formation.[133,134] The hydrogen bonding between the OH groups of starch and the OH groups of PVA prevents chain segment movement to a certain extent,[134] and this effect becomes important for 4 wt % to 6 wt% starch to bring the degree crystallinity slightly back up in Figure 15B. Mirroring a similar trend in monotonic toughness, the molecular chains of PVA can no longer diffuse as freely as before due to the enhanced opportunities for hydrogen bonding with more starch present. Thus, the crystallinity is increased from 3 wt % through 6 wt% starch, where starch brought a mechanical stiffening effect to the samples, as seen in the representative stress-strain curves in Figure 14A.

3.2.6 Fatigue Behavior

With 4 wt% starch having improved monotonic tensile behavior, this sample was selected for further study of its tensile fatigue behavior compared to the control, native PVA sample. This decision was based on the ability to enhance tensile properties without sacrificing ease-of-processing, a category in which cotton flock did not meet expectations. Tensile fatigue testing imparts irreversible damage in a material as a function of reversed loading and unloading cycles.[1] The hydrogel undergoes a cyclic strain of amplitude *E*, and the test counts the numbers of cycles *N* of this applied strain until failure.[1] Collecting this data would lead to the development of an *E-N* curve, otherwise known as a strain-life curve. As a point of clarification, this testing does not entirely occur at stress or strain levels that lead to immediate, catastrophic failure. Rather, it is the development and summation of minor damage at non-catastrophic testing levels (i.e., stresses lower than the ultimate tensile stress and strains lower than the strain at failure).

In the hydrogel research community, cyclic studies that utilize loading and unloading of hydrogels under tensile conditions are important, but they could be improved with 1) systematically varying the applied load or displacement level as well as 2) increasing the number of cycles applied in a test to support the claim that a material is "fatigue resistant" or "anti-fatigue".[6,92,93,95,114,135] If a material is deemed to be

"fatigue resistant", then researchers need a greater number of cycles to validate this claim. As such, it is difficult to assert that a material is "fatigue resistant" or "anti-fatigue" simply because it is tougher or stronger in terms of its monotonic tensile properties. Furthermore, simple tracking of the stress-strain response of a material as a function of cycle number is insufficient if the sample has not failed. The lack of failure for a sample shows that too low of an applied stress or applied strain in cyclic testing conditions was employed, and no true understanding of a material's fatigue resistance as a function of applied load can be understood in this way.

Within the confines of this study, tensile fatigue testing was carried out in a cyclic, displacement-controlled test. Pristine control samples with a custom shape for a soft material to combat sample buckling during testing were tested in monotonic tension. These tensile results were used to establish an average failure strain and its resulting standard deviation. Standard deviation levels from the average were then employed at systematically varying levels to test samples (i.e., one standard deviation below the failure strain was denoted as 1σ). A "runout" sample was considered to last 100,000 cycles without failure. Three control samples were tested using a strain rate of 2.0 s^{-1} at 0.25, 0.5, 1, and 2 standard deviations below the failure strain, respectively. However, it was quickly observed that damage accumulation in the samples was either non-existent or remarkably slow, as almost all samples reached 100,000 cycles without

failure as mentioned in the Mechanical Testing section of Experimental Section. As a result, both control and 4 wt% starch samples were given a sharp notch of a 1, 2, or 3 mm in the gauge section to initiate the growth of a crack in a sample. The use of this crack was to create a damage site that could lead to failure in a sample during fatigue testing. Figure 16 shows the effects of each notch on both the control and 4 wt% starch samples in monotonic tension as compared to their pristine state.

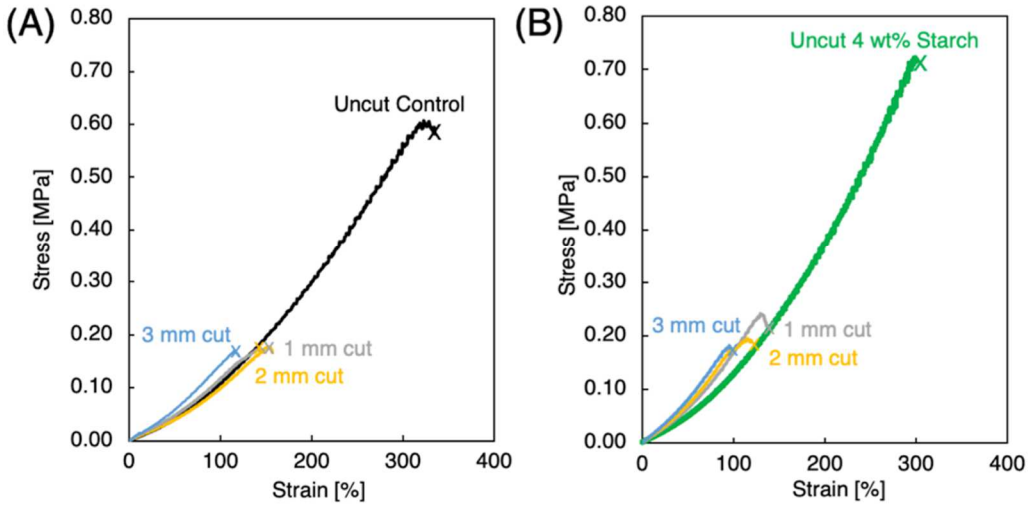

Figure 16: Tensile stress-strain behavior for uncut, 1, 2, and 3 mm cut control samples (A) and 4 wt% starch samples (B) for the customized, thicker fatigue sample shape in both.

These sharply notched hydrogels were tested in monotonic tension in the customized fatigue shape to calculate an average failure strain and subsequent standard deviation levels in a similar manner to the pristine samples. The length of the cut led to a

trend in failure strain (i.e., the longer the cut, the lower the failure strain). Control samples had an average failure strain of 156.78%, 142.81%, and 124.73% for 1 mm, 2 mm, and 3 mm cut samples, respectively. 4 wt% starch samples had an average failure strain of 140.56%, 111.88%, and 92.87% for 1 mm, 2 mm, and 3 mm cut samples, respectively. In terms of average ultimate tensile strength, there was a slight drop from the 1 mm cut samples to the 2 mm and 3 mm samples. The control sample had a 6.2% drop while 4 wt % starch had a 15.0% drop, yet the 2 mm and 3 mm cut samples had extremely similar ultimate tensile strengths for both the control and 4 wt% starch. With the completion of these tests, it was decided that a 2 mm cut would be used to develop the fatigue life curve for both samples due to: 1) the tedious nature of making a 1 mm cut in the gauge section and 2) losing half of the gauge section from a 3 mm cut meant the biggest loss in sample area for testing.

For the fatigue analysis of both the control and 4 wt% starch samples, a strain rate of 2.61 s^{-1} was utilized to retain prolonged tensile loads before buckling of the sample became a dominating effect. In the case of buckling, the sample would spend more time in a compressed state than in a stretched state. In addition, the length of the test was considered with the selection of this strain rate to run 100,000 cycles without prolonged testing periods. The control and 4 wt% starch samples had different monotonic failure strains, which ultimately led to adjusting the testing amplitudes and

frequencies for the applied strain rate to remain constant across both samples. Both the control and 4 wt% starch systems were analyzed with four samples at five different standard deviations levels to make for a total of 20 samples (0.5σ, 1.0σ, 2.0σ, 3.0σ, and 4.0σ). A plot of strain range vs. cycles to failure can be seen in Figure 17 for both the control and 4 wt% starch samples.

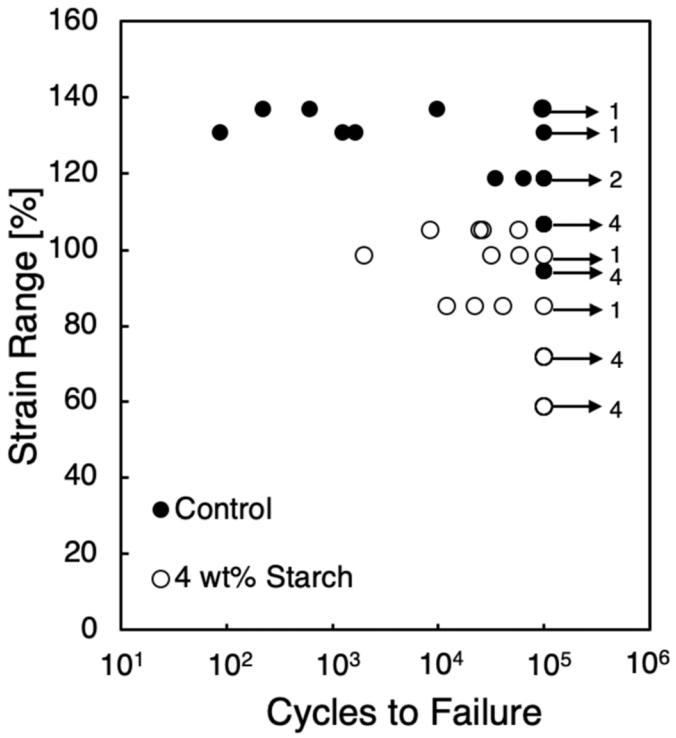

Figure 17: Fatigue data for 2 mm notched control and 4 wt% starch samples based on strain range as a function of cycles to failure. A sample that lasted 100,000 cycles without failure was considered a "runout" sample with an arrow pointing to the right and indicating how many samples had reached this status at a given strain level. Five strain levels for both the control and 4 wt% starch were utilized (0.5σ, 1.0σ, 2.0σ, 3.0σ, and 4.0σ). Once 100,000 cycles were completed, the test was concluded.

As shown in Figure 17, 4 wt% starch had more "runout" samples that lasted 100,000 cycles. In addition, failure was defined as a complete tear of the sample. Some runout samples for both the control and 4 wt% starch incurred damage accumulation to varying degrees with respect to crack growth over the course of 100,000 cycles. In a case of one of the control samples, only a single strand of material was remaining at the end of 100,000 cycles. However, this sample was not considered to be a sample that had failed for the sake of consistency. Future work would need to analyze crack growth rates to more directly compare the samples. To further analyze the results of these fatigue tests, each test was reviewed for the tensile stress range each sample experienced at the median time point of the test. For the purposes of this study, tensile stress range was defined as the maximum tensile stress the sample experienced. With the observation of sample buckling in the hydrogel samples, tensile stresses became an important factor to consider even though strain-controlled loading was employed for the testing.[136] Only the tensile load the sample endured at the median time point of the test was analyzed as a result of the stress relaxation observed in the hydrogels. Thus, these samples were analyzed for their "median life tensile stress range" with regards to the tensile stresses experienced in lieu of the compressive ones. The results of this analysis can be seen in Figure 18 for both the control and 4 wt% starch samples.

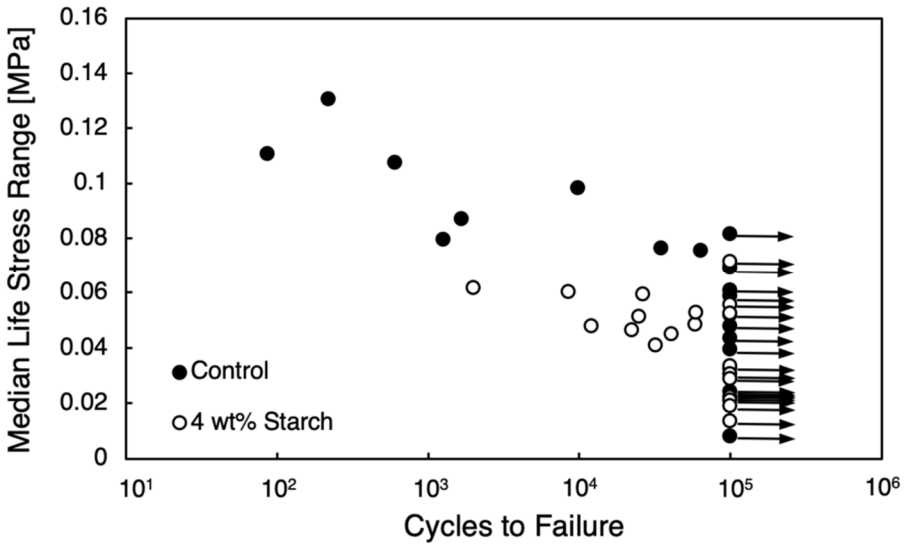

Figure 18: Fatigue data for 2 mm notched control and 4 wt% starch samples based on median life tensile stress range as a function of cycles to failure. A sample that lasted 100,000 cycles without failure was considered a "runout" sample with an arrow pointing to the right, at which point the test was concluded.

We have established a fatigue stress threshold (or fatigue limit) in this work in which a sample would last 100,000 cycles below this threshold without failing. For the control hydrogel sample, that value was 0.061 MPa. For the 4 wt% starch hydrogel sample, that value was 0.033 MPa. All samples were tested with a 2 mm crack to initiate damage accumulation, and the fatigue threshold values presented above are represented with this flaw. Without a flaw the fatigue stress threshold would be higher. Materials researchers have employed crack growth thresholds based on stress intensity factor, although given the large strain deformations experienced here these linear elasticity

formulations would be invalid. Thus, here we have just shown a simple stress-based threshold in the presence of a flaw which represents worst case scenario.

In monotonic tension with the ASTM Type V sample shape, the 4 wt% starch sample brought about an average increase of 43.5% in ultimate tensile strength compared to the control sample. For the uncut, customized fatigue shape in monotonic tension, the 4 wt% starch sample exhibited an average increase of 28.9% in ultimate tensile strength compared to the control sample. For the 2 mm cut, customized fatigue shape in monotonic tension, the 4 wt% starch sample displayed an average increase of 27.8% in ultimate tensile strength compared to the control sample. However, over the range of strengths tested in this particular study, it was fair to determine that these improvements in monotonic properties did not bring about improved fatigue behavior. A closer look at the nominal tensile stress-strain response for some of the conducted tests can be seen in Figure 19.

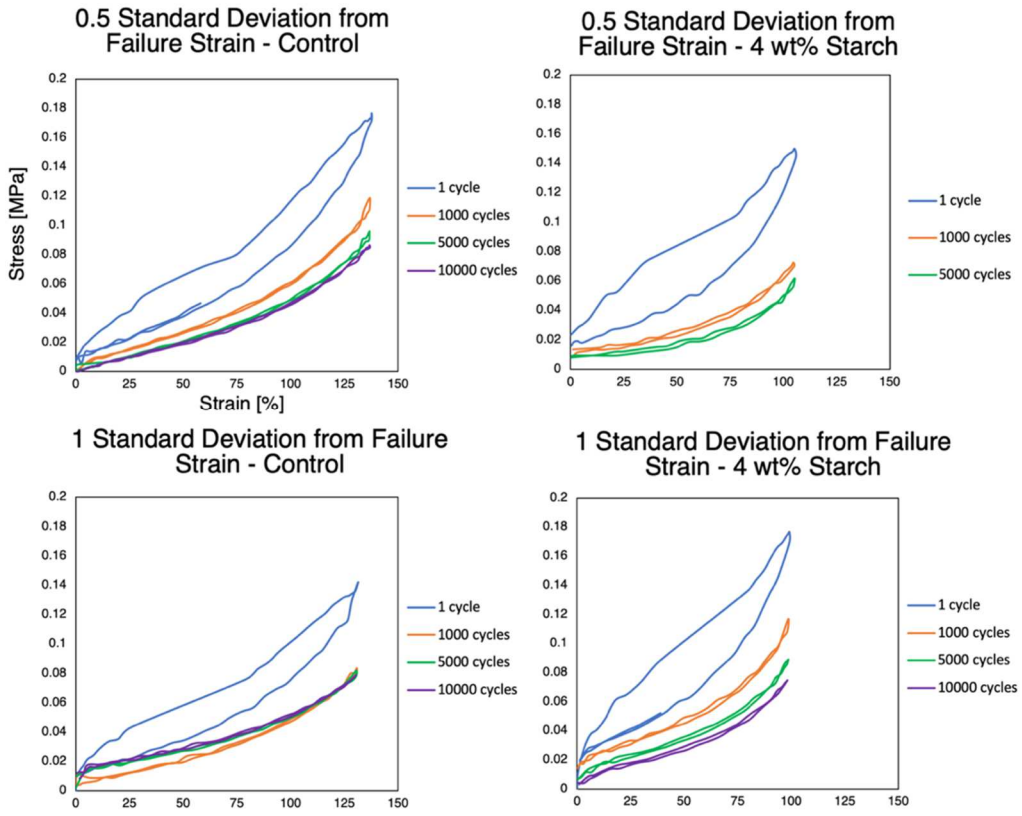

Figure 19: Nominal stress versus strain over cyclic loads for PVA control and 4 wt% starch composite hydrogels at defined strain levels. These strain levels were respectively selected as 0.5 and 1.0 standard deviation from the failure strain for control and 4 wt%

When comparing similar median life tensile stresses from 0.04 MPa to 0.06 MPa in Figure 18, the control system had more runout samples than the 4 wt% starch-based system. In considering this range of stresses when the control and 4 wt% starch systems can be likened to one another, an improvement in the fatigue properties for the 4 wt% starch was not identifiable. Although testing was completed in a strain-controlled manner, analyzing these cyclic tests for their tensile stresses at the median time point

showed that the addition of starch did not lead to samples lasting a greater number of cycles at similar stress levels. With this in mind, it was reasonable to establish that improvements in the monotonic tensile properties for the PVA-based hydrogel did not correlate to superior fatigue behavior with the addition of 4 wt% starch. This result was novel and unexpected, as it was hypothesized that an improvement in monotonic toughness would result in an improvement in fatigue behavior. As a possible explanation for this obtained result, Móczó et al. proposed that the impact of stress concentration increases with particle size in the case of an epoxy composite.[137,138] Due to the large size of the polymers that make up starch,[139] stress concentrations may have been induced to lead to premature failure of the hydrogel.[137] In a similar manner to epoxy resin composites studied in Ferreira et al.,[140] the large molecular structure of amylopectin combined with amylose in the makeup of starch can act as flaws and bulky inhomogeneities for enhanced stress concentration. Thus, the PVA-starch hydrogel is prone to failure before its PVA control counterpart. Further research will be needed to understand if this explanation is sufficient.

For applications such as articular cartilage replacement, this fatigue study illuminated the importance of fully characterizing the impact of hydrogel reinforcement. Often times, researchers seek to make their synthetic hydrogels much stronger in terms of monotonic mechanical properties. This constant pursuit leaves a begging question for

synthetic hydrogels with biomedical applications: Just how strong is strong enough? Unfortunately, this pursuit of continually strengthening hydrogels has created an enormous need in understanding the effects of mechanical reinforcement on long-term mechanical behavior. It has become essential to study the fatigue properties to screen synthetic hydrogels for their suitability in biomedical applications. These synthetic systems require sufficient resistant to damage on a long timescale to be appropriately considered for human use. The fatigue study utilized in this work is crucial to ensure that early failure of a synthetic hydrogel is not due to tensile loads. Otherwise, the hydrogel cannot be employed for long-term use. Although the bio-friendly nature of synthetic hydrogels may be preserved and the strength may be increased through reinforcement techniques, these important adjustments may not always lead to the best long-term behavior, as seen in the case of 4 wt% starch and the control. Ideally, this fatigue analysis created a roadmap for future synthetic hydrogels that seek to be used in biomedical applications such as articular cartilage replacement.

3.3 Conclusion on Tensile Fatigue of Poly(Vinyl Alcohol) Hydrogels with Bio-Friendly Toughening Agents

In conclusion, we have prepared a tough hydrogel composed of poly(vinyl alcohol) and starch that can be studied for its tensile fatigue properties. After carrying out a screening process of 13 bio-friendly additives, starch was selected as the additive

for further mechanical study. With ease in terms of processing, the PVA-starch hydrogel was able to withstand both high stress and high strain in tension in the realm of soft materials. The hydrogen bonding between PVA and starch aided in dissipating mechanical energy for improved toughness. The addition of starch had minimal effects on the ability of the hydrogel to take up water. Crystallinity had a slight uptick with the amount of starch being tuned accordingly for the highest toughness results. In addition, we were able to create a fatigue life curve for both the PVA control sample and the top performing PVA-starch sample. To our knowledge, this study is the first to construct a tensile fatigue life curve for a synthetic hydrogel system.

Poly(vinyl alcohol) hydrogels hold a great deal of promise in the realm of soft materials, especially as a potential cartilage-like structure. Advanced studies for the full range of biomedical applications are needed in order to deeply explore their tissue-like mechanical properties. In addition, different bio-friendly additives as well as a variation in the freezing-thawing cyclic processing can be utilized to tune the elastic properties accordingly. In this work, we set out to characterize the fatigue behavior of double-network PVA-based hydrogels. Improvements in monotonic toughness were observed through bio-friendly additives, and the swelling ratio of the top performing additive samples was not significantly impacted. A trend between enhanced monotonic tensile behavior and crystallinity could be observed with the top performing additive, starch.

Pristine samples could not be used for tensile fatigue testing due to the lack of damage accumulation in the samples. The shape of the prepared hydrogels had to be adjusted and a defect of a specified length in the gauge section were used to generate fatigue analysis. Hydrogel tensile specimens with a crack of 2 mm were employed to generate the strain range curve and subsequent median life tensile stress range curve. As a result of these tests, it was concluded that the addition of starch to the control sample did not bring about an identifiable improvement to the fatigue behavior. Thus, the central hypothesis of this work was only partially correct: mechanical improvements were observed for monotonic behavior but not fatigue behavior. As the first fatigue analysis of its kind for synthetic hydrogels, the intention of this study was to design a pathway for future tensile studies of synthetic hydrogel systems that undergo an improvement in monotonic properties.

With the successes discovered in this PVA-based hydrogel, this dissertation will continue to highlight basic structure-property relationships for hydrogels studied for fatigue behavior in tension. The hypothesis of this work was using biofriendly agents to improve monotonic toughness to enhance fatigue behavior. Though part of this hypothesis did not come to fruition in the case of starch, the work in Chapter 4 opens up continued study of systems that show long-term mechanical promise based on monotonic testing. In identifying a different system and carrying out similar mechanical

analysis, it will be possible to conclude starch's behavior as an anomaly to the hypothesis or a repeated observation.

3.4 Methods and Materials

3.4.1 PVA-based Hydrogel Fabrication

The materials in this study were used without further purification and purchased from Sigma-Aldrich, St. Louis, MO, USA, unless otherwise denoted. These materials include poly(vinyl alcohol) (PVA, molecular weight (M_w) 85,000 – 124,000 Da, 99+% hydrolyzed), starch powder, 2-Hydroxy-4'-(2-hydroxyethoxy)-2-methylpropiophenone (Irgacure 2959), cyanuric acid, folic acid, d-sorbitol, maltitol, k-carrageenan, chitosan, cellulose powder, cellulose fibers, hydroxyapatite, agar powder (Alfa Aesar), xanthan gum, and cotton flock (Freeman Manufacturing and Supply Company, Avon, OH, USA). PEGDMA 1,000 g mol^{-1}, PEGDMA 8,000 g mol^{-1}, and PEGDMA 20,000 g mol^{-1} were all acquired from Polysciences, Inc. Deionized water used in this study was acquired from a Pureflow Inc. Portable Exchange Type II system.

For preparation of control samples, the necessary amount of PVA was combined with deionized water in a 100 mL round bottom flask to create a 16 wt% mixture with the weight of PVA based off the weight of deionized water. This mixture was capped with a rubber septum, and it was heated and stirred for a minimum of three hours at

95°C in an oil bath until the PVA was fully dissolved. In cases where a bio-friendly additive was used, the required amount of bio-friendly additive was based on the weight of PVA. For example, a 4 wt% Agar sample with PVA (9.518 g) and deionized water (50 mL) would utilize Agar powder (0.381 g). The bio-friendly additive would be combined with PVA and deionized water at the beginning. The process of stirring and heating began once the round bottom flask was secured with the rubber septum and flask clamp. After a minimum period of three hours, the resulting solution was then removed from the 95°C oil bath and sonicated for 30 seconds to remove any surface bubbles. The solution was then poured into customized stainless-steel molds with slots that matched the dimensions of an ASTM D638-14 Type V shape for monotonic tension testing and other characterization techniques.[141] Control samples were composed of PVA dissolved in deionized water with no selected additive present. Fatigue tension testing samples were prepared from a customized stainless-steel mold with a thicker gauge section. Parafilm was placed and taped over the top of the material to create a seal, and a stainless-steel lid was then placed on top. The molds were frozen at -23°C for 1.5 hours followed by 7 hours of thawing at 20°C. Once this initial freeze-thawing cycle was complete, another cycle was employed. The molds were again frozen at -23°C for 1.5 hours followed by 7 hours of thawing at 20°C. At this point, the samples could be removed from the stainless-steel molds using a spatula and analyzed for their

properties. Samples could be stored in a 15 mL centrifuge tube with deionized water (11 mL) until tensile testing had occurred. For samples with a small cut of a specific length in the gauge section, a razor blade was used to introduce this defect.

For PEGDMA-based samples, a given molecular weight of 1,000, 8,000, or 20,000 g mol^{-1}, respectively, was selected (16 g) and combined with deionized water (84 mL) and Irgacure 2959 (0.016 g) in a 200 mL glass jar. A Teflon stir bar was then added to the jar and the mixture was stirred at 300 RPM for 1 hour until homogeneous. The solution was then transferred to a Teflon mold with slots that matched the dimensions of the custom fatigue tensile specimen. The mold was placed inside a Dymax ECE 5000 Series UV Light-Curing Flood Lamp System. Samples were then cured for 3 minutes, at which point they were easily removable from the Teflon mold and placed into a 50 mL centrifuge tube filled with deionized water (30 mL) to prevent drying out until tensile testing.

3.4.2 Mechanical Testing Protocol

All tensile measurements were performed on an Instron 1321 (Instron, Norwood, MA, USA) instrument, and monotonic tension samples were tested at a rate of 15 mm min^{-1}. Monotonic samples were prepared from an ASTM D638-14 Type V shape, while fatigue samples were prepared from a customized shape due to sample buckling while

testing. An extensometer was used to determine an experimental effective length for both monotonic and fatigue samples on a TestResources 830 (TestResources, Shakopee, MN, USA) load frame with a 50-lb load cell. All monotonic mechanical data was obtained from corresponding individual stress-strain curves. Fatigue tensile testing occurred in a tap water bath at 37°C to prevent samples from drying out during prolonged tests. We ran three fatigue tests of control samples with a strain rate of 2.0 s^{-1} at 0.25, 0.5, 1, and 2 standard deviations below the failure strain, respectively. All but one of these samples lasted 100,000 cycles without failing, and this sample failed on the first cycle due to a possible bubble defect in the gauge section. As a result, we chose to use cuts of a controlled length (1 mm, 2 mm, and 3 mm) in the gauge section with the goal of reducing variability and establishing an idea of tensile strain range vs. cycles to failure for both the control sample and the top performing additive.

3.4.3 PVA-based Hydrogel Swelling Study

The water uptake of the top performing PVA hydrogels was measured by recording the mass variation of the hydrogels after swelling in a 15 mL centrifuge tube of deionized water (12 mL) at room temperature for 24 hours. Samples were prepared in the ASTM D638-14 Type V shape. Excess water on the external surface of the hydrogels was removed by lightly tapping the samples on a piece of filter paper. The samples were

then weighed and subsequently dried to constant weight at 80°C for 14 hours in a Yamato drying oven. The ratio of the swollen weight to the dry weight was used to calculate a swelling ratio, q, below. The swelling ratio (q) of the hydrogel samples was defined as the ratio of the weight of swollen sample (W_s, swollen in deionized water for 24 hours) divided by the weight of the dried-out sample (W_d, dried out at 80°C for 14 hours to constant weight) in Equation 2.

$$q = \frac{W_s}{W_d} \quad (2)$$

Each reported swelling ratio is an average of at least seven parallel measurements.

3.4.4 X-Ray Diffraction of Hydrogel Samples

PVA-starch DN hydrogel samples were also characterized via XRD measurements on a PANalytical X'Pert PRO MRD HR XRD System (Malvern Panalytical Inc., Westborough, MA, USA). Samples were prepared in the ASTM D638-14 Type V shape. The prefix module selected was Mirror Cu W/Si (parabolic MRD) with a K-alpha wavelength. The following parameters were used for measurement of hydrogel samples via XRD: Generic Configuration with a start angle of 10°, end angle of 60°, step size of 0.05°, time per step of 1 second, scan speed of 0.05°s^{-1}, and number of steps at 1,000. XRD scans were repeated for a minimum of three times for each sample, and an average of the resulting scans was reported.

3.4.5 Differential Scanning Calorimetry for Crystallinity

Control and PVA-starch DN hydrogel samples were evaluated for their crystallinity via DSC measurements on a TA Instruments Discovery DSC (TA Instruments, New Castle, DE, USA). Samples were prepared in the ASTM D638-14 Type V shape. For each analysis, the hydrogel sample (about 5 mg) was placed into a hermetically sealed aluminum pan. The following protocol for DSC measurements was used: equilibrate to 40°C, isotherm for 1 min, ramp 10°C/min to 250°C, isotherm for 3 min, ramp 10°C/min to 40°C, isotherm for 3 min, ramp 10°C/min to 250°C, isotherm for 3 min, and ramp 10°C/min to 40°C. DSC scans were repeated, and an average was taken between the two measurements.

Chapter 4. A Synthetic Hydrogel Composite with the Mechanical Behavior and Durability of Cartilage

The primary focus of Chapter 3 was centered around PVA as a material system for the creation of a hydrogel. The research in Chapter 3 successfully established a tough, bio-friendly double-network hydrogel via freezing-thawing cyclic processing. Several interesting discoveries encouraged further examination in PVA as a polymer of interest for use in synthetic hydrogels. In brief, these findings included an improvement in the monotonic tensile properties when starch was present, an uptick in crystallinity with gradual additions of starch, and a lack of improvement in the tensile fatigue properties when starch was introduced. The work in Chapter 4 will aim to build on the key findings of Chapter 3 through different components and processing techniques. The central hypothesis of this work was examining the impact of modification to processing techniques and addition of tough composite additives to ultimately improve fatigue properties.

4.1 Introduction to Heavy Load-Bearing Cartilage Mimic

Although PVA as a double-network hydrogel has suitable properties as an articular cartilage replacement in the MTP joint, there still exists a shortcoming in the strength of the hydrogel for larger weight-bearing applications of other joints. Damage to cartilage in these load-heavy joints often results in worsened pain and decreased

range of motion for the patient. To make matters worse, the current state-of-the-art for cartilage repair/replacement involves a few expensive techniques such as stimulation with the use of bone marrow, transplantation from another region of cartilage, and implantation of cartilage cells to kickstart growth that have amplified frequencies of failure.[142–145] These techniques often bring about extensive rehabilitation and prove minimal efficacy in older patient populations.[146,147] In addition to these techniques, the use of metal alloys such as cobalt-chromium as well as ultra-high-molecular-weight polyethylene have been tried but often lead to areas of stress concentration from stiffness differences as compared to native tissue.[148,149] As a result, the abnormal stresses brought on from these materials can lead to even faster joint degeneration. To avoid increased failure rates for synthetic hydrogels used in these types of applications, it has become necessary to create a hydrogel that matches the mechanical strength, lubrication, and wear properties of the cartilage for a particular load-bearing joint. In doing so, the patient would have a reduction in pain, a shortened recovery time, and a longer lasting hydrogel that would not require multiple removals and subsequent implantations. With issues of properly assimilating the techniques mentioned above, the completed work in this section sought to understand mechanical failure of cartilage-like materials in lieu of integration-related concerns.

The Food and Drug Administration's approval of PVA to treat osteoarthritis in the first MTP joint marked a major step for the use of hydrogels in load-bearing

joints.[150] An estimated 30 million U.S. adults (or 13.4% of the adult population) endure osteoarthritic complications in which the knee is most commonly impacted from damage to articular cartilage.[151] Furthermore, an anticipated 78 million U.S. adults will suffer from arthritic conditions by 2040, as most of these issues coming from osteoarthritis lead to a higher prevalence in older adults with an aging U.S. population.[152] Unfortunately, the proverbial "line in the sand" was drawn for these PVA hydrogels due to their inability to match the compressive and tensile strength of other types of cartilage in joints that experience severe mechanical conditions, such as the knee.[153–155] Even though the MTP joint can withstand up to 119% of a person's body weight while walking, the knee can bear up to 400% of a person's body weight.[156,157] In addition, the compressive strength (~10-20 MPa) and tensile strength (~20 MPa) of knee cartilage extend beyond the realm of FDA-approved hydrogels with PVA as the sole polymeric component.[35,155,158,159] The large deformation and lower compressive modulus of a PVA-only hydrogel suggest it would transfer stress to surrounding tissue and bone if used in heavy-loading joint like the knee.[160]

With this challenge in view, scientists turned to a variety of candidates to improve the tensile and compressive properties of hydrogels. One such material included the use of bacterial cellulose to improve the tensile strength and tensile modulus of hydrogels.[161,162] Other researchers have focused efforts on improving the compressive properties on hydrogels through nanoparticle reinforcements.[163,164] With

the advances in these adjustments to the composition of a hydrogel, there exists a trade-off between improving either the tensile or compressive properties, but not both. In this manner, a unique opportunity has presented itself to synthesize a hydrogel that matches the tensile and compressive properties of cartilage in the knee. Figure 20 highlights progress in the realm of improving mechanical behavior of synthetic hydrogels as well as the results of the work to be discussed in the remaining parts of Chapter 4 of this document.

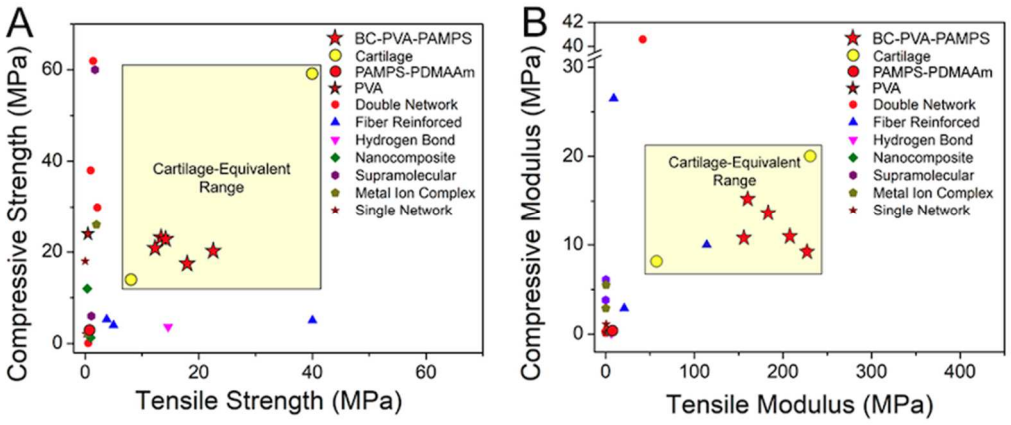

Figure 20: A plot of the compressive vs. tensile (A) strength and (B) modulus for BC-PVA-PAMPS (this work) and other strong hydrogels.

Although there have been considerable advances in improving the tensile and compressive strength of hydrogels, Figure 20 highlights that no prior hydrogel matches both the tensile and compressive strength of cartilage. One such example includes bacterial cellulose bringing the tensile strength of a polyacrylamide hydrogel up to 41

MPa, but its compressive strength of 5.1 MPa fell short of native cartilage.[161] Another system utilized Laponite, a synthetic layered silicate, to be added to an existing double network hydrogel to improve its compressive strength to 61 MPa; however, its tensile strength registered at a much lower 1.4 MPa.[165] With respect to the data of Figure 20 and references utilized, Table 2 provides the varying compositions as well as tensile and compressive results. Both strength and modulus in tension and compression were compared across of variety of hydrogel systems.

Table 2: Mechanical properties of hydrogel created in Chapter 4 of this document and previously published materials.

Composition	Tensile Strength (MPa)	Tensile Modulus (MPa)	Compressive Strength (MPa)	Compressive Modulus (MPa)	Reference number
BC-PVA-PAMPS (22.1%-40%-146kDa- 30%-60 mM)[a]	*13.4*	*155*	*23.0*	*10.8*	This Work
BC-PVA-PAMPS (22.1%-40%-146kDa- 20%-60 mM)[a]	*22.6*	*158*	*20.0*	*15.2*	
BC-PVA-PAMPS (22.1%-40%-146kDa- 30%-40 mM)[a]	*18.0*	*181*	*17.3*	*13.7*	
BC-PVA-PAMPS (22.1%-40%-146kDa- 30%-20 mM)[a]	*12.3*	*227*	*20.6*	*9.49*	
BC-PVA-PAMPS (22.1%-40%-146kDa- 30%-0 mM)[a]	*14.1*	*206*	*22.7*	*10.9*	
Human cartilage	8.1-40	58-228	14-59	8.1-20.1	[154,155,166]
PVA	0.35[a]	0.14[a]	*>24*	0.31-0.80	[160]
PAMPS-PDMAAm	0.49[a]	0.96[a]	3.1	0.2	[167]
PVA-PAMPS-PAAm	0.55	0.4	0.06	0.25	[168]
Agar-PAAm	1	0.08	38	0.123	[169]
3D printed PAMPS-PAAm	1.41	1.01	*61.9*	0.44	[165]
Polyaramid nanofiber-PVA	5	9.1	4	26.5	[170]

BC-PAAm	*40*	*114*	5.1	*10*	[161]
BC-gelatin	3.8	21	5.3	2.9	[167]
PVA-Agarose	*14.6*	6.38	3.66	0.09	[83]
PVA-Fe-alginate-PAAm	0.5	0.15	2.25	2.89	[171]
PVA-CPBA-Ca	2	0.5	*26*	5.5	[172]
PVA-HA/PAA	0.98	3.71	1.3	0.3	[173]
Tetra-PEG	0.032	0.008	*18*	0.16	[174]
Chitosan-gelatin-multivalent sodium phytate	1.75	0.25	*60*	6.1	[175]
PVDT-PEGDA	1.1	0.12	6	3.81	[80]
CNC-PA-PAAm	*16.5* 4.4	232.4 40.6	*31.1* *21.2*	65.4 41.8	[176]
PVA-HA/HACC	3.05	0.7	*40.15*	0.88	[177]
Peptide-Zn^{2+}	3.02	0.27	1.0	0.22	[178]
3D printed PCL scaffold-PVA	4.41	9.53	3	1.2	[179]
PVA-CS	4.02	2.07	*18*	1.5	[180]
K-CG-PAA-Fe^{3+}	2.7	1.17	*26.5*	1.2	[181]

(a) BC-PVA-PAMPS hydrogels with a formula of X wt. % BC, Y wt. % PVA, a PVA molecular weight of Z kDa, M wt.% PAMPS and N mM MBAA was denoted as BC-PVA-PAMPS (X%- Y%-Z kDa-M%-N mM).

(b)Tensile strength and modulus of PVA and PAMPS-PDMAAm were tested as described in Section 4.4 Materials and Methods.

(c) Abbreviations used in this table: BC: bacterial cellulose; PVA: Poly(vinyl alcohol); PAMPS: poly(2-acrylamido-2-methyl-1-propanesulfonic acid sodium salt); PDMAAm: poly(dimethylacrylamide); PAAm: polyacrylamide; CPBA: 4-carboxyphenylboronic acid; HA: hydroxyapatite; PAA: poly(acrylic acid); Tetra-PEG: Tetra-polyethylene glycol; PVDT: poly(2- vinyl-4,6-diamino-1,3,5-triazine); PEGDA: polyethylene glycol diacrylate; CNC: cellulose nanocrystal, PA: phenyl acrylate; HA: hydroxyapatite, HACC: 2-hydroxypropyltrimethyl ammonium chloride chitosan, PCL: polycaprolactone, CS: chitosan, K-CG: K-carrageenan

(d) With the exception of PVA and PAMPS-PDMAAm, on which we performed tensile tests ourselves, this table is limited to publications that report all four metrics, i.e., strength and modulus in tension and compression.

(e) The metrics that fall in the cartilage equivalent range in *italics*.

The work in this section set out to utilize biomimetic design strategies to create a hydrogel that matches these properties of cartilage for a higher load-bearing application. Ultimately, it was the goal of this work to study a hydrogel for its fatigue tensile properties that achieved the strength and modulus of cartilage in tension and compression.

The tensile fatigue testing conducted in this work will lead to a direct comparison with the work completed in Chapter 3. The improvement in monotonic mechanical behavior for this system and the system in Chapter 3 will show if persistently toughening hydrogels brings about an improvement in long-term mechanical behavior. No such hydrogel that meets or surpasses the properties of cartilage in heavy load-bearing joints has been studied for its tensile fatigue properties.

4.2 Design of Fiber-Reinforced Double-Network Hydrogel

Although the use of fibers for reinforcement does present some limitations in prior discussing of this document, their application in a rational design strategy must not be discounted. Fibers may be included in a hydrogel's system to ensure a sufficient mimic of the properties of cartilage with what is readily available synthetically. Given that nature utilizes collagen fibers for higher sustained tensile loads for cartilage, the use of fibers in a synthetic system may prove to be more beneficial than problematic. Cartilage equivalent properties can be mimicked in taking a closer look at the structure

and synergy that exists between the components of cartilage. Articular cartilage is primarily composed of water (60-85% by weight), with collagen fibers of diameter ~100 nm consisting of ~15-22% all components, and negatively charged aggrecan making up ~4-7%.[182–184] Nature has successfully utilized the combination of these materials to work in harmony for the favorable mechanical behavior of articular cartilage.

In terms of the tensile behavior, the collagen fiber network provides cartilage with a mechanism to attain its high tensile strength.[182] As for the compressive properties, a brush-like molecule known as aggrecan contains negatively-charged sulfate groups from glycosaminoglycan chains.[185,186] In combination with hyaluronan, aggrecan forms large aggregates to aid with higher sustained compressive loads through a balance of osmotic pressure.[183–185,187–193] Aggrecan also participates in the dissipation of mechanical energy in cartilage by adding to the drag that water experiences as it moves in the cartilage matrix.[187] In this way, it can further aid cartilage with absorbing shocks and dampening vibrations.[188,194]

With this blueprint in mind, the process of selecting materials to create a cartilage-like hydrogel began. Unfortunately, the high failure rate of decellularized allografts from degradation in the human body led to the exclusion of collagen in design of the hydrogel.[195] As a result, bacterial cellulose was selected as the nanofiber network to replace the favorable tensile behavior of collagen. Bacterial cellulose is biocompatible, and it is comprised of a cellulose fiber network that the human body is incapable of

enzymatically degrading.[196–200] Furthermore, bacterial cellulose can be swelled in water to mimic the high-water content in articular cartilage. The second network in the form of a polyvinyl alcohol (PVA) hydrogel was interwoven into the existing bacterial cellulose network to contribute an energy dissipation mechanism and elastic restoring force.[201–203] The PVA network can act as a "shock absorption" network to dissipate energy and prevent areas of high stress concentration in the hydrogel.[90] In addition, the polyvinyl alcohol chains were able to help the BC nanofibers with sharing mechanical load, thus improving the tensile strength of the overall hydrogel.[35,170,204] A poly(2-acrylamido-2-methylpropyl sulfonic acid sodium salt) (PAMPS) network was also incorporated into the hydrogel to improve the compressive strength of the overall hydrogel by mimicking the negative charge of the sulfate groups of aggrecan in cartilage.[188,194] In turn, the negatively charged groups bring about osmotic pressure that swells cartilage and aids its compressive strength. The graphic in Figure 21 encapsulates the composition of the proposed hydrogel system as compared to that of cartilage.

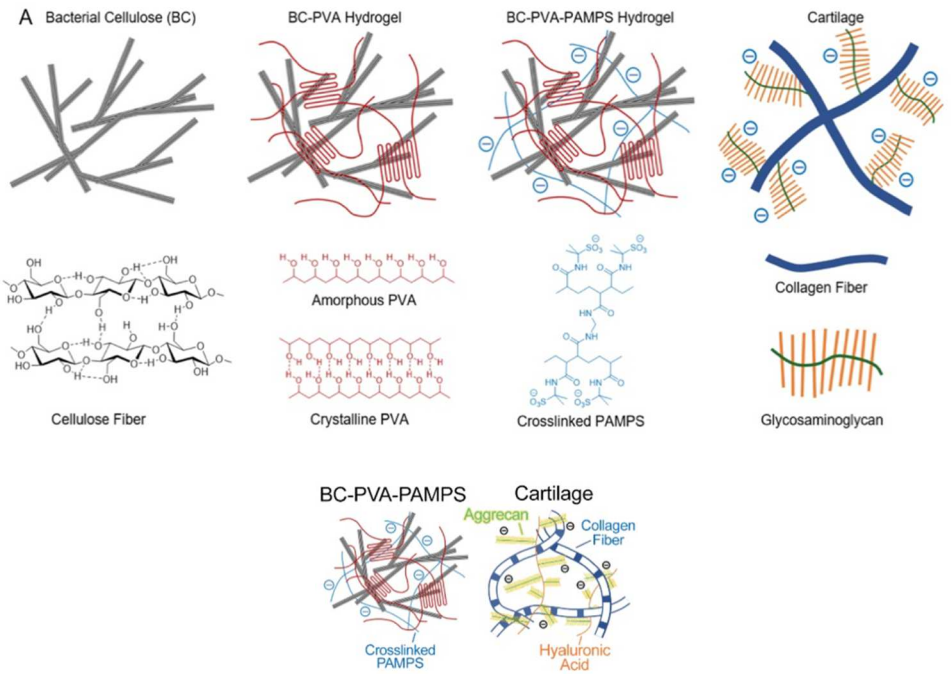

Figure 21: Composition of fiber reinforced double-network hydrogel as compared to cartilage. In addition, schematic comparison of structure of BC-PVA-PAMPS hydrogel as compared to that of cartilage

This system would require a delicate balance between the components to not only achieve cartilage-equivalent tensile properties but cartilage-equivalent compressive properties as well. A brief view of the synthetic route to create this hydrogel system can be seen in Figure 22 for a step-by-step look at the manufacturing process.

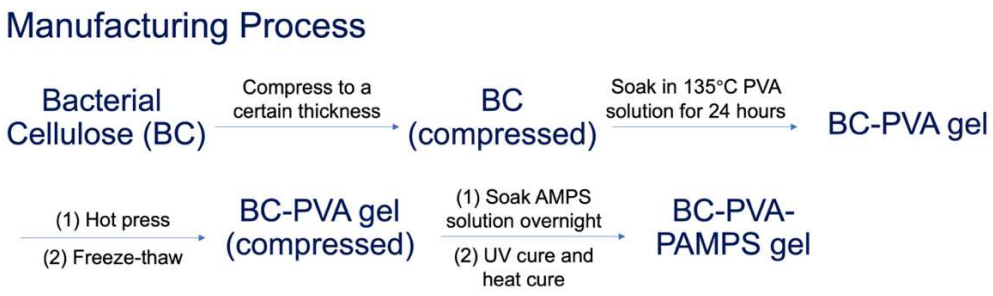

Figure 22: Manufacturing process of BC-PVA-PAMPS hydrogel

The following manufacturing process was used for a hydrogel of the following composition: 22.1 wt% BC, 40 wt% PVA (molecular weight: 146 000 g mol^{-1}), 30 wt% PAMPS, and 60 x 10^{-3} M MBAA. First, a piece of BC was pressed to a controlled thickness, typically 0.5 mm, by using spacers between 2 metal plates. Next, the pressed BC was soaked in an aqueous solution of 40 wt% PVA (molecular weight of 146 000 g mol^{-1}) at 135°C for 24 hours to diffuse the PVA solution into the BC. The BC-PVA gel was then frozen at -78°C for 30 minutes and thawed to room temperature to physically crosslink the PVA network.[204] The BC-PVA hydrogel was then soaked in a solution of 30 wt% AMPS, 60 x 10^{-3} M MBAA, 50 x 10^{-3} M I2959 and 0.5 mg mL^{-1} potassium persulfate (KPS) solution for 24 hours. The hydrogel was cured with a UV transilluminator (VWR) for 15 minutes on each side, and then heat cured in an oven at 60°C for 8 hours to ensure even and complete curing. The resulting BC-PVA-PAMPS hydrogel was stored in 0.15 M phosphate buffered saline (PBS) solution for at least 24 hours before further characterization. The next section will unveil the characterization results of different compositions to understand the impact on mechanical behavior.

These results influenced the selection of a composition for advanced study of tensile fatigue behavior.

4.3 Characterization of Fiber-Reinforced Double-Network Hydrogel

Principally, this work began with characterizing a variety of combinations of the components. Particular attention was given to matching the tensile strength of cartilage first, and then taking these combinations for study of compressive properties. This is due to tensile tests creating clear failure in a sample, whereas determining compressive failure is more arbitrary in nature. We first set out to understand the synergy among the composition of the hydrogel in terms of the anticipated role each material would play. Figure 23 provides the (A) tensile and (B) compressive stress-strain curves for BC-PVA, BC-PAMPS, and BC-PVA-PAMPS hydrogels. These results aided in narrowing down the range of possible combinations to achieve cartilage-equivalent properties, as shaded in light blue in Figure 23.

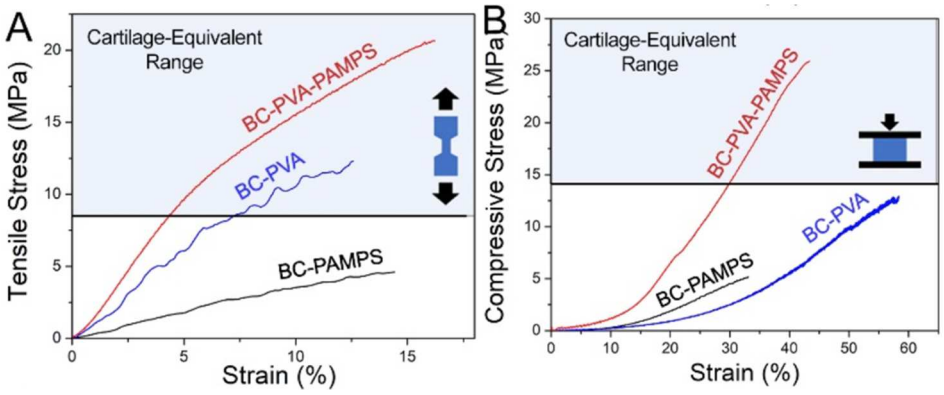

Figure 23: (A) Tensile and (B) compressive stress-strain curves for BC-PVA, BC-PAMPS, and BC-PVA-PAMPS hydrogels

As shown in Figure 23A, a BC-PAMPS hydrogel achieved a tensile strength of 4.6 MPa. However, the requirement for cartilage-equivalent properties set the baseline at 8.1 MPa. A BC-PVA-PAMPS and a BC-PVA were able to achieve tensile strengths of 20.7 MPa and 12.3 MPa, respectively, which safely put them into the range of cartilage-equivalent tensile strengths. As shown in Figure 23B, the BC-PAMPS and BC-PVA hydrogel failed to meet the baseline of compressive strength of cartilage. In addition, the compressive modulus of the BC-PVA hydrogel was 6.2 MPa, which fell lower than the compressive modulus of cartilage (~10-20 MPa) as the sample was much more ductile.[155] The higher compressive modulus of the BC-PAMPS hydrogel had a shortcoming in the form of brittleness. However, the incorporation of the PAMPS network into the existing BC-PVA framework to create the BC-PVA-PAMPS hydrogel brought the compressive modulus and strength to be within acceptable values for the cartilage-equivalent threshold. It must be noted that the tensile strain at failure of

cartilage falls in the range of 20-30%,[205] which happens to be barely higher than the 17% tensile strain at failure of the BC-PVA-PAMPS hydrogel. In comparing the closeness of these results, the strain at failure for BC-PVA-PAMPS is similar to cartilage. The PVA-PAMPS hydrogel, on the other hand, had a tensile strain at failure of 66%. The separation of these values gives support to the idea that BC lowers the strain at failure. Previous study of bacterial cellulose fiber show that it has a fracture strain <25%.[206] As a result, the ductility of BC limits the ductility of BC-reinforced hydrogels.

To discover the boundary conditions for the various combinations of components for cartilage-like properties, we performed thirty mechanical tests with different molecular weights of PVA and different concentrations of BC, PVA, AMPS, and MBAA cross-linker. These tests aimed to quantify the relationship between the hydrogel's mechanical properties and these variables. The outcome of this screening process would bring about the selection of an ideal composition that could balance the baseline tensile and compressive properties to match cartilage. The results of these mechanical tests are shown in Figure 24.

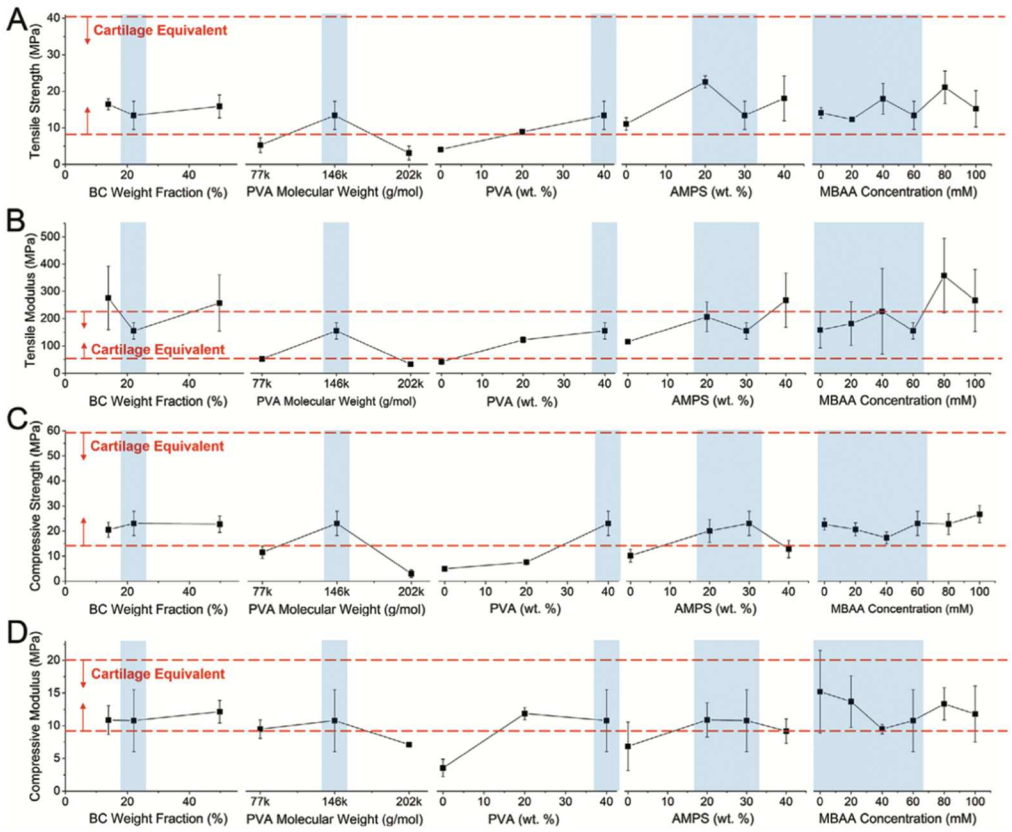

Figure 24: Tensile strength (A), tensile modulus (B), compressive strength (C), and compressive modulus (D) of BC-PVA-PAMPS hydrogels with different formulations. The concentrations of BC, PVA, PAMPS, MBAA are 20 wt%, 40 wt%, and 60 x 10^{-3} M and the molecular weight of PVA was 146 000 g mol^{-1} unless otherwise indicated. The range of compositions that corresponds to cartilage-equivalent hydrogels are denoted with blue shading.

A list of the hydrogel compositions tested in Figure 24, including their water content and swelling ratios, is provided in Table 3. The swelling ratio was defined as the ratio of the mass of a fully swollen hydrogel to the mass of a fully dried hydrogel.

Table 3: The varying hydrogel compositions that were tested for the creation of Figure 24.

Initial BC Weight Fraction (wt.%)	PVA Concentration (wt.%)	PVA Molecular Weight (g mol-1)	AMPS Concentration (wt.%)	MBAA Concentration (mM)	Swelling ratio[a]	Final Water Content (wt. %)	Composition
22.1%	40%	146k	30%	60	2.46	59.4	BC-PVA-PAMPS
0	40%	146k	30%	60	2.69	62.8	PVA-PAMPS
22.1%	0%	146k	30%	60	3.79	73.6	BC-PAMPS
22.1%	40%	146k	0%	60	5.13	80.5	BC-PVA
22.1%	40%	146k	30%	0	2.2	55.2	BC-PVA-PAMPS
13.9%	40%	146k	30%	60	2.39	58.1	BC-PVA-PAMPS
49.8%	40%	146k	30%	60	5.29	81.1	BC-PVA-PAMPS
22.1%	20%	146k	30%	60	2.77	63.9	BC-PVA-PAMPS
22.1%	40%	77k	30%	60	3.57	72.0	BC-PVA-PAMPS
22.1%	40%	202k	30%	60	4.42	77.4	BC-PVA-PAMPS
22.1%	40%	146k	30%	20	2.30	56.5	BC-PVA-PAMPS
22.1%	40%	146k	30%	40	2.25	55.5	BC-PVA-PAMPS
22.1%	40%	146k	30%	80	2.07	51.8	BC-PVA-PAMPS
22.1%	40%	146k	30%	100	2.19	54.4	BC-PVA-PAMPS
22.1%	40%	146k	20%	60	1.99	49.7	BC-PVA-PAMPS
22.1%	40%	146k	40%	60	2.21	54.8	BC-PVA-PAMPS

In first narrowing down the weight fraction of bacterial cellulose, all three wt.% tested (13.9%, 22.1%, and 49.8%) matched the tensile and compressive strength requirements for cartilage. However, only 22.1% achieved cartilage-equivalent tensile modulus. Next, the PVA network was screened based on molecular weights of 77 000, 146 000, and 202 000 g mol^{-1}. Using 146 000 g mol^{-1} for the molecular weight of PVA brought the tensile and compressive strengths to be within the range for cartilage-equivalent properties. With the increase from 77 000 g mol^{-1} to 146 000 g mol^{-1}, the polymer chain entanglement and hydrogen bonding of the PVA network improved, leading to an enhanced strength.[204,207] Bringing the molecular weight up to 202 000 g mol^{-1} made it difficult to achieve to full infiltration with the bacterial cellulose network, which led to a decrease in the true concentration of PVA within the bacterial cellulose sheet. Ultimately, this brought about a decrease in strength to fall below the lower bound for cartilage-equivalent tensile and compressive properties.

With no PVA present, both modulus and strength for tension and compression fell below the minimum for cartilage-equivalent properties. However, an increase in tensile and compressive strength was observed as the PVA concentration increased from 20 wt.% to 40 wt.%. The only PVA concentration that achieved sufficient compressive strength was 40 wt.%. Attempts to utilize even higher PVA concentrations were unsuccessful, as these concentrations did not fully dissolve at 135°C. As a result, the 40 wt.% concentration was close to the upper limit of the amount of PVA that can be infiltrated into the hydrogel. In terms of improving the tensile and compressive moduli, efforts turned to utilizing PAMPS due to its ability to form a stiff, brittle hydrogel by itself. With no AMPS present, the compressive modulus did not reach cartilage-equivalency. The use of 20 wt.% and 30 wt.% AMPS helped achieve cartilage-equivalent strength and modulus for both tension and compression. As the AMPS addition was brought to 40 wt.%, the hydrogel became brittle, and the resulting compressive strength was lowered outside of the acceptable cartilage-equivalent range.

The last variable of interest came in discovering the need to crosslink the PAMPS network. The material of choice for crosslinking purposes was N,N'-methylenediacrylamide (MBAA). Surprisingly, an MBAA concentration of 0×10^{-3} M still gave way to achieving cartilage-equivalent mechanical properties. From 0×10^{-3} M to 80×10^{-3} M, the MBAA addition did not impact the ability of the hydrogel to stay within the tensile and compressive range for matching cartilage. At 80×10^{-3} M and 100×10^{-3} M, the

tensile modulus became too high for the upper limit to cartilage-equivalent properties. As a result, this work concluded that a range of MBAA additions from 0 to 60 x 10^{-3} M brought about cartilage-equivalent mechanical properties. Based on the results in Figure 24, the composition of the hydrogel termed to be "BC-PVA-PAMPS" as the top performing hydrogel for subsequent testing was 22.1 wt% BC, 40 wt% PVA (molecular weight: 146 000 g mol^{-1}, fully hydrolyzed), 30 wt% PAMPS, and 60 x 10^{-3} M MBAA.

Given the numerous studies of strong hydrogels based on polyacrylamide (PAAm) from Table 2, this work also attempted to make cartilage-equivalent hydrogels composed of BC, PAMPS, and PAAm. Similar concentrations of BC and PAMPS were used to compare with the BC–PVA–PAMPS hydrogel. Although several of the compositions tested achieved a cartilage-equivalent compression strength in Table 4, none of the compositions tested achieved a cartilage-equivalent tensile strength.

Table 4: Mechanical properties of BC-PAMPS-PAAm hydrogels. Metrics that fall in the cartilage equivalent range are in bold.

Initial BC Concentration (wt.%)	AMPS Conc. (wt.%)	MBAA Conc. (mM)	AAm Conc. (wt.%)	Tensile Strength (MPa)	Tensile Modulus (MPa)	Compressive strength (MPa)	Compressive modulus (MPa)
49.8	15	90	22.1	1.99	5.39	**40.69**	21.65
22.1	30	90	12.4	3.47	29.10	**14.96**	6.85
22.1	15	120	29.8	3.43	16.12	4.75	2.06
49.8	20	120	12.4	3.99	20.55	2.60	1.06
1.00	30	120	22.1	3.72	51.00	7.49	**9.94**
49.8	30	60	29.8	5.91	33.15	10.73	7.70
22.1	20	60	22.1	3.74	14.24	12.34	**12.81**
13.9	15	60	12.4	2.66	8.15	3.83	2.03
13.9	20	90	29.8	3.90	30.21	**14.64**	**13.88**

This difference can be attributed to the lower strength of the PAAm hydrogel relative to PVA.

In identifying a candidate that matched the tensile and compressive properties of cartilage, the next portion of this project was dedicated to testing wear and frictional properties. In addition to matching the requirements of the mechanical behavior of cartilage, the fiber-reinforced double-network hydrogel must also mimic the functional properties of cartilage. These include the hydrogel's ability to fight degradation and loss of mass during a typical wear test as well as how smooth the surface of the hydrogel is for an analysis of its coefficient of friction. Furthermore, the movement of fluid through the hydrogel can be studied in a confined compression test and biocompatibility analysis can be arranged. However, it is important to note that these tests are not the focal point of Chapter 4; they are merely complementary to the full mechanical characterization of the durability of the BC-PVA-PAMPS hydrogel. This testing was carried out by the research group of Dr. Benjamin Wiley. For information pertaining to the time-dependent mechanical properties, osmotic effects, coefficient of friction, wear resistance, and biocompatibility of the BC-PVA-PAMPS hydrogel, please refer to Yang et al. (2020).[208]

4.3.1 Fatigue Study of Fiber-Reinforced Double-Network Hydrogel

Upon analyzing the top hydrogel system through the series of durability and biocompatibility tests, the goal of this work shifted toward analyzing its tensile fatigue

properties with the hope of creating a tensile fatigue life curve. The importance of characterizing cyclic behavior for this cartilage-equivalent material becomes critical due to the cyclic stresses that cartilage experiences in vivo.[100,109,209] As justification for employing this type of testing on the hydrogel system, tensile fatigue stresses may contribute to the mechanical failure of cartilage. The failure of collagen fibers over a long-time frame may be due to experiencing prolonged, cyclic loads in tension.[109,210–212] Furthermore, carrying out cyclic tensile tests provided a clear definition of failure as opposed to establishing failure in compression for soft, cartilage-like materials.[155] As a material experiences repetitive loading, local tensile stresses arise even if the predominant force is compressive due to the complex nature of how stress is distributed around an indentation.[213] With these considerations in view, characterizing the impact of such stresses with regard to the lifetime of a synthetic cartilage replacement is critical.

To have a wide breadth of understanding of each component's role, it would be best to select a combination to be considered a control with no components such as bacterial cellulose by itself. The next combination to test would exceed both the tensile and compressive properties of articular cartilage, otherwise termed the top-performing combination. The final two combinations could be utilized to better understand the role of PVA and PAMPS, respectively. These combinations could be BC-PVA with no PAMPS as well as BC-PAMPS with no PVA. In this way, isolation of the impact of each component on long-term tensile behavior could be achieved. To ensure the hydrogel did

not change significantly over the duration of the fatigue experiments, hydrogel samples were stored in PBS solution for up to 12 days. Their tensile strength and thickness were measured, and the results can be seen in Figure 25.

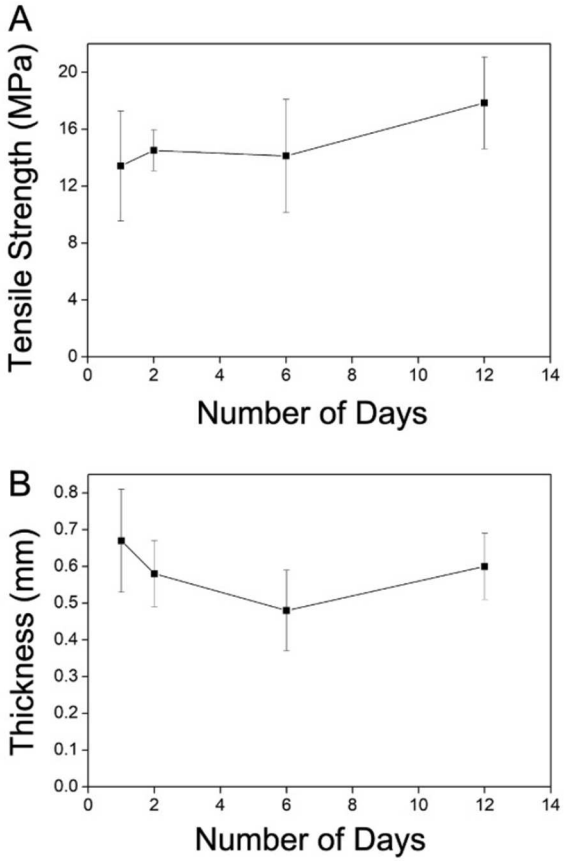

Figure 25: (A) Tensile strength and (B) thickness of the BC-PVA-PAMPS hydrogel samples after storage in PBS for a given number of days at room temperature.

This data confirms that the tensile strength and thickness of the hydrogel remained relatively constant over 12 days.

Results from cyclic tensile testing are provided in Figure 26 for the BC-PVA-PAMPS hydrogel (top-performing combination) and different combinations to understand the specific role of each component. In addition, porous titanium was included in this figure for the purpose of comparison.[214]

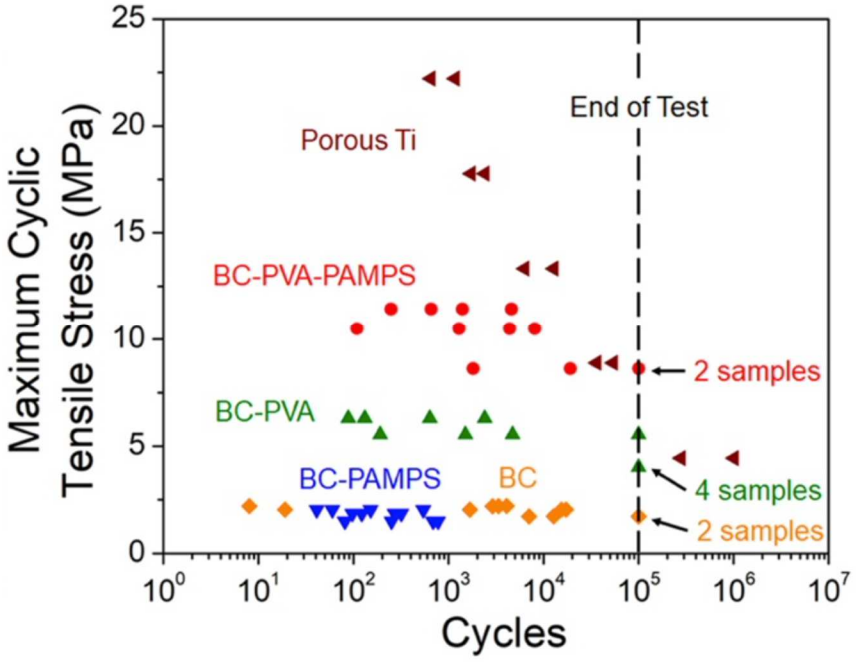

Figure 26: Maximum cyclic tensile stress applied vs. the number of cycles before failure. Eight samples indicated by arrows did not fail after 100,000 cycles.

In this work, all cyclic tests were carried out at a constant frequency of 2.5 Hz for all samples. As a result, samples with higher tensile strengths were tested at higher stress rates. A test of 100,000 cycles would take 11.1 hours, and input load parameters were 1 N for the minimum and specific load of interest for the maximum. Testing conditions

can be seen in Table 5 of 4.5.2.7 Fatigue Tensile Testing. The first five loading–unloading cycles for the BC–PVA–PAMPS fatigue test and the associated hysteresis energies are shown in Figure 27.

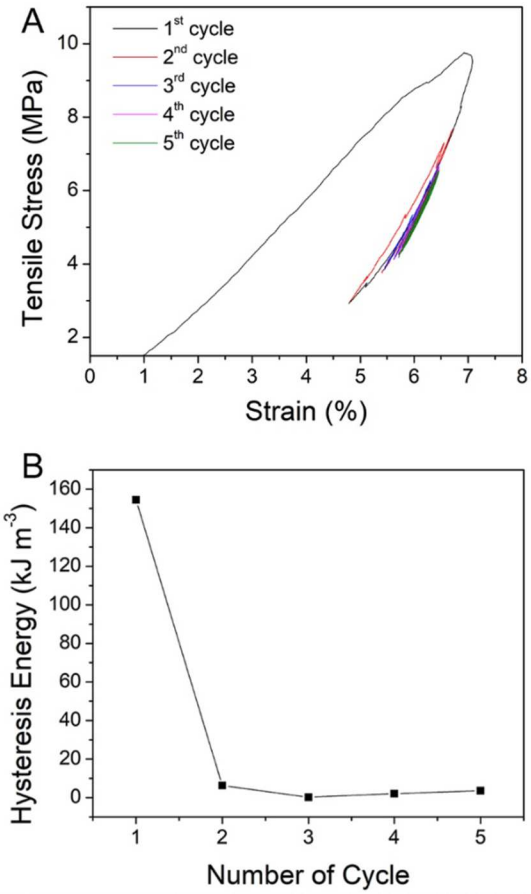

Figure 27: (A) Stress-strain curve for the first 5 tensile loading-unloading cycles for the tensile fatigue test of BC-PVA-PAMPS. (B) Hysteresis energies for the first 5 cycles.

The BC-PVA-PAMPS hydrogel had two samples that lasted 100,000 cycles without failure at 8.62 MPa, which is comparable to the performance of 85% porous 3D-

printed titanium.[214] The BC-PAMPS sample performed poorly in fatigue testing due to the brittleness of the PAMPS network which caused the samples to failure at early time points.[215] The BC-PVA sample had improved fatigue resistance due to PVA's inherent toughness,[201–203] and all four of its samples lasted 100,000 cycles at 4.02 MPa with no signs of damage at the end of the tests. BC-PVA-PAMPS displayed superior fatigue behavior due to PVA's prominence in acting as a toughening agent, thus negating the brittle impact and poor fatigue response of PAMPS. In a promising fashion, the observed fatigue strength of the BC-PVA-PAMPS combination is comparable to the fatigue strength seen in cartilage of middle-aged adults.[109] With a holistic view of the mechanical durability of the BC-PVA-PAMPS hydrogel, it has exciting candidacy as a material for repairing articular cartilage lesions.

4.4 Concluding Remarks of Fiber-Reinforced Double Network Hydrogel

With regards to comparing the work in this chapter with the Chapter 3, greater insight was shown for understanding the lifetime of an extremely strong hydrogel for high load-bearing applications. In Chapter 3, toughening the existing PVA framework with starch did not bring about an improvement in fatigue behavior. However, the extreme strengthening of the base BC network in Chapter 4 through PVA and PAMPS led to enhanced fatigue strength in comparison to the system studied in Chapter 3. Perhaps starch as a toughening agent was an anomaly in its specific case with

interacting with the PVA network. The work in Chapter 4 proves that improving the mechanical behavior of a base network can lead to an improvement in fatigue behavior. Further studies in this realm would be needed to determine if the behavior of starch in Chapter 3 was an outlier from expectation.

In conclusion, a bio-inspired design strategy was employed to synthesize the first composite hydrogel with comparable strength and modulus as human articular cartilage in compression and tension. Bacterial cellulose nanofibers were used to add tensile strength similar to the collagen nanofibers found in cartilage. Polyvinyl alcohol gave the composite hydrogel an elastic restoring force, viscoelastic energy dissipation, and prevented stress concentration on individual BC fibers. PAMPS supplied the hydrogel with a source of fixed negative charge, and it also provided an osmotic restoring force similar to the role of aggrecan in cartilage. BC-PVA-PAMPS hydrogel also had an aggregate modulus (0.78 MPa) and permeability (3.2×10^{-15} m^4 N^{-1} s^{-1}) that give it the same time-dependent mechanical response as cartilage under confined compression. The BC-PVA-PAMPS hydrogel exhibited a coefficient of friction (0.06) about half that of cartilage, was 4.4 times more resistant than a polyvinyl alcohol hydrogel and exhibited cartilage-equivalent fatigue strength at 100,000 cycles. BC-PVA-PAMPS was not cytotoxic and is comprised of materials that have been previously demonstrated to be biocompatible.

In re-creating the essential functions of cartilage, the hypothesis of this work was confirming if such a design strategy of processing and composite additives for improving monotonic mechanical behavior would enhance fatigue behavior. As observed in the enhanced fatigue behavior with all components present, this work established a connection between improvement of monotonic mechanical behavior to fatigue behavior, thus confirming the central hypothesis of Chapter 4. As a result, it became fair to conclude that starch's behavior may be isolated to starch solely in the specific work of Chapter 3. Further work would be needed to investigate different toughening agents or processing techniques for impact on fatigue behavior, although the remaining portions of the document will be dedicated to study of interesting observations of flaw development in Chapter 3. In lieu of focusing exclusively on the translation from monotonic strength or toughness to fatigue, the final portion of this work was concentrated on understanding the progression of monotonic flaws as it relates to untimely failure in fatigue (i.e., early implant failure for a synthetic cartilage substitute). To summarize, the specific deliverables of this aim were the following:

- Successful matching of tensile and compressive properties of BC-PVA-PAMPS hydrogel with heavy load-bearing cartilage
- Full mechanical characterization of a range of system combinations for the BC-PVA-PAMPS hydrogel, including tension and compression

- Development of a fatigue life curve for four different variations of the BC-PVA-PAMPS hydrogel through load-controlled tensile fatigue testing

4.5 Materials and Methods

4.5.1 Materials

Bacterial Cellulose (BC) was purchased from Gia Gia Nguyen Co. Ltd. Poly(vinyl alcohol) (PVA) (fully hydrolyzed, molecular weight: 146 000 g mol^{-1}), N,N'-methylenediacrylamide (MBAA, 97.0%), 2-hydroxy-4'-(2-hydroxyethoxy)-2-methylpropiophenone (I2959), potassium persulfate (KPS) and 2-acrylamido-2-methylpropanesulfonic acid sodium salt (PAMPS) (50 wt% solution in water) were purchased from Sigma Aldrich. Phosphate buffered saline (PBS) was purchased from VWR International. Bovine serum (New Zealand origin, collected from cattle typically 12-24 months old) was purchased from Fischer Scientific.

4.5.2 Methods

4.5.2.1 Fabrication of BC-PVA-PAMPS hydrogel

BC sheets were pressed to a controlled thickness between two aluminum plates (typically 0.5 mm, controlled by spacers between the aluminum plates) and placed into a

hydrothermal reactor with a mixture of 40 wt% PVA and 60 wt% deionized water. The hydrothermal reactor was sealed and heated at 135°C for 24 hours to allow the PVA to diffuse into the voids of BC and form a BC-PVA hydrogel. The BC-PVA hydrogel was removed from the reactor when hot (>85°C). Note the hydrothermal reactor was pressurized with hot steam and created a burn hazard, so personal protective equipment including lab coat, heat resistant gloves and full-coverage face shields should be used when opening the reactor. The residual PVA solution was removed by scraping the surface of the BC-PVA samples with a metal spatula. The samples were frozen in a -78°C fridge for 30 minutes and thawed at room temperature to physically crosslink the PVA network.

The BC-PVA hydrogel was then soaked in a solution of 30 wt% AMPS, 60 x 10^{-3} M MBAA, 50 x 10^{-3} M I2959 and 0.5 mg mL^{-1} KPS solution for 24 hours. The hydrogel was cured with a UV transilluminator (VWR International) for 15 minutes on each side, and further cured in an oven at 60°C for 8 hours to ensure even and complete curing. The resulting BC-PVA-PAMPS hydrogel was stored in PBS for at least 24 hours before further characterization.

4.5.2.2 Fabrication of PVA hydrogel

To fabricate PVA hydrogel with a PVA concentration of 40 wt%, a slurry of 40 wt% PVA and 60 wt% deionized water were mixed in a glass petri dish (diameter: 90

mm) and heated at 121°C for 30 minutes in an autoclave sterilizer. The resulting hydrogel was frozen in a -78°C fridge for 30 minutes and thawed to room temperature. The hydrogel was frozen and thawed for 4 additional cycles. The resulting PVA hydrogel was cut into the desired shape and stored in PBS for at least 24 hours before tests.

4.5.2.3 Fabrication of PAMPS-PDMAAm hydrogel

The PAMPS hydrogel was synthesized following a modified procedure from previous work.[216] An aqueous solution of 1 M AMPS, 40 x 10^{-3} M MBAA and 50 x 10^{-3} M I2959 was made and cast in a silicone rubber mold and sandwiched between a pair of glass slides. The solution was cured with a UV transilluminator (VWR International) for 1 hour on each side. The PAMPS hydrogel was then removed from the mold and submerged in an aqueous solution of 3 M DMAAm, 3 x 10^{-3} M MBAA and 50 x 10^{-3} M I2959 for 24 hours. The hydrogel sample was then cured with a UV transilluminator for 30 minutes on each side to form a PAMPS-PDMAAm double network hydrogel. The resulting hydrogel was soaked in PBS for at least 24 hours before mechanical testing.

4.5.2.4 Fabrication of PVA-PAMPS hydrogel

PVA hydrogel was made with the previously described procedure (see 4.5.2.2 Fabrication of PVA hydrogel). The PVA hydrogel was then soaked in a solution of 30

wt% AMPS, 60 x 10^{-3} M MBAA, 50 x 10^{-3} M I2959 and 0.5 mg mL^{-1} KPS solution for 24 hours. The hydrogel was cured with a UV transilluminator (VWR International) for 15 minutes on each side, and then heat cured in an oven of 60°C for 8 hours to ensure even and complete curing. The resulting PVA-PAMPS hydrogel was stored in PBS for at least 24 hours before testing.

4.5.2.5 Monotonic Tensile Testing

Monotonic tensile measurements were carried out on an Instron 1321 (Instron, Norwood, MA, USA) instrument as well as a TestResources 830 (TestResources, Shakopee, MN, USA) load frame at a rate of 0.25 mm s^{-1}. Monotonic samples in an ASTM D638-14 Type V shape with a titanium hollow punch that was created through additive manufacturing. The dimensions of the samples were measured with a caliper before testing. The ultimate tensile strength (UTS) was the maximum stress measured before fracture. The tensile modulus was taken as the slope of the stress-strain curve at a stress of 1 MPa for comparison with previous studies of human cartilage.[166]

4.5.2.6 Monotonic Compressive Testing

The compressive properties of all samples were measured with an axial Torsion System (Test Resources 830LE63). The cylindrical samples were cut out of films of hydrogel samples with a hollow steel punch (diameter: 4 mm). The dimensions of the

samples were measured with a caliper before testing. The compressive properties were measured with a rate of 0.05 mm s^{-1}. The ultimate compressive strength was taken as the maximum stress measured before fracture. The compressive modulus was derived as the slope of the stress-strain curve at the stress of 0.4 MPa. The 0.4 MPa stress point was chosen for comparison with previous studies of human cartilage.[155]

4.5.2.7 Fatigue Tensile Testing

Hydrogel samples for fatigue were prepared in an ASTM D638-14 Type V shape. Samples were initially analyzed for their ultimate tensile strength (UTS) in monotonic tension in a 37°C tap water bath. A minimum of four samples for each hydrogel was tested to obtain an average UTS value, which are listed in Table 5.

Table 5: Average UTS and standard deviation values for hydrogels in tensile fatigue tests.

Composition	UTS (MPa)	Standard Deviation (MPa)
BC-PVA-PAMPS	12.37	1.87
BC-PVA	7.06	1.52
BC-PAMPS	2.21	0.35
BC	2.36	0.32

Cyclic tensile tests were carried out with the hydrogel samples in a water bath at 37°C. Cyclic tests were conducted at 2.5 Hz. Input load parameters were 1 N for the

minimum and specific load of interest for the maximum. Target load values were based on the stress at 0.5, 1 and 2 standard deviations below the UTS. A maximum of 100,000 cycles were carried out. Every sample that did not fail after 100,000 cycles had no visible signs of damage accumulation or crack formation.

Chapter 5. Flaw Sensitivity and Tensile Fatigue of Poly(Vinyl Alcohol) Hydrogels

For a deeper understanding of the lifetime of synthetic hydrogel systems, proper attention must be given to the connections between improved strength and damage accumulation as a result of fatigue testing. As mentioned before, PVA hydrogels derive their tunable properties through freezing and thawing cyclic processing. Most often, researchers focus on developing mechanically robust hydrogels with the hope of increasing durability and reliability in fighting the accumulation of damage in a sample.[217] Prolonging the lifetime of a hydrogel is successful to the point that formation of cracks and subsequent crack growth become important factors.[218,219] The work completed in Chapter 3 utilized sharply notched samples for the formation of a tensile fatigue life curve. As such, observation of the growth of the sharp notch during tensile fatigue testing in Chapter 3 introduced a range of possibilities for future study. Different processing techniques such as the number of freezing-thawing cycles and variation of flaw type and dimension will ideally create a roadmap for future study of the advanced

mechanical behavior of synthetic hydrogels.

The sharply notched flaw type was arbitrarily chosen to complete the tensile fatigue testing in Chapter 3. As observed during testing, a graphic of a sample being tested in a cyclic, strain-controlled manner with an initial flaw that was perpendicular to the direction of the applied tensile stress can be seen in Figure 28.

Figure 28: Tensile specimen of a PVA hydrogel with a controlled flaw that was originally perpendicular to the direction of the applied tensile stress

The motivation behind this concept grew out of the observation that fatigue samples in Chapter 3 did not fail in similar manners, as observed with some tests in Figure 17. Rather, samples exhibited failure pathways of some variation of Mode I, Mode II, and/or Mode III, often termed mixed mode failure.[220] A schematic to show the difference between Mode I, Mode II, and Mode III can be seen in Figure 29.[221]

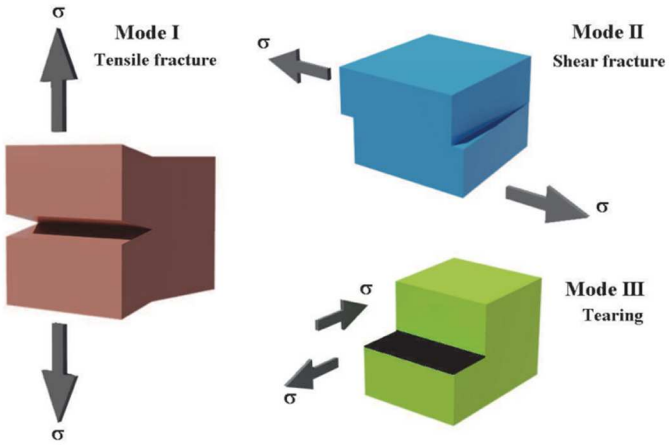

Figure 29: Schematic of the differences between Mode I, Mode II, and Mode III fracture modes from indentation fracture[221]

Variation of the type of flaw and subsequent tensile testing are needed to extract valuable information of failure pathway for a given synthetic hydrogel. Furthermore, the dimensions of these flaws can be tuned accordingly to achieve sufficient tensile strength values for fatigue testing. There exists a distinctive opening in the field of fracture mechanics and the behavior of flaws in synthetic hydrogel samples for superior understanding of fatigue properties. Furthermore, crack blunting strategies in terms of increasing fracture toughness have been pursued with regards to monotonic tensile properties of hydrogel systems.[222–224] As noted before, researchers generally agree that increasing the fracture toughness of the synthetic hydrogel is the best strategy to confront the formation or growth of a flaw. However, these adjustments to a material system turn a blind eye to long-term, fatigue properties. In addition, there is very little

attention given to the development of these flaws and if a certain type of flaw will ultimately lead to quicker failure. Understandably, this field is difficult to pursue due to the lower strength and toughness of a variety of synthetic hydrogel systems.

With this in view, the goal of this proposed aim will be pursuing a freezing-thawing cycle process for a PVA-based hydrogel that maximizes toughness and ultimate tensile strength while balancing processing conditions. In this way, the hydrogel will alleviate issues that come with testing lower strength materials for the development of controlled flaws in terms of size and shape. Prior work focused on a sharp, 2 mm cut that penetrated the full thickness of the gauge section. In this work, the type of flaw will be adjusted as well as its dimensions for an understanding of impact on fatigue properties. The central hypothesis of this work was that flaw type (sharp, crack-like flaws vs. blunted, cylindrical hole-like flaws) was critical to monotonic and fatigue behavior. To the author's knowledge, this work is novel with regards to synthetic hydrogel systems.

5.1 Rationale of PVA-based Hydrogel with FT Cycle Steps and Controlled Flaws

In lieu of continuing with two freezing-thawing (FT) cycles for the creation of the hydrogels, a range of freezing-thawing cycles starting from one cycle to eight cycles will be analyzed for any improvement in monotonic tensile properties such as toughness.

Each cycle will consist of a 20-hour freezing step followed by a 4-hour thawing step. This work describes a poly(vinyl alcohol) hydrogel utilizing the top-performing FT cycle for future fatigue study based off the greatest monotonic toughness value. In pursuing a similar synthetic strategy to Chapter 3 due to familiarity and ease of processing, controlled flaws will be designed and tested. The monotonic tensile responses of relatively strong and weak versions of the hydrogel are studied with cylindrical hole and crack-like flaws of different size to develop an understanding of monotonic strength in the presence of two different, extreme defect types. The monotonic strength of the samples with cylindrical defects is reasonably predicted using nominal stress which accounts for a loss of load bearing area, while linear-elastic fracture mechanics gives a first order approximation of the impact of crack-like flaw size on monotonic strength. Study of crack propagation in hydrogels is abundant in monotonic tension,[225–227] though the pursuit of this analysis for the development of a fatigue life curve based on the designed flaw is lacking. Two subsets of key defected samples were further subjected to c loading and fatigue failure at varying stress amplitude. The cylindrical defect samples outperformed cracked samples in fatigue, and the utilization of four FT cycles instead of two improved both monotonic toughness and fatigue properties. This work represents the first tensile fatigue analysis on defected hydrogel materials, sheds light on the behavior of hydrogels in cyclic loading environments, and evaluates both the monotonic toughness and fatigue behavior of soft materials with and without defects.

5.2 Background of Flaw Sensitivity Analysis of Hydrogels

Design and control over the mechanical properties of tissue-like hydrogels has led to a plethora of research for soft materials. Repair or replacement of cartilage, soft tissue engineering, and drug delivery highlight just a few of the extensive applications for this class of materials.[228–231] The onset of opportunities to use hydrogels has introduced a pressing need to understand the long-term behavior of these soft and wet materials for many potential uses in the human body. To ensure a continued wide range of applications, hydrogels must be able to withstand cyclic mechanical loads over prolonged periods of time while still exhibiting functionality and mechanical robustness. In particular, the response of a hydrogel to the existence and growth of various types of flaws either broadens or limits the scope of their applicability. A facile, straightforward synthetic hydrogel with reasonable toughness and structure-property control provides opportunity to understand the impact of flaws on hydrogel mechanical behavior and how improved monotonic toughness potentially translates to improved fatigue performance.

One such model system that allows for the study of how different flaw types impact monotonic and cyclic failure in soft materials is poly(vinyl alcohol) (PVA). This hydrogel system is suitable due to the following factors: adjustable mechanical properties, facile synthetic preparation, biodegradability, biocompatibility, and low

toxicity.[14,15,33–36,42,232] PVA hydrogels can be crosslinked through a freeze-thaw method allowing for simple preparation of relatively tough hydrogels. This method physically crosslinks the polymer network through microcrystalline domains and imparts intrinsic toughness (area under the stress-strain curve, or resistance to crack propagation) to the hydrogel.[33,120] Through freezing-thawing cyclic processing of PVA hydrogels, scientists have added another tool to attain high-level control over the mechanical properties of PVA hydrogels. With relative ease-of-processing and structure-property control for a soft material, a PVA hydrogel can be used as a model system to understand the impact of the progression of different kinds of mechanical flaws under monotonic and cyclic loading conditions.

Aiming to understand the early formation of damaging flaws like cracks and cavities in hydrogels, researchers have shifted focus to using synthetic strategies to prevent the creation of cracks and cavities during materials processing. Widespread studies in the realm of developing "flaw-insensitive" or "notch-insensitive" hydrogels have grown recently to prevent catastrophic failure.[135,233–237] Due to the variable nature of the environment in which they are being used, such as the human body, the specific type of flaw is critical to a material's ability to endure mechanical stresses for two reasons: 1) direct loss of sample area to carry load and 2) amplification of applied stresses to a local region in a material (stress concentration or stress intensity). Cracks and less severe rounded cavities can hinder a soft material from sustaining mechanical

loads under both monotonic and cyclic loading conditions. Edge-based cracks present the worst-case scenario due to an intensity of stress at the tip of the crack and exposure to environment. On the other hand, cylindrical holes or notches away from the edge of the material are blunt stress concentrators and are the least detrimental geometrical defects. Several researchers have studied the impact of flaws with regards to the material's sensitivity toward the imposed flaw.[98,224,238–240] However, very little has been studied as flaw size increases in materials capable of very large strain deformations.[240] Accounting for the initial growth and subsequent long-term development of these flaws as it relates to strength of a hydrogel is critically important for hydrogels in biomedical applications.

In the deformation and fracture of materials, it is critical to consider the impact of flaws with regards to a material's ability to maintain strength. Various approaches can be used to estimate the impact of flaws on the strength of a material for different flaw geometries and severities such as nominal stress, stress concentration, and stress intensity (fracture mechanics). Nominal stress analysis is simply a reduction in the load bearing area of a sample due to the presence of a geometric defect. In this highly non-conservative approach, a sample losing a percentage of its area will lose only that same percentage in strength. Nominal stress is a reasonable predictor of strength drop when a soft or low modulus material easily deforms and geometric defects have minimal stress localizing impact. Stress concentration is a quantitative measure of the amplification of

local stresses relative to the global applied stresses, and it provides a measure of the local driving force for a specific flaw to propagate or the stability of a flaw at a certain global stress value.[241] Unfortunately, the major issue with using stress concentration approximations for hydrogels comes from the strong link between flaw geometry and stress concentration value. As hydrogels experience large strains, the flaw shape evolves rapidly and typically lowers the stress concentration value. For example, under uniaxial tension, a perfectly circular flaw is quickly turned into an ellipse with its loading axis aligned in the loading direction which has minimal local stress amplification.

Stress intensity factor (fracture mechanics) is used for predictions of the strength of a material with a crack or crack-like flaw based on scaling with the magnitude of local stresses experienced at the tip of the crack.[242] The assumption of this model relies on the tip of the crack coming to a mathematical singularity (crack tip radius of zero) instead of being blunted. Although fracture mechanics has geometrical small strain and deformation limitations akin to stress concentrations, its worst-case scenario assumption about crack tip geometry and stresses can provide some insight into the behavior of cracked soft samples. For soft materials, nominal stress analysis provides an upper bound on strength due to a flaw (smallest possible strength loss for a given flaw size) while fracture mechanics provides a lower bound on strength due to a flaw (greatest possible strength loss for a given flaw size).

The impact of flaws in hydrogels is even less characterized and understood under tensile cyclic loading, where damage can progress and result in sample failure even if a flaw is not "critically" sized. Moreover, tensile testing removes the non-conservative nature of determining failure for a sample that can recover from extreme compressive deformation. The progression of flaws under cyclic tensile loading will help to understand one failure mode in hydrogel materials used in load-bearing applications. The common focus on a hydrogel's sensitivity towards the existence and behavior of an initial flaw under monotonic testing is often idealistic since it requires the material to exist in pristine condition, which is practically impossible. In addition, flaw analysis in many "cyclic" papers on hydrogels is commonly halted before completing a large number of cycles or true fatigue failure of a sample is reached. Without sufficient cycles to observe the ultimate failure from longer-term repetitive loads, the hydrogel's resistance to the growth of a flaw has not been truly evaluated over the appropriate range of stress levels. The ultimate goal in this work is to use a PVA hydrogel system with a simple preparation and tunable mechanical properties to understand the impact of different flaw types and sizes on cyclic behavior in both high cycle-low stress and low cycle-high stress fatigue.

In this work, PVA hydrogels were prepared with the use of freezing-thawing cyclic processing as a means to study mechanical behavior of a hydrogel with varied inherent toughness in the presence of cylindrical holes and sharp cracks with

systematically increasing size. Freeze-thaw cyclic processing was used to improve monotonic toughness through crystallization of the hydrogel network. Once a chosen freezing-thawing cyclic process was selected for its enhancement of mechanical properties, attention was turned to the resulting hydrogel's response to different flaw types and dimensions under monotonic loading. This study set out to create the worst-case flaw scenario (sharp crack after freezing-thawing) and best-case flaw scenario (cylindrical hole before freezing-thawing). The PVA hydrogel was relatively insensitive to the cylindrical hole type of flaw, but extremely sensitive to the crack-like flaw, despite both of them deforming significantly from their initial geometry on loading. Nominal stress analysis and stress intensity modeling demonstrated how these two flaw types impact the sample strength just within the upper and lower bounds, and thus encompass the impact of flaw type on hydrogel strength. Tensile testing in a cyclic manner was then employed on the PVA hydrogels to study the growth of crack-based flaws and cylindrical hole-based flaws toward ultimate failure of the material. The utilization of additional freeze-thawing cycles enhanced fatigue behavior in comparing 2 FT cycles to 4 FT cycles. Moreover, samples with sharp crack flaws did not perform as well as those with cylindrical hole flaws for both 2 FT and 4 FT cycles, in line with decreases in monotonic strength with crack-like flaws. These tensile fatigue results provide a blueprint for analyzing tough but defected hydrogels under long-term, cyclic loading conditions.

5.3 Characterization of PVA-based Hydrogels with Varying FT Cyclic Steps and Flaws

5.3.1 Chemistry and Sample Geometry

Using methods from prior work,[209] homogenous solutions consisting of PVA (16 wt% with respect to the total weight of deionized water combined with PVA) were obtained with a high degree of processability. The screening process of FT cycles provided a quantitative tracking of the improvement of mechanical properties through crystalline domain development and non-covalent interactions. The synthetic approach utilized in the study is illustrated in Figure 30.

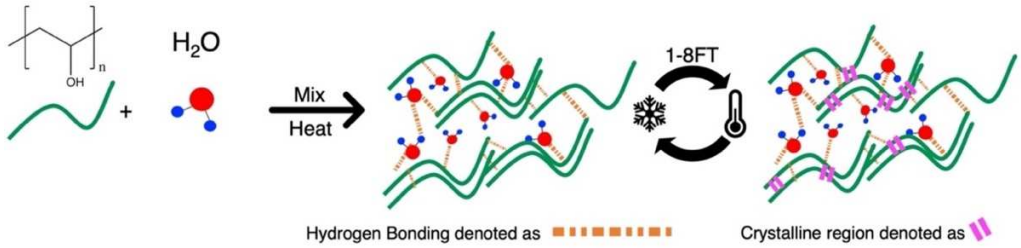

Figure 30: Schematic representation of the PVA-based tough hydrogel preparation strategy using freeze-thawing cyclic processing.

A given amount of PVA was combined with deionized water and maintained at 95°C until PVA had fully dissolved for pouring the solution into the stainless-steel molds. Freezing and subsequent thawing of the samples took place to create the

hydrogel. Hydrogen bonding could occur between PVA with itself and PVA with water. Development of crystalline regions was solely attributed to PVA interacting with itself. Representative images of typical monotonic tension samples after final preparation can be seen in Figure 31A for the FT cycle screening process, while typical fatigue tension samples can be seen in Figure 31B for samples that had a sharp crack and Figure 31C for samples that had a cylindrical hole.

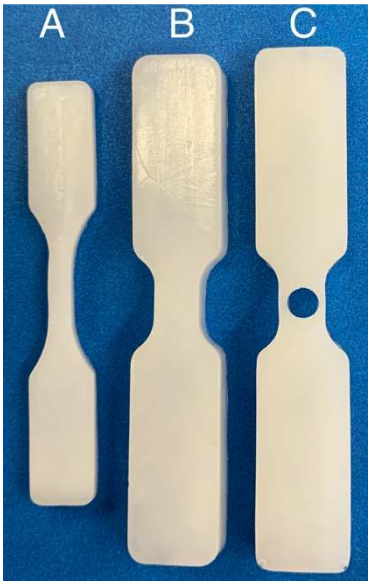

Figure 31: Representative optical images of PVA hydrogel samples: (A) ASTM D638-14 Type V shape for monotonic tension, (B) customized fatigue tension sample for a sharp edge crack, and (C) customized fatigue tension sample for a cylindrical hole.

Adjustment of the shape of the sample was necessary for the following three reasons: 1) the Type V sample had a gauge section that was too small to accommodate larger cracks and cylindrical holes, 2) the Type V samples had a tendency to buckle

when tested cyclically in strain-controlled tension, and 3) the Type V-shaped samples had previous issues with failure near the grip section instead of the gauge section when stretched in a cyclic fashion.[209] With these reasons in mind, the same customized fatigue shape previously developed in our work was utilized for fatigue testing herein.[209] This difference in sample geometry of a thicker, shorter gauge section can be seen in comparing Figure 31 A to B and C.

5.3.2 Screening Process of FT Cycles

Analogous to our prior work,[209] PVA hydrogels were prepared by dissolving the polymer in deionized water and pouring the solution into a designated mold. Subsequently, freezing and thawing the solution was used to physically crosslink the polymer network through crystalline domains, thus creating the hydrogel.[53,111] The starting point of this study took the form of investigating the mechanical properties of the PVA hydrogel by systematically varying the number of freezing-thawing cycles from one to eight. As opposed to the previous work of utilizing two freezing-thawing cycles for both control and all bio-friendly toughening agents,[209] this work sought to understand the impact of the number of freezing-thawing cycles. The hydrogel samples were tested for their monotonic tension properties using the ASTM D638-14 Type V shape to obtain the top performing FT cycle number based solely on "flaw-free" toughness, which is once again defined as the area under the stress-strain curve.

Toughness was selected as the key factor for screening FT cycles due to its practical applications in the realm of soft materials when considering the ability of a hydrogel to dissipate mechanical energy, which is a direct, quantitative relationship to toughness.[84,114–116]

The goal of the screening process of the FT cycles was to determine a processing cycle number for which toughness was maximized without sacrificing ease-of-processing. Figure 32A illustrates the trend for tensile toughness for each FT cycle. Representative tensile stress-strain curves for the PVA samples of differing FT cycles can be seen in Figure 32B.

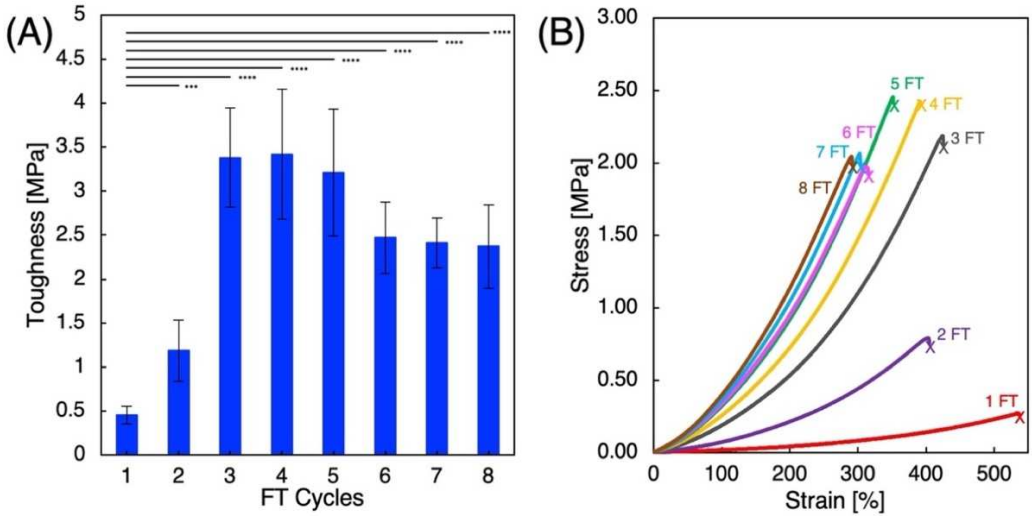

Figure 32: (A) Average toughness values for all FT cycles obtained from monotonic tensile stress-strain behavior with ASTM D638-14 Type V shape. Minimum of n=9; data depict mean toughness value ± standard deviation; compared with 1 FT cycle by one-way analysis of variance (ANOVA); α=5%; * depicts statistical significance in the following manner: * p<0.05; ** p<0.01, *** p<0.001, **** p<0.0001. (B)

Representative tensile stress-strain behavior of all FT cycles (1 FT to 8 FT) obtained from monotonic tension testing with ASTM D638-14 Type V shape.

The toughness values from 1 FT to 8 FT cycles were: 0.46 MPa ± 0.10 MPa, 1.19 MPa ± 0.35 MPa, 3.38 MPa ± 0.57 MPa, 3.42 MPa ± 0.74 MPa, 3.21 MPa ± 0.72 MPa, 2.47 MPa ± 0.40 MPa, 2.41 MPa ± 0.28 MPa, and 2.37 MPa ± 0.47 MPa. As shown in Figure 32A, the toughness values increased until the maximum at 4 FT cycles, followed by a slow drop off until the toughness values saturated for 6 FT, 7 FT, and 8 FT cycles. This trend in mechanical results can be explained in considering the development, or densification, of crystalline domains of the hydrogel's structure with subsequent FT cycles.[111] As a well-studied physical crosslinking strategy, the development of crystalline domains within a hydrogel's network to bear mechanical load is a direct result of freezing-thawing cyclic processing.[53,111,243] With the onset of additional freezing-thawing cycles, the size of existing microcrystalline domains grows and new domains can also form.[111] Similar to this work, the densification process of prior work progressed continually for additional freezing-thawing cycles.[111] By the 6 FT, 7 FT, and 8 FT cycles, a saturation point was reached in this densification process and the toughness values had leveled off. Similar to the trend in toughness, the ultimate tensile strength increased starting from 1 FT until reaching a plateau. Upon leveling off, the ultimate tensile strength dropped for 6 FT, 7 FT, and 8 FT. The strain-to-failure trend can also be explained in terms of densification of the network structure and microcrystalline

domains. The highest strain-to-failure values were observed with minimal FT cycles when the microcrystalline domains were not as developed. The lowest strain-to-failure values were obtained with the higher number of FT cycles due to a highly dense network with developed microcrystalline domains.

To understand the impact of the FT cycles on the functional properties of the PVA hydrogels, a swelling ratio comparison study was performed. The ability of a hydrogel to uptake water is crucial for potential drug release and tissue engineering applications as well as understanding different stress dissipative mechanisms in articular cartilage and the degree of crosslinking.[117–119] Figure 33 shows the impact of each FT cycle on the ability of the hydrogel to swell in deionized water at room temperature.

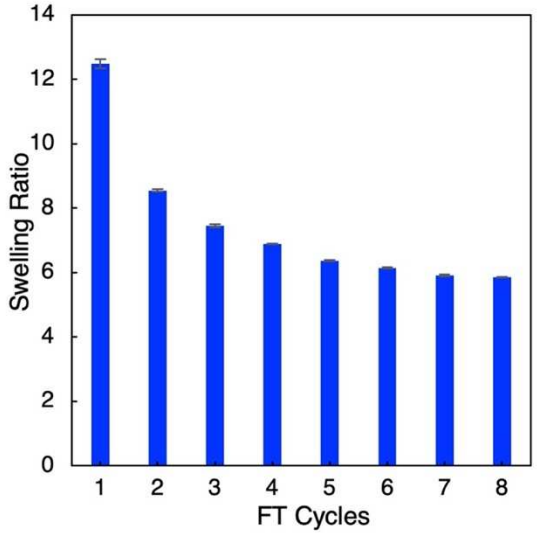

Figure 33: Swelling ratio comparison of all FT cycles using tensile testing samples; data depict mean swelling ratio ± standard deviation.

The average swelling ratios were 12.48 ± 0.14, 8.55 ± 0.03, 7.45 ± 0.05, 6.90 ± 0.01, 6.37 ± 0.02, 6.15 ± 0.01, 5.91 ± 0.03, and 5.86 ± 0.02 for each of the FT cycles from one cycle to eight cycles, respectively. In accordance with similar work,[111,203,244] the ability of each FT cycle hydrogel to uptake water decreases with increasing number of FT cycles. This occurs because continually freezing and thawing the hydrogel leads to significant densification of the gel structure with each FT cycle and an overall increase in effective crosslinking density.[111] Additional FT cycles restrict the movement of PVA chains, making it much more difficult for water molecules to penetrate into the polymer chain network.[245] In observing the shift in the swelling capability of the hydrogel based on FT cycles, the next portion of this study sought to understand the physical impacts in terms of crystallinity on hydrogel structure and network interactions.

5.3.3 Crystallinity Analysis of FT Cycles

Phase separation of PVA with water, intramolecular hydrogen bonding (PVA with itself), and intermolecular hydrogen bonding (PVA with water) were identified as non-covalent molecular interactions in this system.[111] These interactions ultimately paved the way for physical crosslinking of the network structure from the freezing-thawing cyclic processing steps. It became critical to understand the connection of each

FT cycle on the degree of crystallinity in a quantitative manner. The crystallinity of samples from their as-prepared state is subject to change if samples experience an aging or a drying process.[120,121] These aging or drying changes can also impact the functional properties of the hydrogel such as its swelling and mechanical behavior.[122,123] As a result, the analysis of the degree of crystallinity would need to preserve the hydrogel in its as-prepared state to avoid any drying or aging process. In preventing a drying or aging process from occurring, the role of the FT cyclic process could be clearly understood as it relates to any alterations in the crystalline nature of the hydrogel. With these considerations in view, some of the common characterization techniques, such as X-ray diffraction (XRD), scanning electron microscopy (SEM) and atomic force microscopy (AFM), could not be utilized due to concerns of an aging or drying process taking place during analysis. As a result, differential scanning calorimetry (DSC) was employed to characterize the impact of FT cycles on the degree of crystallinity in the as-prepared state.

The amorphous network structure of the PVA hydrogel is comprised of tiny, highly ordered regions of PVA chains that form "knots" as a result of freezing at very cold temperatures.[124] These "knots", or microcrystallites, form as a result of reduced molecular motion for the chains of PVA at low temperature.[129] As PVA chains remained locked in close proximity to one another with the freezing of water, they can interact favorably to create microcrystallite pockets that are physically crosslinked sites for

bearing mechanical load. Formation of the "knots" continues to progress with additional freezing and thawing cycles.[53,126,130] Utilizing the endothermic melting of PVA crystallites, the crystallinity degree of a hydrogel sample can be obtained.[121] The crystallinity degree ($\chi_{\%}$) of the hydrogels was calculated using Equation 1.

$$\chi_{\%} = \frac{\Delta H}{\Delta H^{\circ} \times W_{PVA}} \times 100 \quad (1)$$

where ΔH was calculated as the area under the endothermic melting peak, ΔH° is the heat needed to melt PVA that is 100% crystalline (138.6 J g^{-1}) , and W_{PVA} is weight fraction of the PVA polymer in the hydrogel sample with respect to deionized water.[38,131,132] Figure 34 provides representative DSC curves from the first heating DSC cycle from which the crystallinity degree was calculated.

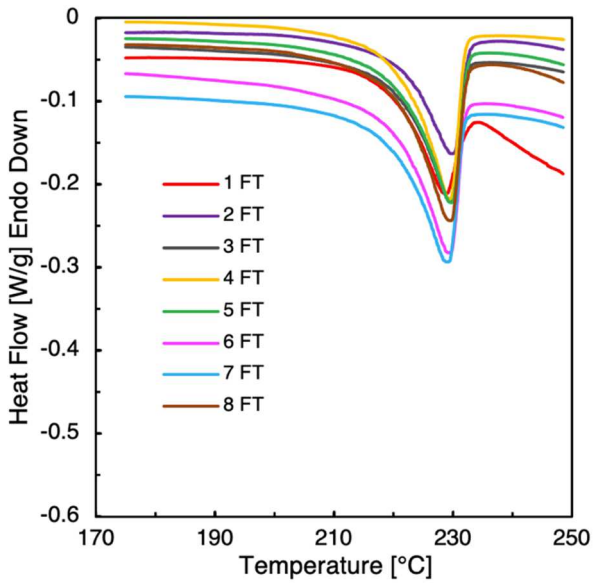

Figure 34: Representative DSC heating curves for each FT cycle with Heat Flow [W/g] vs. Temperature [Celsius] for the first heating step from 40°C to 250°C.

For a more quantitative analysis of change in hydrogel crystallinity, Figure 35 provides a view of the trend of crystallinity degree versus an increasing number of FT cycles.

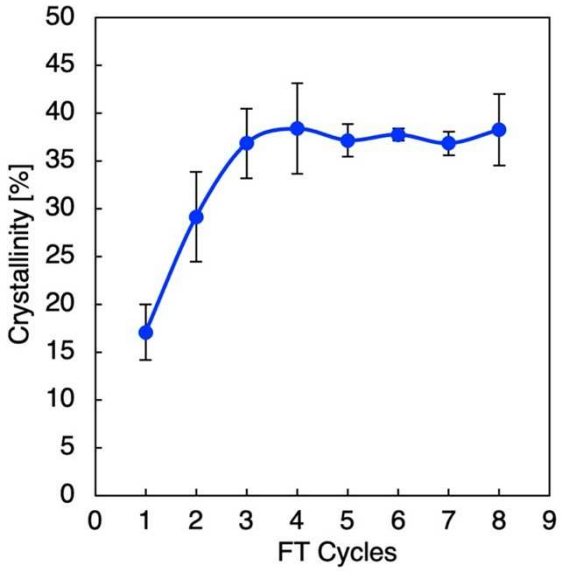

Figure 35: Crystallinity of PVA samples with varying numbers of FT cycles obtained from DSC measurements. Data depict mean crystallinity value ± standard deviation.

Crystallinity values from 1 FT to 8 FT were the following: 17.08% ± 2.91%, 29.17% ± 4.74%, 36.86% ± 3.63%, 38.39% ± 4.75%, 37.17% ± 1.72%, 37.78% ± 0.65%, 36.86% ± 1.23%, and 38.29% ± 3.72%. From the data in Figure 35, the degree of crystallinity increased as the number of freeze-thawing cycles increased until reaching a saturation point after the first 3-5 FT cycles, as observed in previous work.[121] This result can be explained in that consecutive FT cycles build upon the foundation that was laid in

creating the "knots" in the network during the first FT cycle.[246] The loosely-formed crystallites from the first FT cycle were continually developed due to further molecular chain aggregation with subsequent FT cycles, and the creation of new crystallites progresses until reaching a plateau.[126,129,228] In characterizing the changes to crystallinity with increasing number of FT cycles, it became evident to fix the number of FT cycles for continued tensile flaw and fatigue studies.

In terms of ease-of-processing concerns, the only sample that was difficult to remove from the mold due to insufficient mechanical stability was 1 FT cycle. Each cycle after that made the processing easier, with the only difference between FT cycles in terms of ease-of-processing was the amount of time it took for additional FT cycles. Based on the small difference between 3 FT and 4 FT in terms of ease-of-processing, the deciding factor for selecting an appropriate FT cycle number for subsequent mechanical testing came down to maximizing toughness. Since the 4 FT cycle sample had the largest toughness value, it was selected as the FT cycle number for further tensile study. In addition, the 2 FT cycle sample was selected for further tensile study due to its near matching of the toughness of the control sample in a prior PVA hydrogel study.[209]

5.3.4 Monotonic Mechanical Characterization of Samples with Macroscale Flaws

Using 4 FT and 2 FT samples as starting blocks, the next portion of this study set out to characterize the impact of two different macroscale flaw types on the tensile

strength of the PVA hydrogel. The flaws utilized were 0.5 mm, 1 mm, 2 mm, 3 mm and 4 mm sharp cracks as well as 0.5 mm, 1 mm, 2 mm, 3 mm, and 4 mm cylindrical holes. Tensile properties of the PVA hydrogel were analyzed using the customized sample shape depicted in Figure 31B for sharp cracks and Figure 31C for cylindrical holes depending on the chosen hole diameter, with the testing rate remaining the same from the FT screening process at 15 mm/min. Further consideration of the introduction of flaw type during synthesis (before or after freezing-thawing) may be considered in future work. The results of this testing for 2 FT cycles can be seen below in Figure 36A for sharp cracks and Figure 36B for cylindrical holes. Accordingly, the results of this testing for 4 FT cycles can be seen below in Figure 36C for sharp cracks and Figure 36D for cylindrical holes. The area used to calculate the stress values was the load bearing area, taking into account the dimension of the given flaw. The force divided by the load bearing area for these tests is called the “nominal stress”, as provided on the y-axis.

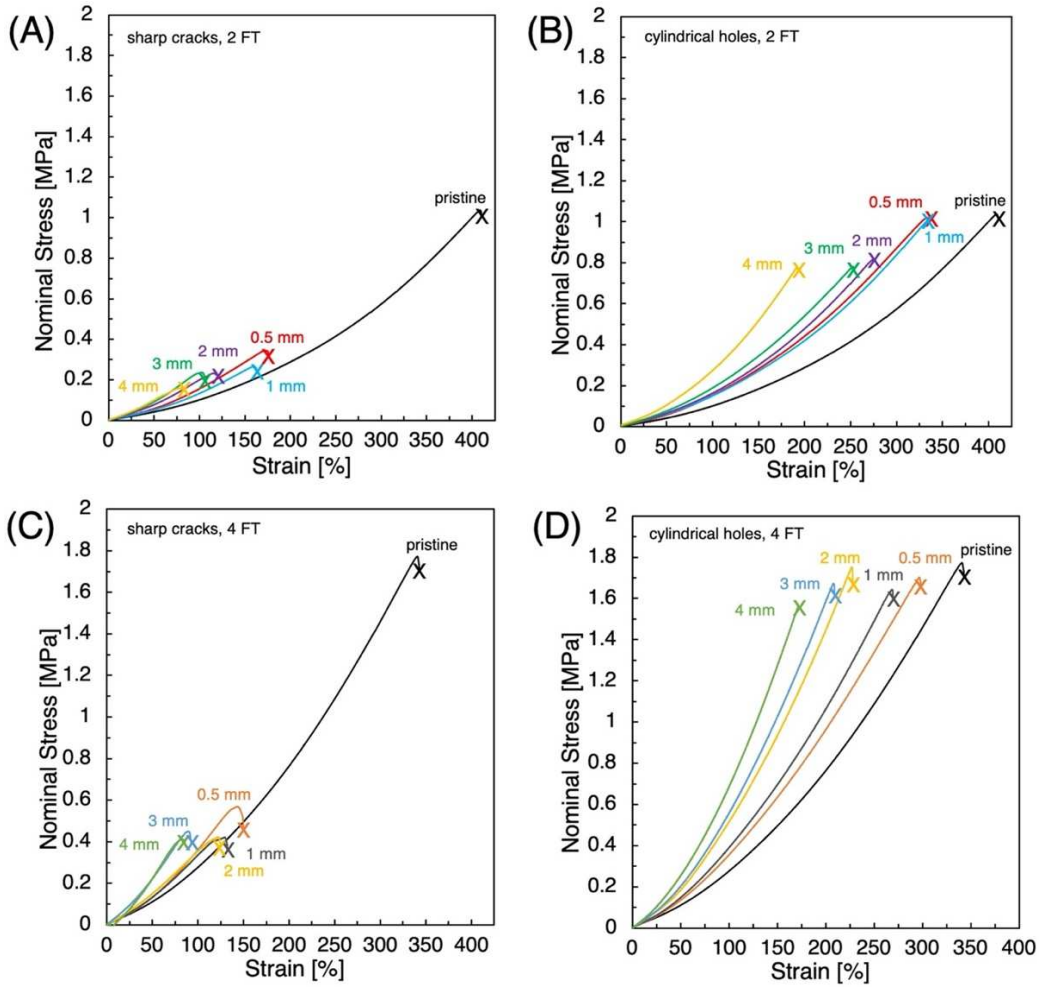

Figure 36: Nominal tensile stress-strain behavior for pristine, 0.5, 1, 2, 3, and 4 mm sharp crack 2 FT (A) and 4 FT (C) PVA samples, and pristine, 0.5, 1, 2, 3, and 4 mm cylindrical hole 2 FT (B) and 4 FT (D) PVA samples in monotonic tension for the customized, thicker fatigue sample shape.

In evaluating Figure 36, samples with a sharp crack experienced a significantly greater degree of ultimate tensile strength loss than those with a cylindrical hole. As the dimension of the flaw increased, the failure strain became smaller for both sharp crack and cylindrical hole samples. Samples that had undergone 4 FT cycles with cylindrical

holes did not experience the same gradual decline in ultimate tensile strength as compared to samples that had undergone 2 FT cycles with cylindrical holes. The goal of comparing cylindrical hole and sharp crack in 2 FT and 4 FT cycles was to obtain a possible similarity in properties across different flaw types to investigate in tensile fatigue testing. As seen in Figure 36, the 0.5 mm sharp crack and 4 mm cylindrical hole have comparable failure strain values for both 2 FT and 4 FT cycles. In this way, tensile fatigue testing can be carried out in a displacement-controlled manner based on failure strain to compare the cylindrical hole and sharp crack across different FT cyclic processing steps. As a result, these two specific flaw types and dimensions (0.5 mm sharp crack and 4 mm cylindrical hole) were selected for completing tensile fatigue testing for the development of a fatigue life curve.

Two simple models were used to evaluate the losses in mechanical properties with flaws, one based on nominal stress (load bearing area impact) and another based on fracture mechanics for a Modified Single Edge-Crack tension specimen, known as MSE(T).[242] For the purposes of this discussion, the terms “fracture mechanics”, “stress intensity”, and “Modified Single Edge-Crack tension” will be used interchangeably. The process of creating these two models can be found in the Experimental Section. Briefly, the nominal stress model simply considers a decrease in sample area to translate to a proportional drop in sample strength. This model gives way to an upper bound in predicting loss of strength in the presence of a flaw (i.e., smallest possible strength loss

for a given flaw size). On the other hand, the fracture mechanics model gives way to a lower bound in predicting loss of strength in the presence of a flaw (i.e., greatest possible strength loss for a given flaw size). Comparison of experimental data to these two models can be seen in Figure 37A for 2 FT cycles and Figure 37B for 4 FT cycles.

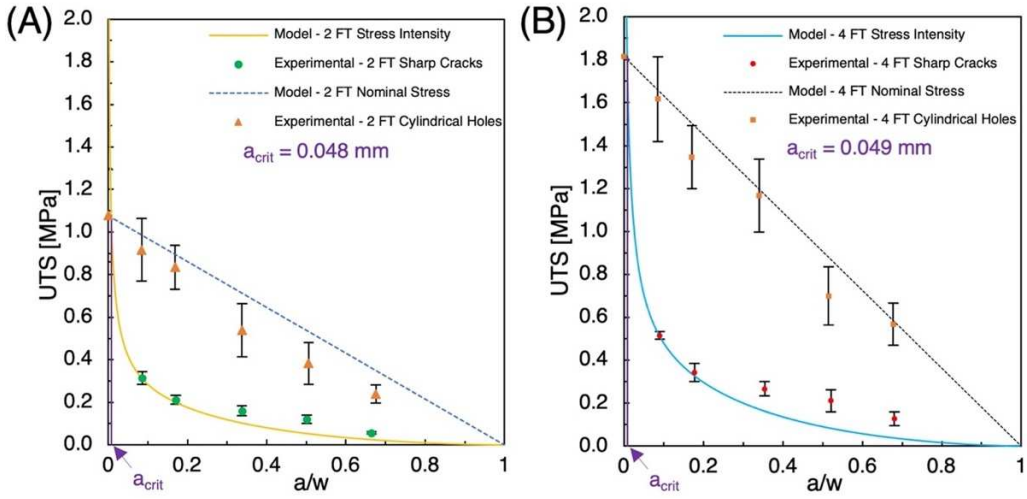

Figure 37: Comparison of experimental tensile strength with nominal stress and stress intensity models for varying cylindrical holes and sharp cracks for (A) 2 FT and (B) 4 FT cycle PVA samples. The x-axis a/w is defined as the ratio of the flaw size "a" to the width of the sample "w".

The results in Figure 37 highlight the extreme sensitivity of both 2 FT and 4 FT hydrogels toward the type of flaw despite the ability of the material to deform significantly and blunt flaw geometry. The experimental strength dropped dramatically for even the smallest sharp crack flaw of 0.5 mm. This large decrease was not observed in the cylindrical hole defect from pristine to 0.5 mm cylindrical hole. In observing these trends, the PVA hydrogels were far more sensitive to the crack-based flaw as opposed to

the cylindrical hole-based flaw, as originally hypothesized and common for other much stiffer non-hydrogel materials. The geometric shape change of the cylindrical hole-based flaw shows effective blunting in comparison to the intensification of local stresses at the tip of the crack-based flaw which blunts, but much less effectively. In addition, the data in Figure 37 confirmed an accurate deployment of the two extreme models. The stress intensity (fracture mechanics) model provided a lower bound of strength loss, while the nominal stress (load bearing impact) model provided an upper bound of strength loss. The experimental data trend for crack-based flaws finished above the model due to the difficulty of perfectly ensuring the crack tip came to a sharp, geometrical point. This was unrealistic to provide a perfect crack tip, just as it would be in practical applications of sustaining such damage. The experimental data trend for the cylindrical hole-based flaws fell slightly below the predicted nominal stress model due to idealistic nature of the model. It accounted for pristine samples with no other defects present in order to show a proportional drop in strength from sample area, and this was difficult to ensure experimentally. The critical flaw size was determined from the intersection of the stress intensity model curve and nominal stress model curve. Assuming a 6 mm width for a sample, this value was 0.048 mm for 2 FT cycle samples and 0.049 mm for 4 FT cycle samples. As such, in theory, any flaw larger than about 50 micrometers would ensure rapid loss in ultimate tensile strength for the hydrogel samples at a rate much more

significant than loss of load bearing area. Flaws smaller than 50 micrometers would have, in theory, minimal impact on the hydrogel strength under monotonic loading.

5.3.5 Progression and Development of Flaw Type in Cyclic Tensile Testing

The remaining work of this study sought to characterize the progression and development of flaws under cyclic loading. As previously mentioned, the sensitivity of hydrogels toward a specific type of flaw is critical to understand what type of damage and how long will it take to lead to untimely failure. For this testing, PVA hydrogel samples were prepared with 2 FT and 4 FT cycles with 0.5 mm sharp cracks and 4 mm cylindrical hole-based flaws, respectively. The monotonic tensile data from Figure 37 was used to establish an average failure strain and subsequent standard deviation levels (minimum n=7 tests for each flaw type and size). Table 6 illustrates the target failure strain testing levels for 2 FT and 4 FT cycles of both cylindrical holes and sharp cracks.

Table 6: Target failure strain testing levels for PVA samples with 2 FT and 4 FT cycles with cylindrical holes and sharp cracks.

Sample Type	0.5σ	1σ	2σ	3σ
2 FT – 0.5 mm sharp crack	175.10%	171.99%	165.79%	159.58%
2 FT – 4 mm cylindrical hole	184.53%	171.24%	144.65%	118.05%
4 FT – 0.5 mm sharp crack	149.65%	146.82%	141.16%	135.51%
4 FT – 4 mm cylindrical hole	175.76%	166.24%	147.20%	128.16%

These flaw types were selected due to the similarity in their failure strain values, and they were tested in a strain-controlled manner at a constant strain rate of 2.6 s^{-1} based on the strain levels in Table 6. This strain rate was used to reduce the total time for each test with the assumption of samples lasting 100,000 cycles (runout samples). In addition, this strain rate aimed to prolong tensile loads before buckling of the sample became a more prominent effect in keeping the sample in a compressed state rather than a stretched one.[209] Both types of flaws for 2 FT and 4 FT samples had different monotonic failure strains as seen in Table 6. As a result, the testing amplitudes and frequencies had to be slightly adjusted for the applied strain rate of 2.6 s^{-1} to remain approximately constant across all tests.

Both the 2 FT and 4 FT systems were analyzed with four tests (n=4) at four different standard deviations levels (0.5σ, 1.0σ, 2.0σ, and 3.0σ) to make for a total of 16 samples for each type of flaw (0.5 mm sharp crack and 4 mm cylindrical hole). Nominal stress versus strain over cyclic loads for 2 FT and 4 FT at one standard deviation level from the failure strain for both 0.5 mm crack and 4 mm cylindrical hole samples can be seen as Figure 38.

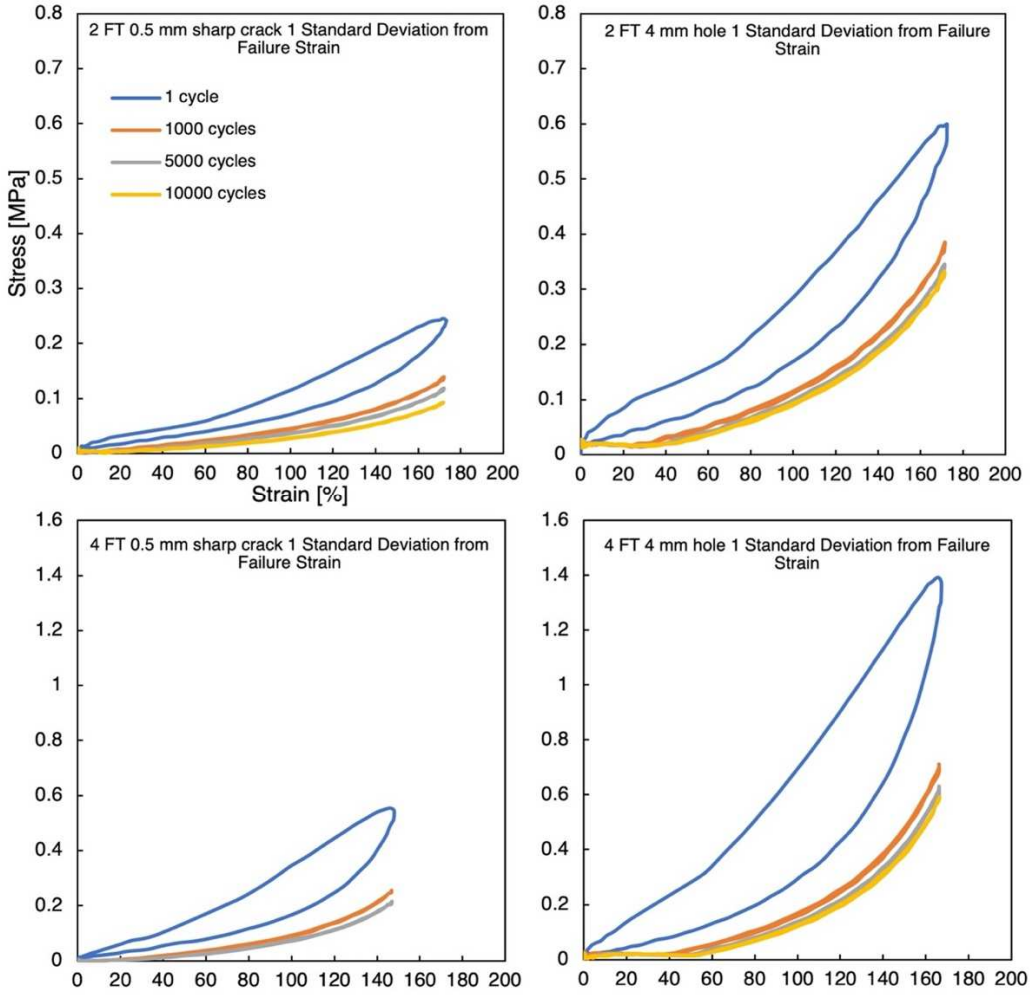

Figure 38: Nominal stress versus strain over cyclic loads for 2 FT and 4 FT at one standard deviation level from the failure strain for both 0.5 mm crack and 4 mm cylindrical hole.

A plot of strain range vs. cycles to failure can be seen in Figure 39A for 2 FT cycles Figure 39B for 4 FT cycles.

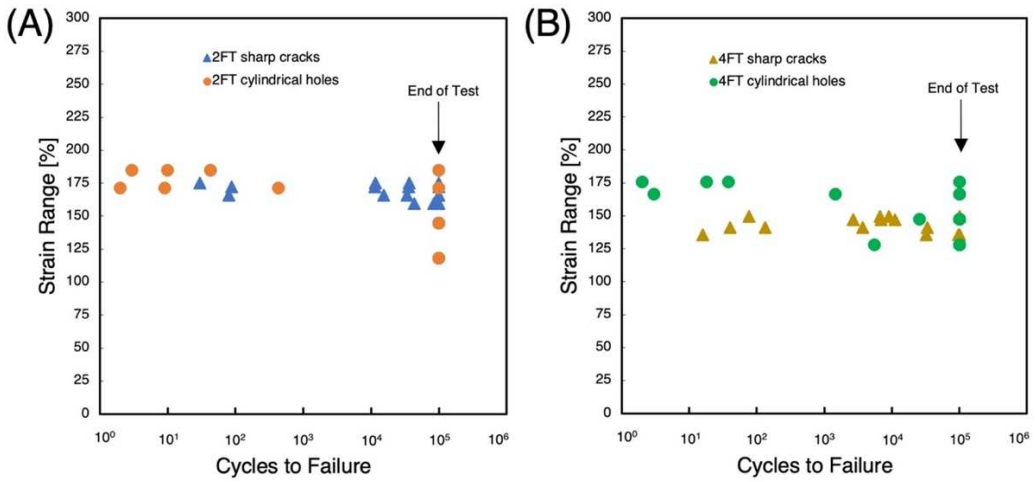

Figure 39: Tensile fatigue data for (A) 2 FT and (B) 4 FT PVA samples with sharp cracks and cylindrical holes based on strain range as a function of cycles to failure. A sample that lasted 100,000 cycles without failure was considered a "runout" sample with an arrow indicating its position in the graph. Four strain levels for both the cylindrical hole and sharp crack samples were utilized for 2 FT and 4 FT (0.5σ, 1.0σ, 2.0σ, and 3.0σ). Once 100,000 cycles were completed, the test was concluded.

As shown in Figure 39, cylindrical hole samples for both 2 FT and 4 FT cycles had more runout samples. Failure of a sample before 100,000 cycles was defined as a complete tear of the sample. Some cylindrical hole samples completed 100,000 cycles as a semicircle (i.e., one half of the circle had broken during the test, leaving the other half intact for the remainder of the test). However, this was not defined as failure of the sample due to part of the sample remaining. In addition, some crack-based samples from 2 FT and 4 FT experienced crack growth to varying degrees over the duration of the test. However, this damage accumulation was not considered a failure since complete tearing of the sample was not achieved. In this sense the runout samples should not be considered "safe-life" endurance limit samples, where stresses below this

result in no fatigue damage progression. Even the runout samples often had visible damage progression in terms of growing flaws.

The data shown in Figure 39 makes it difficult to ascertain sample performance across different failure strain testing levels with each flaw type. In order to fully characterize the results of fatigue testing, each sample was reviewed for the tensile nominal stress range experienced at the median time point of the test according to our previous work.[209] Median tensile nominal stress range was defined as the maximum tensile nominal stress the sample experienced at the median time point of the test. In testing these samples in a strain-controlled manner with constant strain rate, tensile stresses must be invoked to compare samples with different failure strain values. As a result of the samples slightly buckling in the progression of a test, only tensile nominal stress at the median time point was considered in instead of compressive ones brought on as the samples experienced stress relaxation. All samples were evaluated for their median life tensile nominal stress range, and the results of this analysis can be seen in Figure 40A for 2 FT samples and Figure 40B for 4 FT samples. The area used to calculate these tensile fatigue stress values was the load bearing area, taking into account the dimension of the given flaw. The force divided by the load bearing area for these tests is called the “median life tensile nominal stress range”, as provided on the y-axis.

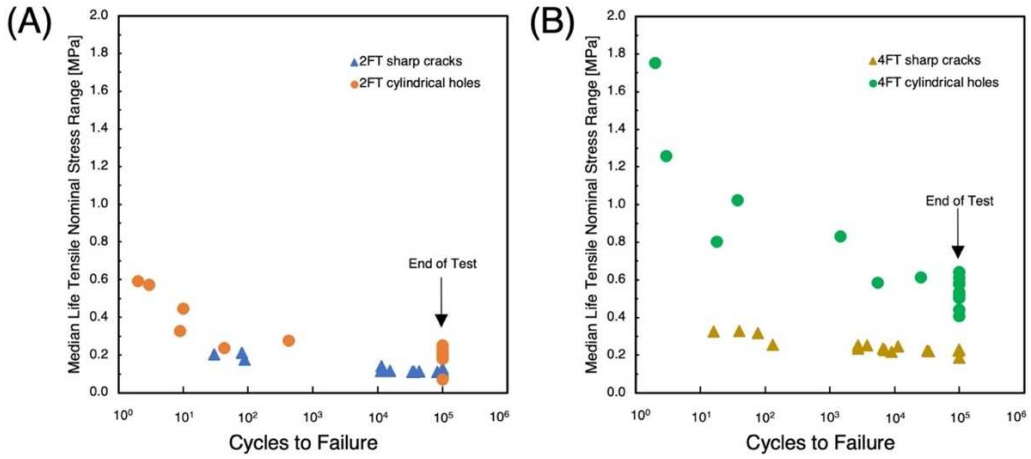

Figure 40: Tensile fatigue data for (A) 2 FT and (B) 4 FT PVA samples with sharp cracks and cylindrical holes based on median life tensile stress range as a function of cycles to failure. A sample that lasted 100,000 cycles without failure was considered a "runout" sample with an arrow indicating this position in the graph. A sample reaching 100,000 cycles marked the end of the test.

In comparing the median life tensile stress range of samples tested, it became clear that samples with much smaller 0.5 mm cracks performed worse than samples with much larger 4 mm cylindrical holes in stress-life space. Furthermore, the 0.5 mm sharp cracks that underwent 4 FT cycles outperformed the 0.5 mm sharp cracks that underwent 2 FT cycles. The same assertion can be made for 4 FT cylindrical holes with respect to 2 FT cylindrical holes. These trends from fatigue testing were consistent with the trends observed in monotonic tensile testing in Figure 36 which implies the increases in monotonic toughness translated to increases in fatigue strength. Tensile fatigue stress threshold was defined here as the largest median tensile nominal stress a sample had endured without failing completely. These values were: 0.1082 MPa for 2 FT-0.5 mm sharp crack, 0.2274 MPa for 2 FT-4 mm cylindrical hole, 0.1865 MPa for 4 FT-0.5 mm

sharp crack, and 0.5812 MPa for 4 FT-4 mm cylindrical hole. Again, damage was still often progressing at these stress levels and with further cycling the samples would likely fails so this stress threshold is not a classical "endurance limit". This fatigue data can be explained in considering the amplification of local stresses at the tip of a sharp crack. These local stresses were far more damaging than a cylindrical hole that did not have a site of extremely concentrated, amplified stress. The stresses in the cylindrical hole samples were more evenly distributed as opposed to the samples with a sharp crack. Although these effects are well known in the fatigue of harder materials, they have not been previously demonstrated in soft, wet hydrogels.

For a complete analysis of the impact of freeze-thaw cyclic processing on monotonic and fatigue behavior, tensile stress values were analyzed across different sample shapes, flaw geometries and testing types for both 2 FT and 4 FT cycles. Ultimate tensile strength was used for monotonic tensile testing, while median life tensile nominal stress range was utilized for tensile fatigue testing in this comparison of additional freeze-thaw cyclic steps. These results are compiled in Table 7, including the percentage increase from 2 FT cycles to 4 FT cycles.

Table 7: Comparison of tensile strength for different sample shapes, flaw geometries, and testing types for both 2 FT cycles and 4 FT cycles.

Sample Type	2 FT cycles [MPa]	4 FT cycles [MPa]	Percentage Increase [%]
No Flaw – Type V shape, Monotonic Testing, Ultimate Tensile Strength (UTS)	0.8042	2.3814	196.1
No Flaw – Custom Fatigue shape, Monotonic Testing, UTS	1.0781	1.8159	68.4
0.5 mm sharp crack – Custom Fatigue Shape, Monotonic Testing, UTS	0.3425	0.5664	65.3
4 mm cylindrical hole – Custom Fatigue Shape, Monotonic Testing, UTS	0.7399	1.7605	137.9
0.5 mm sharp crack – Custom Fatigue Shape, Fatigue Testing, Median Life Tensile Nominal Stress Range	0.1082	0.1865	72.3
4 mm cylindrical hole – Custom Fatigue Shape, Fatigue Testing, Median Life Tensile Nominal Stress Range	0.2274	0.5812	155.6

In all cases, the samples experience an increase in tensile stress values when comparing 2 FT to 4 FT cycles. The greatest jumps in additional freeze-thaw cyclic steps were realized for pristine-Type V shape-monotonic testing, 4 mm cylindrical hole-Fatigue shape-monotonic testing, and 4 mm cylindrical hole-Fatigue shape-fatigue testing. Furthermore, the stress values drop from those without defects and monotonic loading, to those with defects and monotonic loading, and finally to those with defects and fatigue loading. Moving forward, researchers must apply caution in exclusively

evaluating increasing the strength/toughness of their hydrogels without giving attention to the impact of various defects and loading profiles (cyclic versus monotonic). In this study the impact of increased toughness and strength was most significant when measured in a perfect, flaw-free sample. Samples with crack-like defects showed an increase in fatigue strength when monotonic toughness was increased, but not with the same relative quantitative impact.

5.3.6 Conclusion of Flaw Sensitivity and Tensile Fatigue of Poly(Vinyl Alcohol) Hydrogels

In the realm of soft materials, this flaw analysis and subsequent fatigue examination are critical for understanding the initiation and progression of sustained damage toward untimely material failure. Often times, researchers seek to make flaw- or notch-insensitive hydrogels to show resistance to failure. In a practical sense, it is extremely difficult to prevent all types of damage from occurring. This relentless pursuit leaves a critical question for synthetic hydrogels with biomedical applications: What kind of damage is sustainable before it develops and progresses to long-term failure? Unfortunately, this pursuit of creating tough, flaw-insensitive hydrogels has created an enormous need in understanding the effects of unplanned, sustained damage with relation to long-term mechanical behavior. It has become essential to study the progression of different flaw types as it relates to fatigue properties to screen synthetic hydrogels for their suitability in biomedical applications. The nominal stress and stress

intensity analysis created upper and lower bounds for the largest strength loss (sharp crack) and smallest strength loss (cylindrical hole). The fatigue study utilized in this work demonstrated that early failure of a synthetic hydrogel may come from flaws assumed to have no major impact and difficult to observe upon material synthesis. Hydrogels can only be trusted for long-term use if their resistance and response to flaws has been well-characterized across flaw types and *cyclic* loading regimes (low *and* high cycle fatigue).

In conclusion, PVA hydrogels present an excellent model system to understand the progression of flaws as it relates to long-term mechanical behavior. In further characterizing soft materials of similar tunable mechanical properties, PVA hydrogels provide a strong foundation for advanced tensile study for even more biomedical applications. High level control over the mechanical properties was attained via control over the freezing-thawing cyclic processing steps to maximize toughness. This work set out to characterize the fatigue behavior of PVA-based hydrogels with different flaw types of sharp cracks and cylindrical holes. A screening process of a hydrogel's toughness was employed, and it was highly dependent on the number of freezing-thawing cycles. The swelling ratio and crystallinity of samples were also contingent upon the same freezing-thawing cyclic process. The shape of the prepared hydrogels was adjusted to accommodate for a larger range of possible dimensions for flaws from 0.5 mm to 4 mm. Two models were created to account for the strength loss of a hydrogel

sample based on its given type (sharp crack or cylindrical hole) and size. Flaws of controlled dimension were then used for tensile fatigue testing to understand progression of damage toward early sample failure. Hydrogel specimens with a sharp crack of 0.5 mm and cylindrical hole of 4 mm were employed in tensile fatigue testing to generate the strain range curve and subsequent median life tensile nominal stress range curve. As a result of these tests, it was concluded that additional freeze-thawing cycles improved fatigue behavior from 2 FT to 4 FT. In addition, the sharp 0.5 mm cracks for both 2 FT and 4 FT performed poorly in comparison to their 4 mm cylindrical hole counterparts. The cyclic, tensile portion of this study aimed to shed light on the importance of characterizing flaw behavior as it relates to long-term use of soft materials in biomedical applications.

To summarize, the specific deliverables of this aim were the following:

- Successful selection of freezing-thawing cycle number through optimal enhancement of monotonic toughness
- Proper identification of two flaw systems of varying dimension for monotonic tensile testing
- Comparison of hydrogels with same flaw under fatigue tensile testing
- Development of a fatigue life curve for different hydrogels with similar flaw systems

5.4 Experimental Section of Flaw Sensitivity and Tensile Fatigue of Poly(Vinyl Alcohol) Hydrogels

5.4.1 Materials

The poly(vinyl alcohol) (PVA, molecular weight (M_w) 85,000 – 124,000 Da, 99+% hydrolyzed) in this study was used without further purification and purchased from Sigma-Aldrich, St. Louis, MO, USA. Deionized water used in this study was supplied from a Pureflow Inc. Portable Exchange Type II system. Stainless steel dowel pins were acquired from McMaster Carr, Atlanta, GA, USA and Amazon.com, Inc., Seattle, WA, USA. A razor blade was used to create sharp cracks of specified lengths.

5.4.2 Material Preparation

For preparation of PVA hydrogel samples, (9.518 g) PVA was combined with deionized water (50 mL) in 100 mL round bottom flask. This mixture was sealed with a rubber septum, and it was heated and stirred for a minimum of three hours at 95°C in an oil bath until the PVA was fully dissolved to form a homogenous solution. Once fully dissolved, the resulting solution was then removed from the 95°C oil bath and sonicated for roughly 30 seconds to one minute to remove any bubbles close to the surface. The hot solution was then poured into stainless-steel molds that matched the dimensions of the ASTM D638-14 Type V shape for monotonic tensile testing, swelling studies, and DSC characterization.[141] Fatigue tensile specimens were prepared in the same manner in a

customized, stainless-steel mold that had a thicker gauge section. The hot solution was poured into the mold, parafilm was utilized to cover the mold, and tape was used over the top of the parafilm to create a sufficient seal. For fatigue samples with controlled cylindrical defects, a metal hollow punch was used to create a hole in the parafilm that aligned with the center of the gauge section. The hot solution would be poured into the mold with the parafilm placed on top. Next, stainless-steel dowel pins of varying diameters were placed into the hole of the parafilm for each sample, and tape was placed over top of the pin. For example, a 1.5 mm hollow punch was used for a 2 mm cylindrical defect to create a sufficient seal around the stainless-steel pin. Stainless-steel dowel pins were utilized as purchased. When freeze-thawing (FT) cyclic processing was complete, pins were easily removed from the gauge section of the hydrogel to create cylindrical holes of controlled diameters. For fatigue samples with controlled sharp crack defects, a razor blade was used to create this crack once FT cyclic processing was complete. The molds were frozen at -23°C for 20 hours followed by 4 hours of thawing at 20°C to complete one freeze-thawing cycle (1 FT). This freezing and subsequent thawing process was repeated for two through 8 freeze-thawing cycles (2 FT through 8 FT). Depending on the number of FT cycles employed, the samples were easily removed from the stainless-steel molds using a spatula and characterized for their properties. Type V samples and fatigue samples were stored in deionized water until monotonic or fatigue tensile testing and DSC characterization had occurred.

5.4.3 Mechanical Testing

Monotonic tensile measurements were carried out using a 50-lb load cell on either an Instron 1321 (Instron, Norwood, MA, USA) instrument or a TestResources 830 (TestResources, Shakopee, MN, USA) load frame. Comparison of monotonic tensile toughness results was completed with one-way analysis of variance (ANOVA); α=5%; * depicts statistical significance in the following manner: * $p<0.05$; ** $p<0.01$, *** $p<0.001$, **** $p<0.0001$. All fatigue tests were completed on the Instron 1321, while an extensometer was used to determine an experimental effective length for both monotonic and fatigue samples on the TestResources 830 load frame with a 50-lb load cell. Monotonic tension samples were prepared from an ASTM D638-14 Type V shape, tested at a rate of 0.25 mm s^{-1}, and led to the compilation of results from corresponding individual stress-strain curves. Once the screening process of the FT cycles in the Type V shape was complete, the thicker fatigue-shaped samples were tested for monotonic tensile comparison with sharp cracks of controlled lengths (0.5 mm, 1 mm, 2 mm, 3 mm, and 4 mm) and cylindrical holes of controlled diameters (0.5 mm, 1 mm, 2 mm, 3 mm, and 4 mm) at a rate of 0.25 mm s^{-1}. For the purposes of discussion, the term "cut" is interchangeable with "sharp crack". Fatigue samples were prepared from a customized shape in order to characterize larger flaw sizes as well as prevention of sample buckling

during cyclic tests. A tap water bath at 37°C was used to prevent samples from drying out during cyclic testing of fatigue samples.

Upon analyzing these tests with respect to nominal stress and stress intensity models (see Stress Intensity Model and Nominal Stress Model in later sections), this study shifted focus to the progression and development of both flaw types as it related to long-term, cyclic testing. To compare materials of similar properties across different flaws of 2 FT and 4 FT cycles, Figure 36 was consulted. It was determined that similar failure strain values for 0.5 mm sharp crack and 4 mm cylindrical hole would provide the best comparison under similar testing conditions. As such, there became four distinct combinations to be tested: 0.5 mm sharp crack of 2 FT cycles, 0.5 mm sharp crack of 4 FT cycles, 4 mm cylindrical hole of 2 FT cycles, and 4 mm cylindrical hole of 4 FT cycles. For the fatigue analysis of both the 2 FT and 4 FT samples, a strain rate of 2.61 s^{-1} was utilized in order to retain prolonged tensile loads before buckling of the sample became a dominating effect as determined in our previous work.[209] The 0.5 mm sharp crack and 4 mm cylindrical hole had slightly different monotonic failure strains, which ultimately led to adjusting the testing amplitudes and frequencies in order for the applied strain rate to remain constant across all tests. With all distinct testing combinations mentioned previously, it was decided to conduct n=4 tests at each of the standard deviation levels (0.5σ, 1σ, 2σ, and 3σ) for a total of 16 samples for each combination.

5.4.4 Hydrogel Swelling

The ability of all FT cycles to uptake water was measured by recording the mass variation of the hydrogels after swelling in a 15 mL centrifuge tube of deionized water (12 mL) at room temperature for 24 hours. Samples were prepared in the ASTM D638-14 Type V shape. Excess water on the external surface of the hydrogels was removed by lightly tapping the samples on a piece of filter paper. The samples were then weighed and subsequently dried to constant weight at 80°C for 20 hours in a Yamato drying oven. The ratio of the swollen weight to the dry weight was used to calculate a swelling ratio, q, below. The swelling ratio (q) of the hydrogel samples was defined as the ratio of the weight of swollen sample (W_s, swollen in deionized water for 24 hours) divided by the weight of the fully dried-out sample (W_d, dried out at 80°C for 20 hours to constant weight) in Equation 2.

$$q = \frac{W_s}{W_d} \quad (2)$$

Each reported swelling ratio is an average of three parallel measurements.

5.4.5 Differential Scanning Calorimetry (DSC)

All FT cycles were characterized for their crystallinity via DSC measurements on a Discovery DSC (TA Instruments, New Castle, DE, USA). Hydrogel samples were prepared in the ASTM D638-14 Type V shape. For each analysis, the hydrogel sample

(about 5 to 7 mg) was placed into a Tzero aluminum pan with a flat Tzero lid pressed into place. The following protocol for DSC measurements was used: equilibrate to 40°C, isotherm for 1 min, ramp 10°C/min to 250°C, isotherm for 3 min, ramp 10°C/min to 40°C, isotherm for 3 min, ramp 10°C/min to 250°C, isotherm for 3 min, and ramp 10°C/min to 40°C. The percent crystallinity was calculated from the first heating curve to be representative of the freeze-thaw procedure that the sample underwent before DSC analysis. DSC scans were repeated on fresh samples for a minimum of n=4 for each FT cycle.

5.4.6 Stress Intensity Model

All samples tested were in the thicker, customized fatigue shape for 2 FT and 4 FT cycles. Monotonic tensile testing according to *Mechanical Testing* was employed to establish the tensile strength values. As for terminology, a was defined as the length of the crack, h was defined as the height of the sample's gauge section, and w was defined as the width of the sample's gauge section. The x-axis of modeling and experimental data was simply a ratio of the crack length, a, to the width of the sample gauge section, w. For creation of the modeling data, the non-dimensional geometric correction factor, β, was used as defined according to Equation 5 of Hammond et al.[242] This correction factor was calculated for each individual sample of both 2 FT and 4 FT (minimum n=7) for a sharp crack of 0.5 mm (the smallest crack dimension that could be reliably reproduced

with a razor blade). In the same manner as Equation 1 of Hammond et al.,[242] the stress value σ was also calculated based on the applied tensile load, thickness of the sample, and width of the sample (independent of the crack length).[242] In combination with the σ values, the β values were then used to calculate a K_i, or stress intensity factor, according to Equation 2 of Hammond et al. for each 0.5 mm crack-based sample.[242] An average K_i value was established among the samples for 2 FT cycles (K_i = 0.467 MPa $mm^{1/2}$) and 4 FT cycles (K_i = 0.789 MPa $mm^{1/2}$).

Once calculated, the K_i values for 2 FT and 4 FT, respectively, were held constant in order to create a new β value from systematically varying values of crack length *a* (from 0.01 mm to 6 mm) and holding the width *w* at a constant value of 6 mm. In this way, a new stress value could be obtained via the constant K_i value, constant *w* value, and unique β value based on the particular selection of crack length *a* (as observed in Equation 2 of Hammond et al).[242] These stress values were plotted against the ratio of the selected *a* value to constant *w* value (6 mm) to establish the stress intensity model. Experimental stress values were based on the area of the sample with the assumption of no crack present (i.e., height x width independent of crack length). These results were plotted against the ratio of the measured crack length *a* to the measured width *w*. Error bars were included to express the standard deviation value for each experimental tensile strength value.

5.4.7 Nominal Stress Model

All samples tested were in the thicker, customized fatigue shape for 2 FT and 4 FT cycles. Monotonic tensile testing according to *Mechanical Testing* was employed to establish the tensile strength values. As for terminology in this model, *a* was defined as the diameter of the cylindrical hole, *h* was defined as the height of the sample's gauge section, and *w* was defined as the width of the sample's gauge section. The x-axis of modeling and experimental data was simply a ratio of the cylindrical hole diameter, *a*, to the width of the sample gauge section, *w*. For both modeling and experimental data, stress was calculated based on the area of the sample with the assumption of no cylindrical defect present (i.e., height x width independent of cylindrical hole diameter). Model data was established by taking the average ultimate tensile strength of a sample with no defect present (i.e., at y-axis intercept) as a data point. A line was then fitted from this data point to the x-axis intercept, establishing the model. Essentially, this model was created from the idea that a decrease in sample area meant a proportional decrease in sample strength. The experimental stress data compared to this model was calculated in the same manner independent of the cylindrical hole diameter. The average ultimate tensile stress was computed for 0.5 mm, 1 mm, 2 mm, 3 mm, and 4 mm cylindrical holes. These results were plotted against the ratio of the measured diameter *a* to the measured width *w*. The critical flaw size, a_{crit}, was determined to be the intersection of the stress intensity model with the nominal stress model. In this sense, a

sample with a flaw size below the value of a_{crit} was predicted to have no impact on the sample's strength. Any sample with flaw larger than a_{crit} was sensitive to the particular flaw type and dimension. Error bars were included to express the standard deviation value for each experimental tensile strength value.

Chapter 6. Flaw Sensitivity and Tensile Fatigue of a High-Strength Hydrogel and Porcine Cartilage

6.1 Motivation

The work presented in Chapter 5 provided PVA hydrogels as an excellent model system to track the growth of flaws and subsequent long-term mechanical behavior. The PVA hydrogels were created through a facile synthetic process, and their tunable mechanical properties created a groundwork to build on for further tensile study. However, these PVA hydrogels matched suitably with the chosen models as high-strain, lower-strength materials. An exciting opportunity exists in conducting similar analysis on a higher strength hydrogel such as the PVA-based composite from Chapter 5 for load-bearing applications. Mechanical characterization of this stronger hydrogel's response to sharp cracks and cylindrical holes would provide valuable information on the full range of applications for these soft materials. Insight would be gained not just for monotonic behavior but also for cyclic behavior. Furthermore, a source of biological tissue such as porcine cartilage could be utilized for parallel mechanical study for

comparison to the lower strength PVA hydrogels and higher strength PVA-based composite. The work in Chapter 6 investigates the mechanical response to flaws in both monotonic and cyclic testing for the PVA-based composite from Chapter 4 and porcine costal cartilage. The central hypothesis of this work revolves around the ability to replicate last chapter's observation that sharp, crack-like flaws are more damaging than blunted, cylindrical hole-like flaws. In addition, this chapter hypothesizes that the porcine costal cartilage and the stronger BC-PVA-PAMPS hydrogel composite will not be as flaw sensitive as the PVA-only hydrogel.

6.2 Introduction – Soft Materials and Biological Tissue Models

The desire for a comprehensive understanding of structure-property relationships in soft materials has created a plethora of research on hydrogels. [247–249] Given their tunability of mechanical properties such as stiffness, hydrogels have been increasingly pursued for wide-ranging applications from the repair or replacement of cartilage to drug delivery carriers. [228–231] With minimal exceptions, hydrogels are developed to be as mechanically strong or tough as possible, especially if the goal is to mimic soft biological tissue. For hydrogels to be used in the human body as tissue-like materials, it is critical to characterize their mechanical behavior in the presence of geometric defects or flaws. Researchers have given particular attention to developing hydrogels that are "flaw-insensitive" or "notch-insensitive". [135,233–237] However, the

impact of flaws on the strength of hydrogels has not been considered relative to extracted biological tissues. Biological tissues experience damage due to various biological disease states and mechanical trauma. This damage may come in the form of a single acute event or repetitive chronic events before catastrophic failure is observed. Prior to employing a hydrogel as a substitute for biological tissue, sufficient mechanical robustness must be displayed under appropriate loading conditions and defected material states. Full understanding of the hydrogel's response to defects must be explored and evaluated relative to a biological tissue model to create a benchmark for performance in the absence of biological healing.

To investigate the clinical suitability of synthetic hydrogels for soft tissue repair or replacement, their mechanical properties should be compared to a wide range of biologic tissues such as tendon, muscle, and cartilage. While human cadavers provide the most accurate tissue source for mechanical characterization, a number of animal models offer a more cost-effective alternative while maintaining a high degree of mechanical similarity. [250–252] Due to the cost differences of working with animal tissue as opposed to cadaver tissue, there exists a unique opportunity to select a tissue model from animals for comparison of hydrogel performance. Porcine cartilage fills this void due to its similarity to human cartilage in terms of mechanical properties. [250,251,253] In this study, porcine costal cartilage was chosen as a biologic model for tensile testing. A cartilaginous structure was desired given the growing interest in hydrogels as potential

cartilage analogues, and porcine costal cartilage offered a large surface area from which to extract tensile samples. This cartilage serves as a prospect to compare tensile strength with respect to flaw type and size in a biological tissue.

A simple model based on lower and upper bound of tensile strength with respect to flaw system and dimension has been employed in previous work with soft, large strain poly(vinyl alcohol) hydrogels. [209] However, this model has not been applied to a higher strength, lower strain-to-failure hydrogel that would be suitable for tissue implant applications. The present work aimed to test the application of these models for a promising hydrogel candidate for the repair or replacement of soft tissue. The synthetic material is a BC-PVA-PAMPS hydrogel, and its preparation can be found in Section 2.1 Fabrication of BC-PVA-PAMPS hydrogel in the Supplementary Information of Yang et al. (2020). [208] By studying this material in the flawed state of prior work, a high-strength hydrogel such as the BC-PVA-PAMPS hydrogel can be compared to its much softer PVA hydrogel counterpart. In addition, porcine costal cartilage harvested from the rib was tested using the same tensile and flaw models from 5.4 Experimental Section of Flaw Sensitivity and Tensile Fatigue of Poly(Vinyl Alcohol) Hydrogels for comparative purposes to the synthetic BC-PVA-PAMPS hydrogel. For succinct reference for the remainder of this chapter, BC-PVA-PAMPS will be referred to as “hydrogel” and porcine costal cartilage will be referred to as “cartilage”.

6.3 Results and Discussion

6.3.1 Sample Geometry

Using tensile techniques from prior work, a customized sample shape was designed for both the hydrogel and cartilage. The samples were produced through a titanium punch fabricated using 3D printing via selective laser melting. An image of the resulting hydrogel and cartilage samples is in Figure 41.

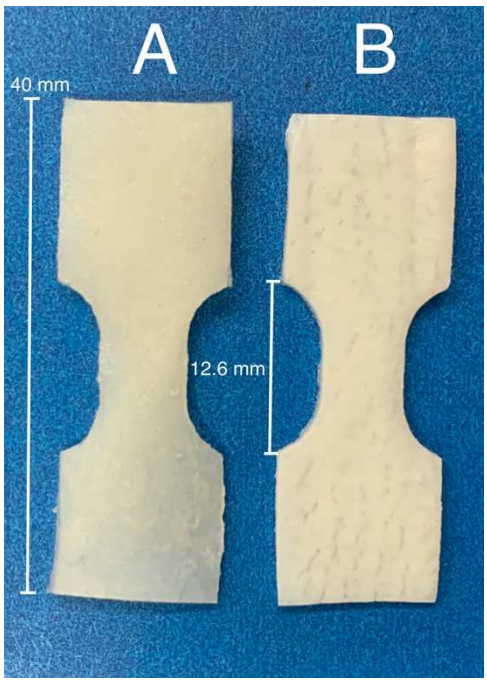

Figure 41: Customized shape of the hydrogel (A) and cartilage (B) tensile samples.

The sample shape depicted in Figure 41 was selected with a larger gauge section to accommodate differing flaw geometries and dimensions such as edge-based sharp cracks and center-based cylindrical holes. This specimen was also selected to prolong the presence of tensile loads during cyclic tensile testing. [209] The ratio of the width of the grip section to the width of the gauge was consistent with prior work. [209] The hydrogel and cartilage were tested in this sample shape to understand the impact of two different flaw types (edge-based sharp cracks and center-based cylindrical holes in the gauge section) and multiple dimensions (0.5 mm, 1 mm, 2 mm, 3 mm, and 4 mm) on UTS at an applied strain rate. The consideration of these flaws was driven by clinical observation of growing defects such as crack-like flaws in human cartilage, as seen in Figure 42.

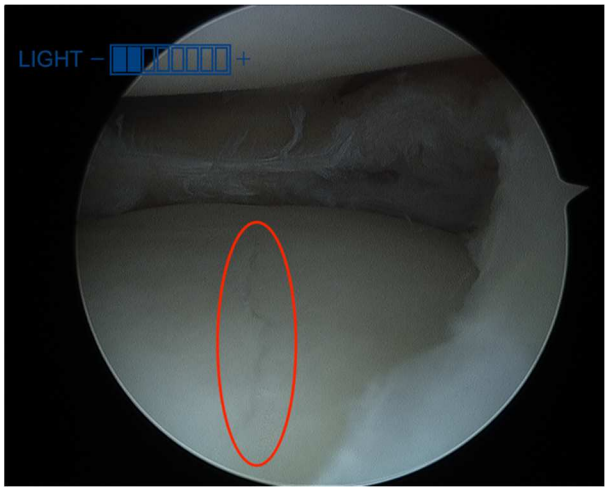

Figure 42: A crack-like flaw (circled in red) in the lateral tibial plateau of a human knee.

The crack-like flaw shown in Figure 42 was part of an arthroscopic surgery to perform a chondroplasty to smooth the articular cartilage crack as a means of preventing further propagation of the defect. Understanding the impact of a flaw as shown in Figure 42 is critical to finding suitable replacements for cartilage and other types of soft tissue with synthetic alternatives. One such proposed substitute comes in the form of the selected BC-PVA-PAMPS hydrogel. The most promising aspect of the hydrogel can be attributed to its tensile strength (13.4 MPa), which is much higher than PVA hydrogels from freeze-thaw (FT) cyclic processing in prior work. [208,209]

6.3.2 Flaw Response at Constant Rate and Tensile Model Construction

To characterize different flaw geometry types, sharp cracks were introduced from the edge of each sample's gauge section toward the center, while cylindrical holes were introduced in the center of the sample's gauge section. Images of cracked samples after testing are shown in Figure 43A and Figure 43B for the hydrogel and cartilage, respectively. Images of cylindrical hole-based samples after testing are shown in Figure 43C and Figure 43D for the hydrogel and cartilage, respectively. Cylindrical holes became elongated as the samples were pulled during tensile testing to form an ellipsoidal shape.

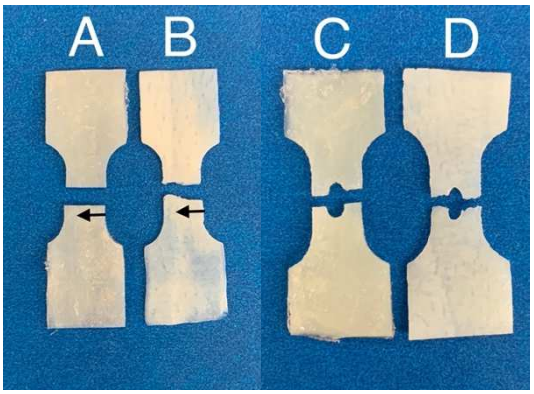

Figure 43: Images of tensile samples after monotonic testing. Cracked samples are provided in (A) for the hydrogel and (B) for cartilage. An arrow is provided for the direction of crack growth from the edge of the sample toward the center. Ultimately, the crack grew across the remaining portion of the gauge section for failure of the sample. Cylindrical hole-based samples are shown in (C) for the hydrogel and (D) for cartilage in the center of the gauge section.

Representative tensile stress-strain curves characterizing monotonic testing for both flaw types and various flaw dimensions for the hydrogel at a strain rate of 0.014 s^{-1} and cartilage at 0.018 s^{-1} are presented in Figure 44. Calculation of sample area for stress values was based on the load-bearing area, which took the dimension of the given flaw into account. The force was then divided by the load-bearing area, giving way to the "nominal stress", as provided on the y-axis. This stress metric allows more direct comparison between groups because it accounts for the fact that the larger flaws naturally remove larger sections of material in similarly sized samples.

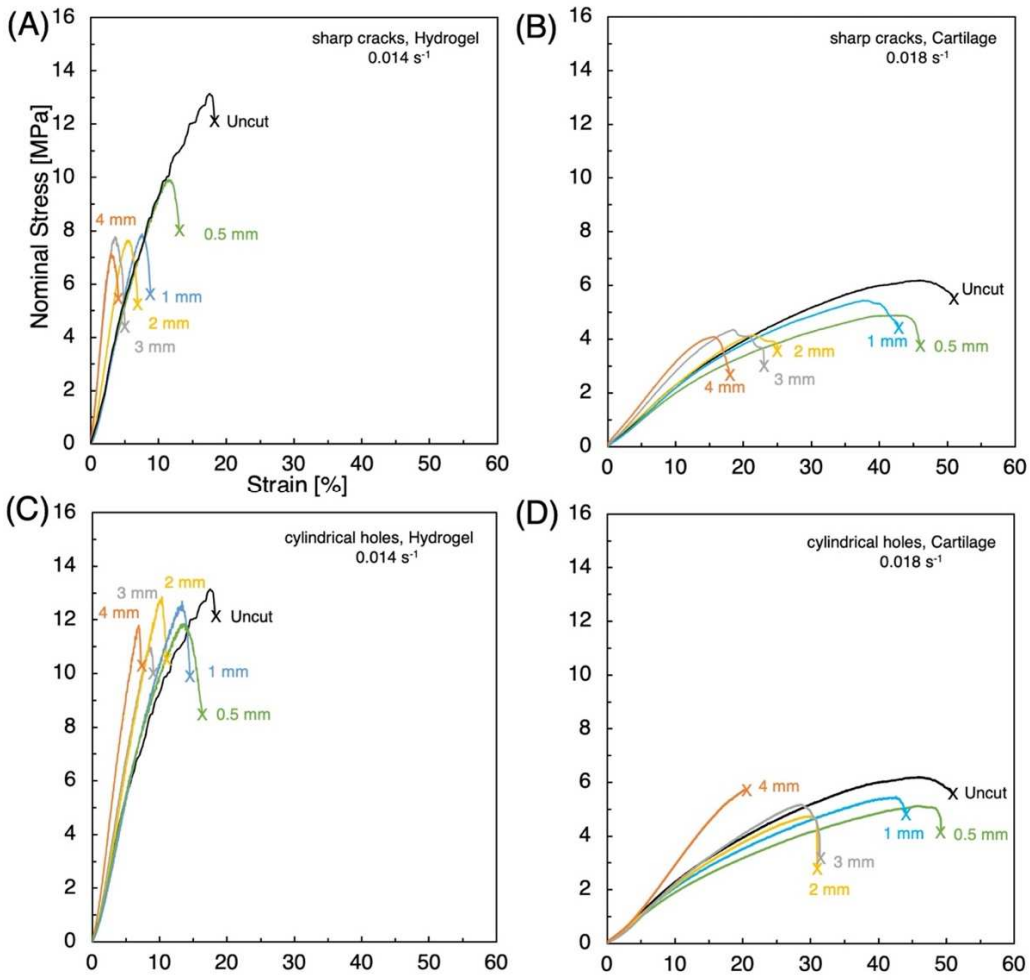

Figure 44: Tensile stress-strain behavior for pristine, 0.5, 1, 2, 3, and 4 mm sharp cracked hydrogel (A), sharp cracked cartilage (B), pristine, 0.5, 1, 2, 3, and 4 mm cylindrical hole hydrogel (C), and cylindrical hole cartilage (D) samples in monotonic tension in a customized tensile shape.

Based on the results in Figure 44, the hydrogel has a higher tensile strength than its cartilage counterpart. Both the hydrogel and cartilage experience a similar trend of decrease in strain-to-failure as the dimension of a given flaw increased. This decrease was more pronounced for sharply cracked samples in both the hydrogel and cartilage with respect to their pristine counterparts. The hydrogel experienced a more significant

decline in tensile strength for samples with sharp cracks compared to the tensile strength loss for samples with cylindrical holes. In comparison to PVA hydrogels from prior work, the hydrogel in the present study was less sensitive to the sharp cracks as measured by loss of tensile strength. [254]

Upper and lower bound models were then used to analyze tensile stress-strain behavior. Comparison of experimental UTS data to the Stress Intensity Model and Nominal Stress Model from 5.4 Experimental Section of Flaw Sensitivity and Tensile Fatigue of Poly(Vinyl Alcohol) Hydrogels is presented in Figure 45A for the hydrogel Figure 45B for cartilage. It should be noted that UTS in Figure 45 is now defined as the ultimate failure load over total sample cross sectional area, as this stress definition does not explicitly account for the loss in load bearing area due to the cylindrical hole or sharp crack. This approach allows comparison of both data sets and the respective failure models, Nominal Stress versus Stress Intensity, both of which inherently account for flaw size (a) relative to sample width (w).

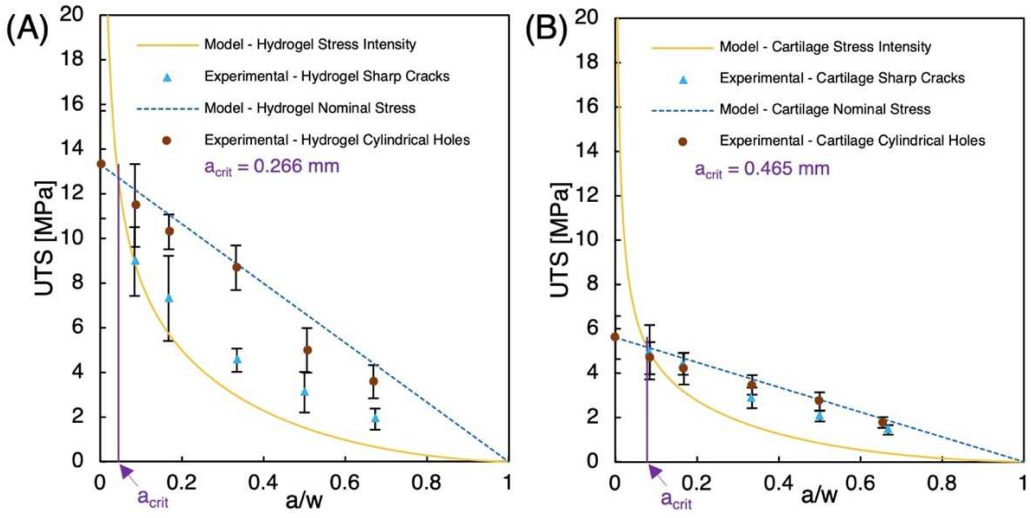

Figure 45: Comparison of experimental tensile strength with Nominal Stress and Stress Intensity Models for varying cylindrical holes and sharp cracks for the hydrogel (A) and cartilage (B).

As shown in Figure 45, the experimental UTS for the sharply cracked cartilage samples differed from the predictions of a simple Stress Intensity Model. The sharply cracked cartilage samples performed similarly to the cylindrical hole cartilage samples which was an unexpected result as a sharp crack is typically a much more severe defect. However, for both the hydrogel and cartilage, the experimental UTS did not drop as drastically for the smallest sharp crack flaw of 0.5 mm as was also observed in a pure PVA hydrogel system. [254] The results from cartilage samples differed from the original hypothesis that tensile strength would be much more sensitive to crack-based flaws compared to cylindrical hole-based flaws. Though the tensile strength for sharp cracked cartilage samples decreased as the size of the flaw increased, this difference was not as pronounced as anticipated. For the hydrogel, the geometric difference of the cylindrical

hole brought about more effective blunting in comparison to the more intense local stresses at the tip of the crack-like flaw. Thus, the experimental tensile strength values for sharp crack hydrogel samples were always lower than their cylindrical hole counterparts.

In light of the simple models, these experimental trends reveal that cartilage was not as sensitive to the type of flaw as the synthetic hydrogel. The critical flaw size, a_{crit}, was defined as the flaw size at which the Stress Intensity Model curve intersected with the Nominal Stress Model curve. At flaw sizes below this critical value both materials have a monotonic strength drop that is theoretically independent of flaw type. Assuming a 6 mm width for a sample, a_{crit} was 0.266 mm for the hydrogel and 0.465 mm for cartilage. Theoretically, any crack-like flaw size larger than 266 micrometers for the hydrogel and 465 micrometers for cartilage would bring about loss in UTS larger than a simple loss of load bearing area calculation would predict. Stated another way, flaws smaller than these dimensions would have a relatively small impact on the *monotonic strength* of the hydrogel or cartilage beyond a simple loss of load-bearing area. In comparison to prior work, the a_{crit} value for PVA hydrogels was around 50 micrometers, [254] about nine times lower than cartilage and five times lower than the hydrogel in this study. Moreover, the data in Figure 45 was bounded by the model predictions. The Stress Intensity Model created a lower bound for both the hydrogel and cartilage experimental data, while the Nominal Stress Model gave way to an upper bound for

strength loss. Experimental strength values finishing above the model can be attributed to the difficulty of ensuring a perfect crack tip radius of zero (i.e., crack tip coming to a sharp, geometrical point). The simple fracture mechanics model assumes a perfect crack tip, and it would be unrealistic to expect a perfect crack tip, particularly in soft materials. Within experimental effort due to creating cylindrical hole-based flaws, the Nominal Stress Model provided an effective upper bound to experimental data for cylindrical hole-based samples.

6.3.3 Rate Sensitivity of the Hydrogel and Cartilage

This study also examined the rate sensitivity of the hydrogel and cartilage in preparation for cyclic tensile testing at a higher frequency. Varying strain rates were selected over a wide range to understand the impact of applied strain rate on mechanical properties. Figure 46 shows the representative tensile stress-strain response for pristine samples of both the hydrogel and cartilage at a variety of strain rates.

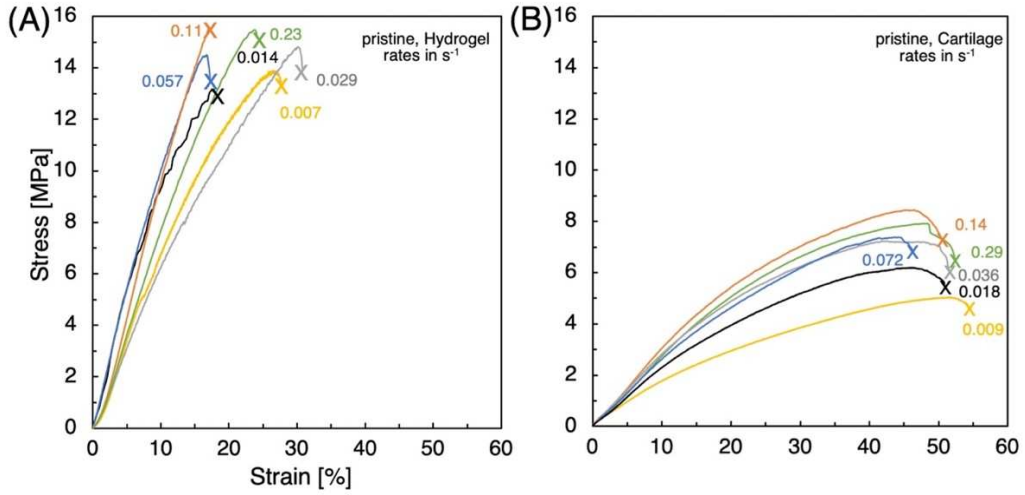

Figure 46: Pristine tensile samples tested under varying monotonic strain rates for the hydrogel (A) and cartilage (B).

As seen in Figure 46, both stiffness and UTS values increased as the applied strain rate increased. This increase was more pronounced for cartilage samples in comparison to hydrogel samples. The increase in stiffness was expected and has been previously reported. [255,256] In addition to samples in their pristine state, flaws of the same dimension (2 mm) but different geometry (edge-based sharp crack vs center-based cylindrical hole) were chosen for comparing tensile response based on applied strain rate. Representative tensile stress-strain curves of all rates for both the hydrogel and cartilage with a 2 mm sharp crack can be seen in Figure 47. The stress calculation of area for the stress values on the y-axis took the dimension of the flaw into account. As a result, the y-axis stress values are reported as "nominal stress" values.

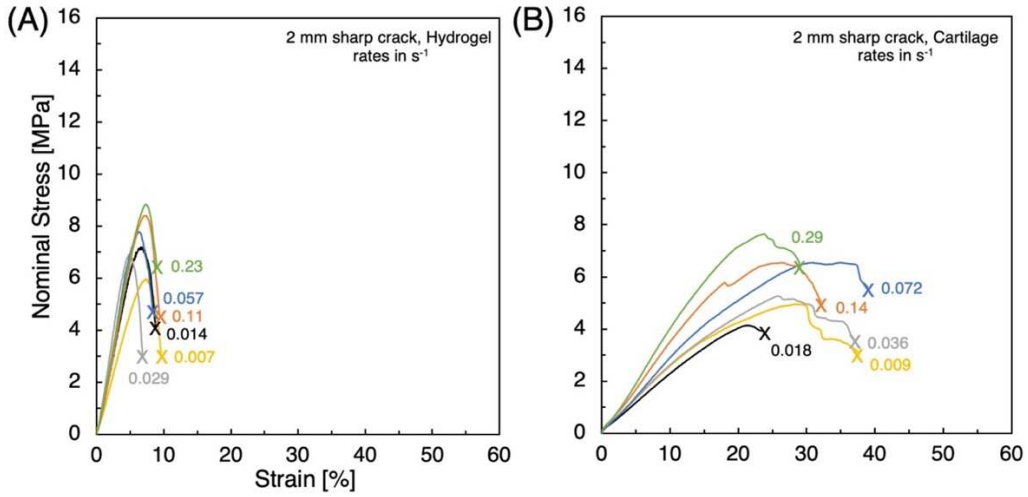

Figure 47: Sharp cracked (2 mm) tensile samples tested under varying monotonic strain rates for the hydrogel (A) and cartilage (B).

As evidenced in Figure 47, strain-to-failure values were much lower for both the hydrogel and cartilage upon introduction of the 2 mm sharp crack on the edge of the gauge section. Once again, strength and slope of the stress-strain curve increase as the strain rate was increased relative to the slower strain rates. Failure patterns for the hydrogel samples were much more direct Mode I growth, as the sharp crack grew straight across the sample. Failure patterns for several of the cartilage samples were not perfectly Mode I growth in that the sharp crack took an uneven path across the gauge section.

In addition to analyzing the monotonic rate dependence of a sample with a 2 mm sharp crack, the same response was considered for a 2 mm cylindrical hole in both the hydrogel and cartilage. Just as in Figure 47, the y-axis stress values in Figure 48 are reported as "nominal stress" values.

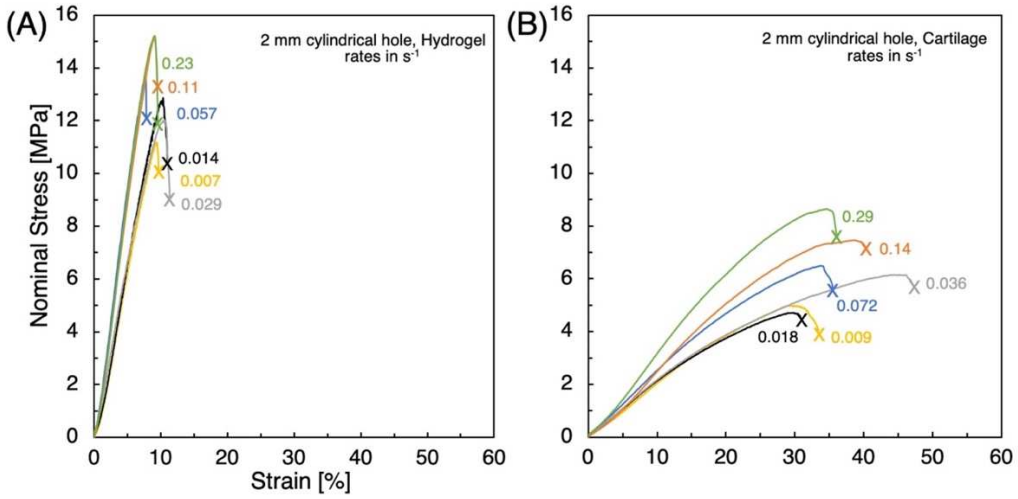

Figure 48: Cylindrical hole (2 mm) tensile samples tested under varying monotonic strain rates for the hydrogel (A) and cartilage (B).

As seen in Figure 48, the hydrogel nominal stress values reach much higher values during monotonic testing as compared to the sharp crack in Figure 47. However, this was not the case for cartilage. The cartilage sample with the cylindrical hole-based flaw behaved similar to the cartilage sample with the sharp crack. Strain-to-failure values for both cartilage and the hydrogel were slightly larger than the sharp crack counterparts from Figure 47. In this sense, the cylindrical hole blunted the growth of the flaw a bit longer than the sharp crack did for both cartilage and the hydrogel.

Figure 49 provides ultimate tensile strength vs. log[applied strain rate] to summarize the strain rate data and examine any connection between rate sensitivity and strength of these materials. The UTS values in Figure 49 were calculated based on the area of the gauge section from the thickness and width (i.e., independent of the 2 mm

flaw) which was different than the nominal stress values used in Figures Figure 46-Figure 48.

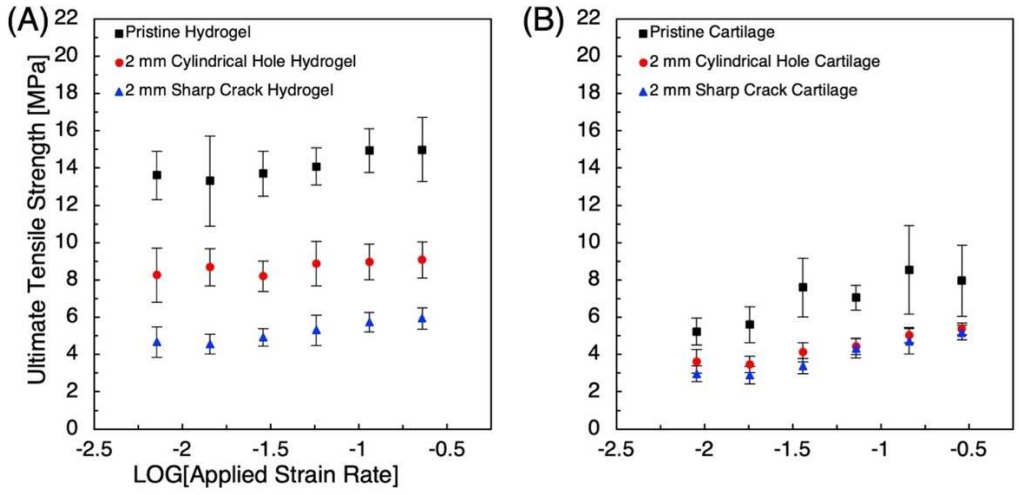

Figure 49: Ultimate tensile strength from monotonic tensile testing vs. LOG[applied strain rate] for the hydrogel samples (A) and cartilage samples (B).

As seen in Figure 49, the tensile strength of the hydrogel is most strongly dependent on its flawed state at all applied strain rates while the cartilage samples were less dependent on flaw type and relatively more dependent on strain rate. The relative flaw insensitivity of cartilage is very impressive, although the inherently stronger hydrogel sample with a 2 mm cylindrical hole still achieves a higher UTS than pristine cartilage. The tensile strength difference in rate between cartilage with a 2 mm sharp crack versus a 2 mm cylindrical hole was essentially non-existent. These two flaw geometries had a comparable impact on tensile strength over a variety of flaw dimensions shown in Figure 45 as well as varying testing rates seen in Figure 49. From the same perspective,

the sharp crack had a greater impact on the tensile strength of the hydrogel than the cylindrical hole. In analyzing the hydrogel and cartilage across a particular condition's testing rates (i.e., the 2 mm sharp crack hydrogel from 0.007 s^{-1} to 0.23 s^{-1}), it becomes clear that cartilage was more sensitive to strain rate than the hydrogel for both flaws and the pristine state. The cartilage samples consistently demonstrated a higher percent change than hydrogel samples when comparing the highest rate to the slowest rate across each sample condition. The hydrogel samples had a minimal trend of increasing tensile strength based on increasing strain rate, whereas cartilage experienced steeper increases.

6.3.4 Fatigue Characterization of the Hydrogel and Cartilage

Cyclic tensile parameters were configured based on the results of the monotonic rate comparisons from Figure 46-Figure 49. Strain-controlled testing at 1 Hz based on strain-to-failure was utilized to carry out the fatigue tests. Given the fixed frequency parameter, monotonic strain-to-failure values from tests with a strain rate of 0.11 s^{-1} for the hydrogel and 0.14 s^{-1} for cartilage were chosen to establish the maximum strain testing levels. Six combinations in total were established from two material types (hydrogel and cartilage) with three testing conditions each: pristine, 2 mm sharp crack, and 2 mm cylindrical hole. The average monotonic strain-to-failure value from each of the three conditions was used to generate all maximum strain fatigue testing levels.

These levels were based on percentages of the average monotonic strain-to-failure value, and the number of samples at each fatigue level was chosen to be $n = 4$. Figure 50 provides a plot of strain range vs. cycles to failure for both the hydrogel and cartilage in a pristine state, with a 2 mm sharp crack, and with a 2 mm cylindrical hole. Strain range percentages shown in Figure 50 are percentages based off the average monotonic strain-to-failure for each condition. Cartilage samples with a 2 mm sharp crack have their 65% and 57.5% runout samples slightly adjusted for cycle number to make them visible in the plot (these tests were concluded upon 100,000 cycles).

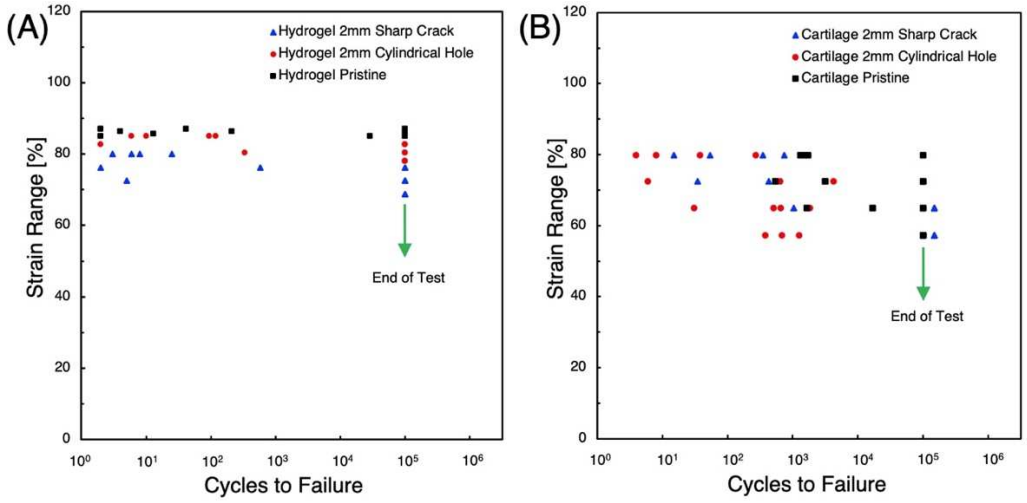

Figure 50: Tensile fatigue data for (A) hydrogel and (B) cartilage pristine samples, 2 mm sharp cracks, and 2 mm cylindrical holes based on strain range as a function of cycles to failure. Strain range is defined as a percentage of the particular sample's average failure strain. A sample that lasted 100,000 cycles without failure is considered a "runout" sample with an arrow indicating its position in the graph. Four strain levels for the pristine, sharp crack, and cylindrical hole were utilized for the hydrogel and cartilage. Once 100,000 cycles were completed, the test was concluded.

Failure of a sample prior to completing 100,000 cycles was defined as a complete tear of the sample. Both hydrogel and cartilage had 2 mm cylindrical hole samples that completed 100,000 cycles as a semicircle (i.e., one half of the circle had torn during the test, but the other half remained intact for the duration of the test). Given that part of the sample remained intact, this was not considered failure for the sample, and as such the strain values at 100,000 cycles are not a "safe-life" level or representative of a sample that has no damage. Damage progression in 2 mm sharp crack samples was also observed due to crack growth over the duration of the test. However, the growth of a crack within a sample did not lead to a tearing of the sample. For these reasons, the runout 2 mm sharp crack samples that achieved 100,000 cycles should not be considered "safe-life" endurance limit samples either. A "safe-life" endurance would be defined as a threshold below which no fatigue damage would progress through large cycle numbers. In this study, these values cannot establish a "safe-life" endurance due to that the observation that even the runout samples displayed visible growth of flaws and damage accumulation.

The results depicted in Figure 50 provide simple comparison within a sample for its three conditions (pristine, 2 mm sharp crack, and 2 mm cylindrical hole) in terms of what sample lasted the longest. However, the data does not allow for straightforward comparison across different flaw types or material types due to different strain-to-failure performance of the two materials. With the goal of drawing relative comparison

between these fatigue results, all samples were analyzed for their tensile nominal stress range at the median time point of the test according to Koshut et al. (2020). [209] According to Koshut et al. (2020), median life tensile nominal stress range was determine to be the maximum tensile nominal stress the sample experienced at the median time point of a given test. [254] With the strain-controlled cyclic testing employed in this study, nominal tensile stresses were used to compare sample performance across different strain-to-failure parameters. Stress relaxation from the samples was observed to bring about buckling during unloading of the samples while cycling, which ultimately led to minor compressive stresses. However, only tensile stress was considered for a comparison of all samples. Each sample was assessed for its median life tensile nominal stress range, and these results are shown in Figure 51. The load-bearing area was utilized to calculate the median life tensile nominal stress range, and this area took the flaw dimension into account. The forced divided by the load-bearing area gave way to the "median life tensile nominal stress range", as shown on the y-axis. Nominal stress over cyclic loads may be obtained in the 6.5.4 Mechanical Characterization section.

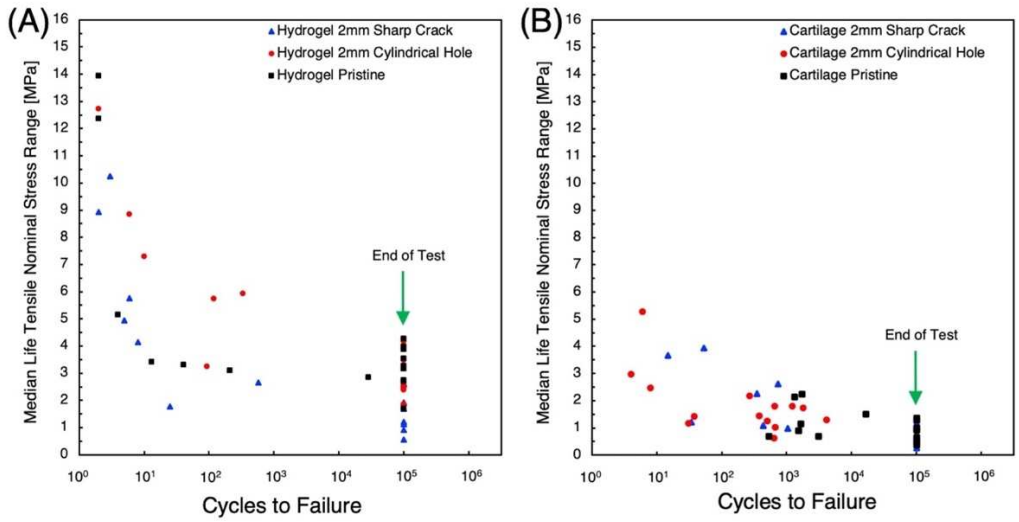

Figure 51: Tensile fatigue data for (A) hydrogel and (B) cartilage pristine samples, 2 mm sharp cracks, and 2 mm cylindrical holes based on median life tensile stress range as a function of cycles to failure. A sample that lasted 100,000 cycles without failure is considered a "runout" sample with an arrow indicating this position in the graph. A sample reaching 100,000 cycles marked the end of the test.

Based on the median life tensile nominal stress range data for cartilage, the 2 mm sharp crack and pristine samples outperformed the 2 mm cylindrical hole samples. This result was unexpected before monotonic testing results. However, it became clear that this result was possible after flaw analysis of cylindrical holes and sharp cracks from Figure 45 established that samples with cylindrical holes and sharp cracks demonstrated similar strength levels. More runout samples were achieved for the sharply cracked cartilage samples, which implies the sharp crack was not as damaging than the removal of more material in a cylindrical cutout of equivalent "size".

Tensile fatigue nominal stress threshold was defined as the maximum median tensile nominal stress that a sample experienced without complete failure (but still

experiencing damage progression). For cartilage samples, these values were: 0.74 MPa for 2 mm sharp crack, 0.40 MPa for 2 mm cylindrical hole, and 0.65 MPa for pristine. This may give the artificial conclusion of enhanced fatigue behavior for the 2 mm sharp crack samples as compared to pristine samples (i.e., that samples with a 2 mm sharp crack would be preferred to those without any damage). However, this stress was calculated based solely on the load-bearing area. When considering the full area of the sample (the width of the gauge section independent of the flaw dimension), the stress values become: 0.50 MPa for 2 mm sharp crack, 0.27 MPa for 2 mm cylindrical hole, and 0.65 MPa for pristine cartilage. The relatively poor performance of the cartilage with a cylindrical hole relative to the sharp crack implies that the removal of more material (exposing a periphery of new surface) is possibly more detrimental than a sharp crack with more localized stresses. Further work would be needed to fully understand this counterintuitive, yet consistent, result.

For the hydrogel, the 2 mm cylindrical hole and pristine samples outperformed the 2 mm sharp crack samples as would be expected based on the local severity of the defects. In addition, more runout samples were achieved for hydrogel samples with a 2 mm cylindrical hole than those with a 2 mm sharp crack. For hydrogel samples, the tensile fatigue nominal stress threshold values were: 1.70 MPa for 2 mm sharp crack, 2.69 MPa for 2 mm cylindrical hole, and 2.73 MPa for pristine. The 2 mm sharply cracked hydrogel samples had a much higher tensile fatigue stress threshold value in

comparison to its 2 mm sharp crack cartilage counterpart. Given the larger tensile fatigue nominal stress threshold values for the hydrogel, the 2 mm cylindrical hole and pristine samples eclipsed the results of the 2 mm sharp crack samples. These results align with observations from monotonic testing in that the hydrogel was more sensitive to the 2 mm sharp crack than the 2 mm cylindrical hole. Analogous to cartilage, these nominal values for the hydrogel provide an impression that a sample with a 2 mm cylindrical hole was similar to the pristine sample. However, when considering the full area of the sample (independent of the flaw), these stress values become: 1.13 MPa for 2 mm sharp crack, 1.81 MPa for 2 mm cylindrical hole, and 2.73 MPa for pristine hydrogel samples.

Finally, the fatigue stress threshold values present an opportunity for comparison to monotonic results for both cartilage and the hydrogel. Based on monotonic testing in this work, the hydrogel and cartilage have different UTS and strain-to-failure values. Further, these materials also had different tensile fatigue nominal stress threshold values. In this sense, it is difficult to truly assess the translation from monotonic to fatigue behavior for the hydrogel against cartilage. However, it is possible to assess the maintenance of strength as a percentage when comparing the monotonic UTS of a sample condition to its tensile fatigue nominal stress threshold value. Analyzing the fatigue behavior of each of these samples relative to their monotonic behavior allows for comparison across material type and condition. The

results depicted in Figure 52 show the relative stress level a sample can support to retain a connection up to 100,000 cycles. These percentages were calculated by taking the tensile fatigue nominal stress threshold for a sample condition and dividing it by the average monotonic nominal UTS based on 0.11 s^{-1} testing for the hydrogel and 0.14 s^{-1} for cartilage.

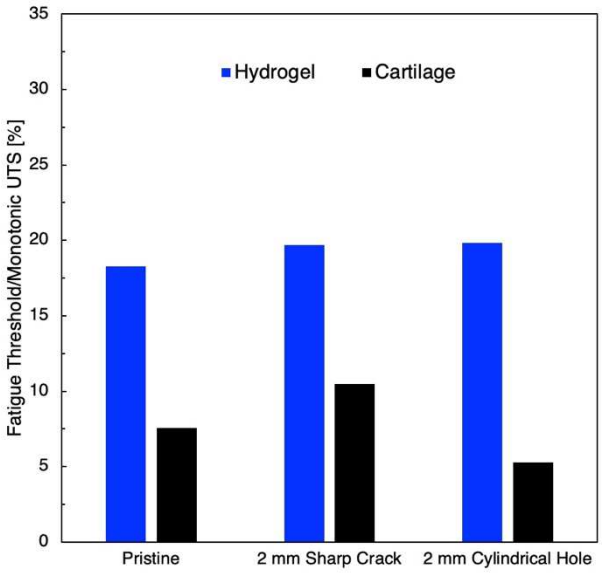

Figure 52: Comparison of drop in strength from monotonic testing to fatigue testing based on sample type and condition.

As seen in Figure 52, the hydrogel was able to maintain a greater percentage of its monotonic strength in comparison to cartilage for all sample conditions. Hydrogel samples maintained roughly 18-20% of their monotonic strength as shown in Figure 52. Cartilage samples, on the other hand, maintained around 5-10% of their monotonic strength. This observation was unexpected based on cartilage's higher a_{crit} value from the tensile models in Figure 45. One possible explanation may come in the form of the

composite's materials. PVA's inclusion in the hydrogel composite may help with improving toughness of the material, which may ultimately enhance fatigue behavior in comparison to cartilage samples.

6.4 Conclusions on the BC-PVA-PAMPS Hydrogel and Cartilage

In consideration of future applications for soft materials, this monotonic flaw analysis and resulting fatigue examination are crucial for realizing the ability of certain flaws to lead to premature failure. In real world applications, it is practically impossible to prevent flaws from arising and sometimes progressing toward material failure. Understanding the long-term response of soft materials toward initial damage and subsequent growth is critical to preserving their scope in biomedical applications. Prior work in Koshut et al. (2021) focused on a lower strength, higher strain-to-failure PVA hydrogel system to explore the impact of flaws on mechanical response. This work set out to characterize a much stronger BC-PVA-PAMPS hydrogel in a similar manner based on flaw type and dimension. Parallel analysis of a biological tissue system in the form of porcine costal cartilage was also carried out.

Principally, both the BC-PVA-PAMPS hydrogel and biological tissue were analyzed for monotonic tensile strength at a constant rate with varying flaw type (sharp edge cracks and central cylindrical holes) and dimension (0.5 mm, 1 mm, 2 mm, 3 mm, and 4 mm). Representative stress-strain curves and tensile strength models were

constructed from this testing. These models have yet to be applied in a high strength hydrogel system like BC-PVA-PAMPS as well as a biological tissue system like that of porcine costal cartilage. The cartilage samples were not as sensitive to the type of flaw (cylindrical hole vs. sharp crack) as the hydrogel samples were. However, both cartilage and the hydrogel selected in this study were not as flaw sensitive as PVA-only hydrogels from prior work. [254] The tensile strength models, through application of the worst-case scenario flaw (sharp edge crack) and best-case scenario flaw (centered cylindrical hole), also provided an accurate lower bound and upper bound on tensile strength loss as a function of flaw type.

The hydrogel and cartilage were then assessed for their monotonic rate sensitivity in preparation for fatigue testing. A variety of monotonic strain rates were selected to study both hydrogel and cartilage in three different sample conditions: pristine, the presence of a 2 mm sharp crack, and the presence of a 2 mm cylindrical hole. A subsequent data analysis of UTS based on applied strain rate was completed. Based on this testing, fatigue parameters were configured around behavior of all three sample conditions at a strain rate of 0.11 s^{-1} for the hydrogel and 0.14 s^{-1} for cartilage. The three sample conditions mentioned previously were utilized for tensile fatigue testing to track the progression or growth of a flaw toward premature failure. A strain range curve and resulting median life tensile nominal stress range curve were generated from these tests. It was concluded that the hydrogel was more sensitive to 2 mm sharp crack, and

cartilage was more sensitive toward the 2 mm cylindrical hole. Hydrogel samples were able to maintain 18-20% of their monotonic strength in fatigue, while cartilage samples were able to maintain 5-10%. The tensile fatigue analysis provided in this work highlighted the importance of considering flaw formation and progression in both synthetic and biological tissue systems. For advanced fatigue pursuit of soft materials and their synthetic alternatives, researchers must thoroughly study across varying sample conditions (pristine or flawed) as well as low and high cycle regimes.

6.5 Experimental Details

6.5.1 Materials

Bacterial cellulose (BC) was purchased from Gia Gia Nguyen Co. Ltd. Poly(vinyl alcohol) (PVA) (fully hydrolyzed, molecular weight: 146,000 g mol^{-1}), N,N'-methylenediacrylamide (MBAA, 97.0%), 2-hydroxy-4'-(2-hydroxyethoxy)-2-methylpropiophenone (I2959), potassium persulfate (KPS), and 2-acrylamido-2-methylpropanesulfonic acid sodium salt (AMPS, 50 wt.% solution in water) were all purchased from Sigma Aldrich. Phosphate buffered saline (PBS) was purchased from VWR International. Porcine tissue sections containing sternum, ribs and associated costal cartilage were acquired from Animal Biotech Industries, Inc., and received in lab within one day of initial tissue harvest. Immediately upon arrival, tissue samples were dissected.

6.5.2 BC-PVA-PAMPS Hydrogel Preparation

Preparation of the BC-PVA-PAMPS was conducted according to Yang et al. (2020).[208] Bacterial cellulose sheets were pressed to a controlled thickness between two aluminum plates (typically 0.5 mm, controlled by spacers between the aluminum plates) and placed into a hydrothermal reactor with a mixture of 40 wt% PVA and 60 wt% deionized water. The hydrothermal reactor was sealed and heated at 135°C for 24 hours to allow the PVA to diffuse into the voids of BC and form a BC-PVA hydrogel. The BC-PVA hydrogel was removed from the reactor when hot (>85°C). Note that the hydrothermal reactor was pressurized with hot steam and created a burn hazard, so personal protective equipment such as a lab coat, heat resistant gloves and full coverage face shields should be used when opening the reactor. The residual PVA solution was removed by scraping the surface of the BC-PVA samples with a metal spatula. The samples were frozen in a -78°C freezer for 30 minutes and thawed at room temperature to physically crosslink the PVA network. The BC-PVA hydrogel was then soaked in a solution of 30 wt% AMPS, 60 mM MBAA, 50 mM I2959 and 0.5 mg/mL KPS solution for 24 hours. The hydrogel was cured with a UV transilluminator (VWR International) for 15 minutes on each side, and further cured in an oven at 60°C for 8 hours to ensure even and complete curing. The resulting BC-PVA-PAMPS hydrogel was stored in 1X PBS for at least 24 hours before further characterization.

6.5.3 Porcine Costal Cartilage Preparation

The porcine costal cartilage in this study was extracted from animals that were typically six months old and weighed about 113 kg with the breed being unknown. To isolate costal cartilage, the cartilaginous structures associated with the 3rd through 5th ribs were sliced axially at their articulations adjacent to the sternum and bony ribs using a scalpel. After removing overlying muscular tissue and associated perichondrium, uniform thin slices of costal cartilage were obtained using a truffle slicer (Urbani Truffles). Cartilage slices were then cut using a custom titanium punch created from additive manufacturing. These samples were either tested immediately for monotonic testing or stored at 4°C in 1X PBS for no more than 14 days for cyclic testing. All porcine tissue processing was performed in accordance with Duke University Animal Safety guidelines.

6.5.4 Mechanical Characterization

Monotonic tensile testing was carried out using a 50-lb load cell on either an Instron 1321 (Instron, Norwood, MA, USA) load frame or a TestResources 830 (TestResources, Shakopee, MN, USA) load frame. All cyclic testing was carried out on the Instron 1321 with a tap water bath at 37 °C in order to prevent hydrogel and cartilage samples from drying out during cyclic testing. For other instances of sample

storage for monotonic testing, 1X PBS was used to maintain sample hydration. A video extensometer was used to determine an experimental effective length for the hydrogel and cartilage samples on the TestResources 830 load frame with a 50-lb load cell. Tensile sample geometry was customized and the same for both monotonic and fatigue testing. Its dimensions were selected to accommodate larger flaw sizes as well as prolonging tensile loads during cyclic testing (6 mm width for the gauge section). Samples with sharp edge-cracks of controlled lengths (0.5, 1, 2, 3, and 4 mm) and cylindrical holes of controlled diameters (0.5, 1, 2, 3, and 4 mm) were first tested at a rate of 0.014 s^{-1} for the hydrogel and 0.018 s^{-1} for cartilage. These tests were analyzed with respect to Nominal Stress and Stress Intensity Models from Koshut et al. (2021). [254] Explanation of the construction of both Nominal Stress and Stress Intensity Models can be obtained in their respective subsections of the Experimental Section from Koshut et al. (2021). [254] Upon analysis of these tests, the hydrogel and cartilage were investigated for rate dependency by selecting one dimension of both flaws (2 mm sharp crack and 2 mm cylindrical) and pristine samples (no flaw) to be tested at a variety of monotonic strain rates. Based on these results, the strain rate of 0.11 s^{-1} for the hydrogel and 0.14 s^{-1} for cartilage was chosen as a benchmark to carry out all fatigue testing at a constant frequency of 1 Hz.

For completion of fatigue testing in a strain-controlled manner, the failure strain results from monotonic tests at strain rates of 0.11 s^{-1} and 0.14 s^{-1} were compiled for pristine, 2 mm sharp crack, and 2 mm cylindrical hole samples for the hydrogel and

cartilage, respectively. Correspondingly, an average failure strain from a minimum of n = 5 tests was calculated. Testing levels for cartilage were configured to be 80%, 72.5%, 65%, and 57.5% of this average failure strain value for 2 mm sharp crack, 2 mm cylindrical hole, and pristine samples. As for the hydrogel, selection of testing levels was more sensitive based on sample condition. The following levels were used for the 2 mm sharp crack: 80%, 76.25%, 72.5%, and 68.75%. The following levels were used for the 2 mm cylindrical hole: 85%, 82.67%, 80.33%, and 78%. The following levels were used for the pristine sample: 87%, 86.33%, 85.67%, and 85%. In total, there were 3 sample conditions for both the hydrogel and cartilage to make 6 total combinations. As mentioned before, a constant frequency of 1 Hz was used for fatigue analysis of all samples. It was decided to conduct n = 4 fatigue tests at each of the testing levels for a total of 16 samples for each combination. A strain-to-failure comparison of aged samples was completed to ensure samples could be properly stored for cyclic testing. This was completed with one-way analysis of variance (ANOVA) based on failure strain as a function of storage time in 1X PBS solution. Nominal stress over cyclic loads can be seen in Figure 53, Figure 54, and Figure 55 for both materials (BC-PVA-PAMPS hydrogel and cartilage) and all three sample conditions (pristine, 2 mm sharp crack, and 2 mm cylindrical hole).

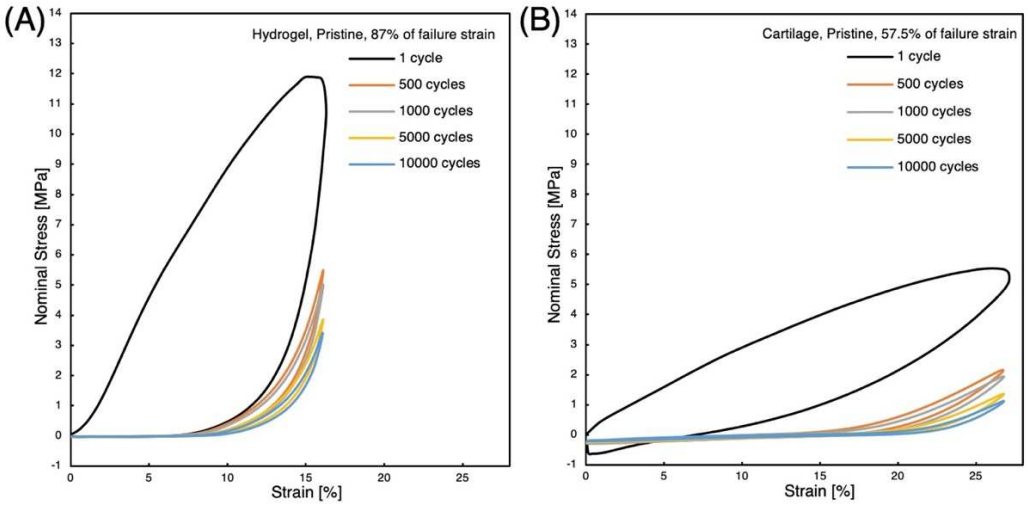

Figure 53: Nominal stress versus strain over cyclic loads for the hydrogel (A) and cartilage (B) in pristine sample condition.

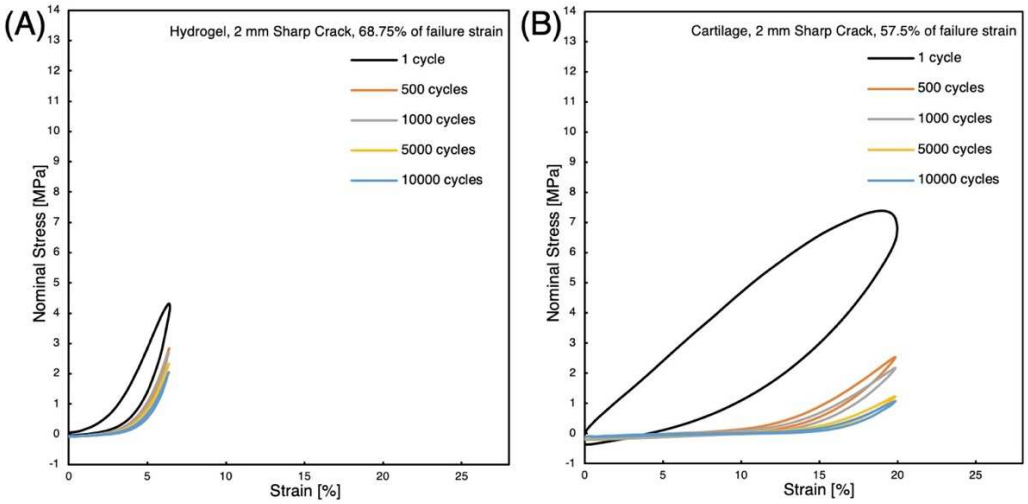

Figure 54: Nominal stress versus strain over cyclic loads for the hydrogel (A) and cartilage (B) with a 2 mm sharp crack for sample condition.

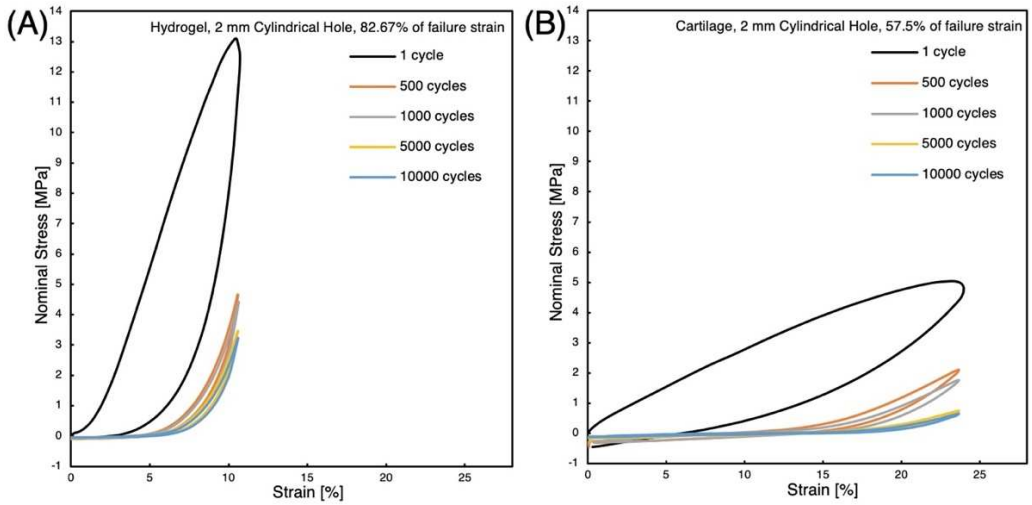

Figure 55: Nominal stress versus strain over cyclic loads for the hydrogel (A) and cartilage (B) with a 2 mm cylindrical hole for sample condition.

Chapter 7. Conclusions

Chapters 3-6 have been dedicated to the characterization of four soft materials, respectively: a PVA-only hydrogel, a PVA-starch hydrogel, a BC-PVA-PAMPS hydrogel, and porcine costal cartilage. The research in Chapter 3 presented a mechanically tunable, robust PVA hydrogel that could be easily synthesized through freezing-thawing cyclic processing. Many common toughening agents were utilized to assess mechanical enhancement of the hydrogel system. Broad chemical and monotonic mechanical analysis of these different toughened hydrogels was carried out. Tensile fatigue characterization with a sharp crack was carried out on the control system (PVA-only as a hydrogel) as well as the top-performing agent (PVA-starch hydrogel). However, both PVA-only and PVA-starch hydrogels had the ability to be improved further with regards to tensile strength. Chapter 4 pursued a composite hydrogel featuring bacterial cellulose, PVA, and 2-acrylamido-2-methylpropanesulfonic acid sodium salt to address the shortcomings of lower strength in the hydrogel systems from Chapter 3. The hydrogel network was strengthened through a variety of synthetic and processing techniques. Once again, broad analysis of the chemical and monotonic mechanical properties of this system was addressed. Ultimately, the role of each component of the system was considered through tensile fatigue study.

The work in Chapter 5 sought to understand the development and progression of flaws observed from cyclic testing in Chapter 3 and Chapter 4. Due to the high-strain

nature of the hydrogels in Chapter 3, a sharp crack was utilized to complete fatigue characterization. Samples in Chapter 4 could be tested in a pristine state for the fatigue study. As a result of these differences of sample conditions, Chapter 5 set out to understand the monotonic and cyclic impact of varying flaw types and dimensions with the PVA-only hydrogel system serving as a model. In addition, Chapter 5 pursued a tuning of the freezing-thawing cyclic processing steps for desired mechanical behavior. The PVA-only hydrogel served as an excellent model to achieve both flaw analysis and freezing-thawing characterization. Fatigue characterization was carried out on samples with chosen flaw conditions such as sharp cracks and cylindrical holes. Chapter 6 carried out a similar monotonic study of varying flaw type and dimension as the PVA-only hydrogel in Chapter 5. However, Chapter 6 examined the BC-PVA-PAMPS hydrogel as well as a biological tissue model of porcine costal cartilage. Further, Chapter 6 investigated the progression of flaws in a cyclic fashion for both the BC-PVA-PAMPS hydrogel and porcine costal cartilage. As for future directions of these soft materials, proposed enquiries are detailed more precisely in the following subsection.

7.1 Future Studies

7.1.1 Processing Considerations of Top-Performing Systems

Given the intense mechanical characterization from Chapters 3-6, the next challenge in realizing the full potential of these soft materials involves functional

processing. For implantation in joints in the human body, these materials must be analyzed for possible improvements to synthetic techniques. For the PVA-only and PVA-starch hydrogels, solution processing and casting into a stainless-steel mold produced controlled shapes and dimensions upon completion of freezing-thawing cyclic processing. In addition, the preparation of the BC-PVA-PAMPS hydrogel can be seen in Figure 22. The shape for tensile testing of the BC-PVA-PAMPS composite material is ultimately created from a flat sheet with a titanium metal punch. As the interest in customizable implants continues to flourish, considerable attention must be given to different methods to make these hydrogels unique to the patient in lieu of generic from a set mold. A great deal of resources and energy would be dedicated to producing a specific mold for each patient before creation of the synthetic implant. As such, there exists a unique opening to pursue processing improvements in these materials.

The ability to 3D-print a range of structures with soft materials would create an endless path of opportunities for use. This may prove difficult for materials like the PVA-only and PVA-starch hydrogels due to their solution casting, but pursuit of the idea nonetheless may reveal information yet to be discovered. As for the BC-PVA-PAMPS composite, strict design and control over the processing of bacterial cellulose could prove to be revolutionary for its applications. For example, 3D-bioprinting with a novel bacterial nanocellulose bio-ink has already led to constructs for cartilage formation.[257] In its current form, the fibers of the bacterial cellulose sheet do not have a

specific, controlled alignment; rather, they are randomly dispersed. By selectively controlling the alignment of the fibers of the bacterial cellulose sheet through exploration of processing options, yet another key variable of its synthesis becomes tunable for mechanical behavior. Ultimately, fiber alignment could be utilized to control mechanical properties based on the soft tissue application of interest. In any case of adapting processing techniques or unlocking new ones, a barrage of mechanical studies will be created. Full mechanical and physiochemical consideration must be given to any alteration of a material's processing. The study of physical and mechanical property changes in tandem will lead to many exciting research endeavors.

7.1.2 Adjustments to Reinforcements

Outside of exploring new processing options for the top-performing hydrogels, the makeup of the hydrogels or treatment of individual components may be altered for future research pursuits. In the case of the PVA-based hydrogels, the top-performing toughening agent based on monotonic toughness analysis was starch. However, an improvement in fatigue behavior was not realized upon the addition of starch to the PVA hydrogel. Selection of a different toughening agent for improved fatigue behavior may proceed based on monotonic results obtained in Figure 12A. Since a monotonic screening process based on toughness has already occurred, this choice of picking a different toughening agent may be simplified. Selection of an agent such as agar or

xanthan gum would be interesting since both of these agents improved the toughness of the hydrogel relative to the control from Figure 12A. Using agar or xanthan gum may prove that the fatigue results of starch were either: 1) an anomaly isolated to that agent only, or 2) the possible development of a trend based on observation from more than one toughening agent. In either case, a batch of mechanical and chemical testing would be needed to fully characterize this new hydrogel system.

In the case of the BC-PVA-PAMPS hydrogel, bacterial cellulose was selected as the fibrous material for improved tensile behavior to mimic the role of collagen in cartilage. One such future direction for this material includes an examination of different types of reinforcement of additional materials such as bacterial nanocellulose.[258–260] However, the use of additional types of reinforcement must be weighed in a cost-benefit manner. Although a fibrous material may bring about improved mechanical behavior, the viscoelastic and chemical behavior of the hydrogel must not be adversely impacted. As a result, advanced mechanical and chemical characterization of the new composition would be thorough in its scope. In addition to different fibrous accompaniments, the treatment of the existing bacterial cellulose component may be studied for alterations in mechanical behavior. Different heat treatments or freeze-drying treatments may improve the tensile behavior of bacterial cellulose.[261,262] Thus, the hydrogel may also be upgraded mechanically as a result. As mentioned previously, extensive mechanical and chemical analysis must be piloted based on any changes to the bacterial cellulose

component. Any observed improvements in monotonic mechanical behavior must be investigated for their impact on tensile fatigue behavior in a cyclic manner.

7.1.3 Differing Animal Model Tissue

The implication of these soft materials to be used as implants in the human body carries enormous weight. As such, establishing a biological tissue model in the form of porcine costal cartilage was critical to the work of Chapter 6. However, further analysis must be performed based on an interspecies comparison before studies involving humans are considered. In this document, porcine costal cartilage was selected due to its cost effectiveness and ease of tensile sample creation. Furthermore, the porcine joint size, weight-bearing requirements, and cartilage thickness are appropriate imitations of their human counterparts.[263–265] However, there may be a different species of animal tissue that is more appropriate for mechanical comparison depending on the final application of the soft material.[250,253,266] In this way, proper selection and study of a different animal model is needed based on the type of biological tissue that the soft material is hoping to mimic.

A step-wise approach based on small laboratory-based animals may be an effective strategy to achieve implantation in humans. Principally, the type of tissue or cartilage targeted for repair or replacement must be identified. A comprehensive literature search may then commence to select a proper animal model that is as close as

possible to a human model. Some examples include repair of the trochlea with rabbits as the animal model or repair of articular cartilage using a sheep model.[252] In either case, sufficient mechanical characterization must be carried out on the animal model of interest to establish a benchmark of comparison. Fatigue characterization of the applied soft material must be done in unison with the selected animal model for a fair depiction of the match. In carrying out mechanical analysis with this strategy, the field of cartilage mimics is strengthened. A growing database of valuable information about the advanced mechanical behavior of each animal model would be created.

The groundwork of this document was based on finding alternatives to treating osteoarthritis in the form of repair or replacement of soft tissue. However, these soft materials must not be limited in their scope. Mechanical adjustment of their properties through synthetic or processing techniques will continue to open doors for use in the human body. It then becomes the great responsibility of material researchers to ensure that the patient receiving the care is always in view when exploring alternatives.

Appendix A: Synthesis of Poly(Vinyl Alcohol)

Poly(vinyl alcohol) is prepared from the free radical polymerization of vinyl acetate to create poly(vinyl acetate) aka PVAc. Subsequent base hydrolysis yields poly(vinyl alcohol), with the full reaction pathway shown in Figure 56 to create the polymer used as a building block for the hydrogels in this dissertation.

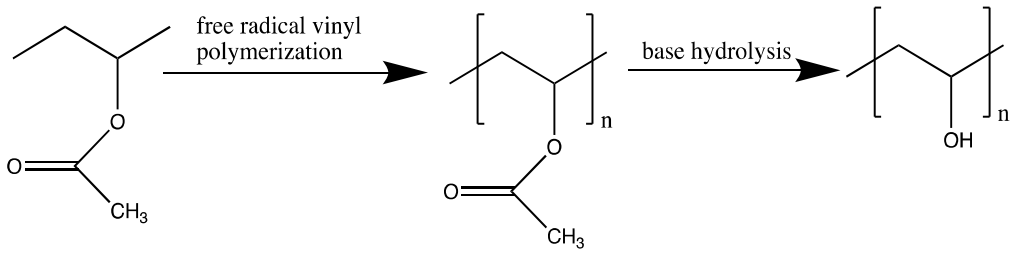

Figure 56: Synthesis of poly(vinyl alcohol)

Appendix B: Structures and Names of Selected Bio-friendly Additives

The additives selected in Chapter 3 were chosen due to being classified as either potentially biocompatible or non-toxic. As a result, they were termed as "bio-friendly". All chemical structures shown in Figure 57 (with the name below the structure) were provided by Sigma Aldrich except for starch (ChemDraw), k-carrageenan (DOI: 10.1016/j.carbpol.2015.01.066), hydroxyapatite (ChemDraw), xanthan gum (DOI: 10.1155/2014/273650), and agar (Fisher Scientific CAS 9002-18-0, A10752).

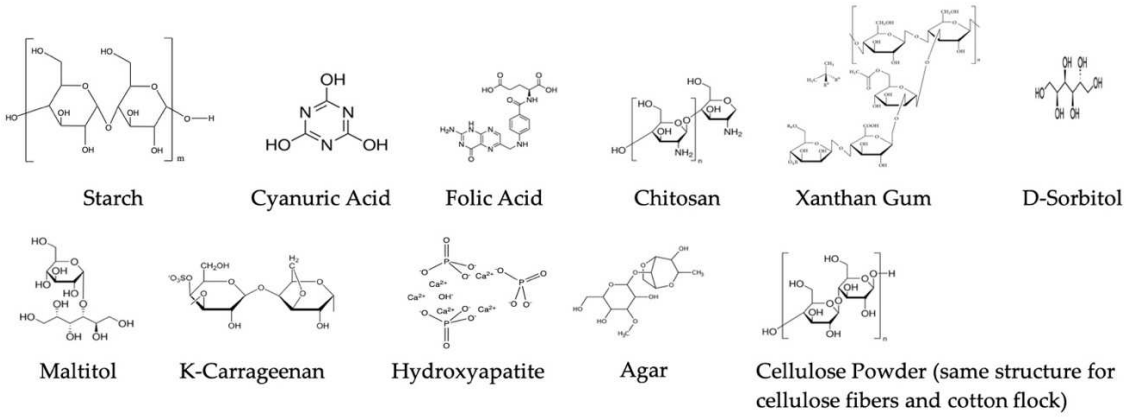

Figure 57: Names and structures of selected bio-friendly additives

References

[1] R. Bai, J. Yang, Z. Suo, *European Journal of Mechanics - A/Solids* **2019**, *74*, 337.

[2] J.-Y. Sun, X. Zhao, W. R. K. Illeperuma, O. Chaudhuri, K. H. Oh, D. J. Mooney, J. J. Vlassak, Z. Suo, *Nature* **2012**, *489*, 133.

[3] T. L. Sun, T. Kurokawa, S. Kuroda, A. B. Ihsan, T. Akasaki, K. Sato, M. A. Haque, T. Nakajima, J. P. Gong, *Nature Materials* **2013**, *12*, 932.

[4] P. Jaipan, A. Nguyen, R. J. Narayan, *MRS Communications* **2017**, *7*, 416.

[5] J. Kopeček, *Biomaterials* **2007**, *28*, 5185.

[6] Z. Zhuang, L. Wu, X. Ma, W. Diao, Y. Fang, *Journal of Applied Polymer Science* **2018**, *135*, 46847.

[7] G. Li, Q. Yan, H. Xia, Y. Zhao, *ACS Appl. Mater. Interfaces* **2015**, *7*, 12067.

[8] P. Song, Z. Xu, Q. Guo, *ACS Macro Lett.* **2013**, *2*, 1100.

[9] B. E. B. Jensen, I. Dávila, A. N. Zelikin, *J Phys Chem B* **2016**, *120*, 5916.

[10] Q. Chai, Y. Jiao, X. Yu, *Gels* **2017**, *3*, 6.

[11] L. Han, X. Lu, M. Wang, D. Gan, W. Deng, K. Wang, L. Fang, K. Liu, C. W. Chan, Y. Tang, L.-T. Weng, H. Yuan, *Small* **2017**, *13*, 1601916.

[12] M. Liu, X. Zeng, C. Ma, H. Yi, Z. Ali, X. Mou, S. Li, Y. Deng, N. He, *Bone Res* **2017**, *5*, 1.

[13] A. Timofejeva, M. D'Este, D. Loca, *European Polymer Journal* **2017**, *95*, 547.

[14] S. Jiang, S. Liu, W. Feng, *Journal of the Mechanical Behavior of Biomedical Materials* **2011**, *4*, 1228.

[15] W. Święszkowski, D. N. Ku, H. E. N. Bersee, K. J. Kurzydlowski, *Biomaterials* **2006**, *27*, 1534.

[16] R. Ma, D. Xiong, F. Miao, J. Zhang, Y. Peng, *Materials Science and Engineering: C* **2009**, *29*, 1979.

[17] L. C. Hughes, C. W. Archer, I. ap Gwynn, *Eur Cell Mater* **2005**, *9*, 68.

[18] E. R. Vina, C. K. Kwoh, *Curr Opin Rheumatol* **2018**, *30*, 160.

[19] B. R. Deshpande, J. N. Katz, D. H. Solomon, E. H. Yelin, D. J. Hunter, S. P. Messier, L. G. Suter, E. Losina, *Arthritis Care & Research* **2016**, *68*, 1743.

[20] C. M. Torio, B. J. Moore, in *Healthcare Cost and Utilization Project (HCUP) Statistical Briefs*, Agency For Healthcare Research And Quality (US), Rockville (MD), **2016**.

[21] S. Lin-Gibson, S. Bencherif, J. A. Cooper, S. J. Wetzel, J. M. Antonucci, B. M. Vogel, F. Horkay, N. R. Washburn, *Biomacromolecules* **2004**, *5*, 1280.

[22] A. K. Whitehead, H. H. Barnett, M. E. Caldorera-Moore, J. J. Newman, *Regen Biomater* **2018**, *5*, 167.

[23] S. Bäckström, J. Benavente, R. W. Berg, K. Stibius, M. S. Larsen, H. Bohr, C. Hélix-Nielsen, *Materials Sciences and Applications* **2012**, *3*, 425.

[24] A. Schmocker, A. Khoushabi, D. A. Frauchiger, B. Gantenbein, C. Schizas, C. Moser, P.-E. Bourban, D. P. Pioletti, *Biomaterials* **2016**, *88*, 110.

[25] E. Zant, D. W. Grijpma, *BIOMACROMOLECULES* **2016**, *17*, 1582.

[26] J. A. Killion, L. M. Geever, D. M. Devine, J. E. Kennedy, C. L. Higginbotham, *Journal of the Mechanical Behavior of Biomedical Materials* **2011**, *4*, 1219.

[27] X. Cui, K. Breitenkamp, M. G. Finn, M. Lotz, D. D. D'Lima, *Tissue Eng Part A* **2012**, *18*, 1304.

[28] J. A. Gavira, A. Cera-Manjarres, K. Ortiz, J. Mendez, J. A. Jimenez-Torres, L. D. Patiño-Lopez, M. Torres-Lugo, *Cryst Growth Des* **2014**, *14*, 3239.

[29] P. Karami, C. S. Wyss, A. Khoushabi, A. Schmocker, M. Broome, C. Moser, P.-E. Bourban, D. P. Pioletti, *ACS Appl. Mater. Interfaces* **2018**, *10*, 38692.

[30] A. Khoushabi, A. Schmocker, D. P. Pioletti, C. Moser, C. Schizas, J. A. Månson, P. E. Bourban, *Composites Science and Technology* **2015**, *119*, 93.

[31] Z. Zhou, D. Yang, J. Nie, Y. Ren, F. Cui, *Journal of Bioactive and Compatible Polymers* **2009**, *24*, 405.

[32] M. Aslam, M. A. Kalyar, Z. A. Raza, *Polymer Engineering & Science* **2018**, *58*, 2119.

[33] C. M. Hassan, N. Peppas, *Adv Polym Sci* **2000**, *153*, 37.

[34] M. Oka, T. Noguchi, P. Kumar, K. Ikeuchi, T. Yamamuro, S. H. Hyon, Y. Ikada, *Clinical Materials* **1990**, *6*, 361.

[35] J. A. Stammen, S. Williams, D. N. Ku, R. E. Guldberg, *Biomaterials* **2001**, *22*, 799.

[36] A. Takasu, K. Aoi, M. Tsuchiya, M. Okada, *Journal of Applied Polymer Science* **1999**, *73*, 1171.

[37] R. H. Schmedlen, K. S. Masters, J. L. West, *Biomaterials* **2002**, *23*, 4325.

[38] A. M. Neres Santos, A. P. Duarte Moreira, C. W. Piler Carvalho, R. Luchese, E. Ribeiro, G. B. McGuinness, M. Fernandes Mendes, R. Nunes Oliveira, *Materials (Basel)* **2019**, *12*, 559.

[39] S. Yarimitsu, S. Sasaki, T. Murakami, A. Suzuki, *Biosurface and Biotribology* **2016**, *2*, 40.

[40] S. Yarimitsu, K. Nakashima, Y. Sawae, T. Murakami, in *5th World Tribology Congress, WTC 2013*, Politecnico Di Torino (DIMEAS), **2014**, pp. 2279–2282.

[41] V. M. Sardinha, L. L. Lima, W. D. Belangero, C. A. Zavaglia, V. P. Bavaresco, J. R. Gomes, *Wear* **2013**, *301*, 218.

[42] M. Kobayashi, Y.-S. Chang, M. Oka, *Biomaterials* **2005**, *26*, 3243.

[43] M. Kobayashi, J. Toguchida, M. Oka, *The Knee* **2003**, *10*, 47.

[44] T. Wang, M. Turhan, S. Gunasekaran, *Polymer International* **2004**, *53*, 911.

[45] Y. S. Zhang, A. Khademhosseini, *Science* **2017**, *356*, eaaf3627.

[46] R. Ramachandran, D. Jung, A. M. Spokoyny, *NPG Asia Materials* **2019**, *11*, 19.

[47] W. Hu, Z. Wang, Y. Xiao, S. Zhang, J. Wang, *Biomater. Sci.* **2019**, *7*, 843.

[48] M. F. Akhtar, M. Hanif, N. M. Ranjha, *Saudi Pharmaceutical Journal* **2016**, *24*, 554.

[49] J. Maitra, V. K. Shukla, *American Journal of Polymer Science* **2014**, *4*, 25.

[50] M. N. Moghadam, D. P. Pioletti, *J Mech Behav Biomed Mater* **2015**, *41*, 161.

[51] X. Jiang, N. Xiang, H. Zhang, Y. Sun, Z. Lin, L. Hou, *Carbohydrate Polymers* **2018**, *186*, 377.

[52] Y. Zhang, M. Song, Y. Diao, B. Li, L. Shi, R. Ran, *RSC Adv.* **2016**, *6*, 112468.

[53] C. M. Hassan, N. A. Peppas, *Macromolecules* **2000**, *33*, 2472.

[54] R. parhi, *Adv Pharm Bull* **2017**, *7*, 515.

[55] H. Li, P. Yang, P. Pageni, C. Tang, *Macromolecular Rapid Communications* **2017**, *38*, 1700109.

[56] A. S. Aroca, M. M. Pradas, J. L. G. Ribelles, J. Rault, *European Polymer Journal* **2015**, *72*, 523.

[57] H. Jiang, L. Duan, X. Ren, G. Gao, *European Polymer Journal* **2019**, *112*, 660.

[58] Q. Chen, X. Yan, L. Zhu, H. Chen, B. Jiang, D. Wei, L. Huang, J. Yang, B. Liu, J. Zheng, *Chem. Mater.* **2016**, *28*, 5710.

[59] N. Yuan, L. Xu, B. Xu, J. Zhao, J. Rong, *Carbohydrate Polymers* **2018**, *193*, 259.

[60] I. Tunn, M. J. Harrington, K. G. Blank, *Biomimetics* **2019**, *4*, 25.

[61] I. M. El-Sherbiny, M. H. Yacoub, *Glob Cardiol Sci Pract* **2013**, *2013*, 316.

[62] H. Bian, L. Wei, C. Lin, Q. Ma, H. Dai, J. Y. Zhu, *ACS Sustainable Chem. Eng.* **2018**, *6*, 4821.

[63] G. K. Tummala, R. Rojas, A. Mihranyan, *J. Phys. Chem. B* **2016**, *120*, 13094.

[64] J. M. Lee, M. T. Sultan, S. H. Kim, V. Kumar, Y. K. Yeon, O. J. Lee, C. H. Park, *International Journal of Molecular Sciences* **2017**, *18*, 1707.

[65] L. E. Millon, W. K. Wan, *Journal of Biomedical Materials Research Part B: Applied Biomaterials* **2006**, *79B*, 245.

[66] N. Sakai, S. Yarimitsu, Y. Sawae, M. Komori, T. Murakami, *Biosurface and Biotribology* **2019**, *5*, 13.

[67] G. Wu, B. Su, W. Zhang, C. Wang, *Materials Chemistry and Physics* **2008**, *107*, 364.

[68] H. Wang, F. Wang, X. Li, X. Peng, Z. Ci, Z. Wang, *Materials Letters* **2018**, *228*, 399.

[69] F. Mirahmadi, M. Tafazzoli-Shadpour, M. A. Shokrgozar, S. Bonakdar, *Materials Science and Engineering: C* **2013**, *33*, 4786.

[70] Y. Pan, Q. Shen, C. Pan, J. Wang, *Journal of Materials Science & Technology* **2013**, *29*, 551.

[71] S. Amadori, P. Torricelli, S. Panzavolta, A. Parrilli, M. Fini, A. Bigi, *Macromolecular Bioscience* **2015**, *15*, 941.

[72] W. R. K. Illeperuma, J.-Y. Sun, Z. Suo, J. J. Vlassak, *Extreme Mechanics Letters* **2014**, DOI 10.1016/j.eml.2014.11.001.

[73] J. Visser, F. P. W. Melchels, J. E. Jeon, E. M. van Bussel, L. S. Kimpton, H. M. Byrne, W. J. A. Dhert, P. D. Dalton, D. W. Hutmacher, J. Malda, *Nat Commun* **2015**, *6*, 6933.

[74] I. Doench, T. Ahn Tran, L. David, A. Montembault, E. Viguier, C. Gorzelanny, G. Sudre, T. Cachon, M. Louback-Mohamed, N. Horbelt, C. Peniche-Covas, A. Osorio-Madrazo, *Biomimetics* **2019**, *4*, 19.

[75] M. Castilho, G. Hochleitner, W. Wilson, B. van Rietbergen, P. D. Dalton, J. Groll, J. Malda, K. Ito, *Scientific Reports* **2018**, *8*, 1245.

[76] D. Benayahu, M. Sharabi, L. Pomeraniec, L. Awad, R. Haj-Ali, Y. Benayahu, *Mar Drugs* **2018**, *16*, DOI 10.3390/md16040102.

[77] S. Xu, L. Deng, J. Zhang, L. Yin, A. Dong, *Journal of Biomedical Materials Research Part B: Applied Biomaterials* **2016**, *104*, 640.

[78] J. P. Chaudhary, F. Kholiya, N. Vadodariya, V. M. Budheliya, A. Gogda, R. Meena, *Arabian Journal of Chemistry* **2018**, DOI 10.1016/j.arabjc.2017.12.034.

[79] K. Y. Lee, K. H. Bouhadir, D. J. Mooney, *Biomaterials* **2004**, *25*, 2461.

[80] X. Dai, Y. Zhang, L. Gao, T. Bai, W. Wang, Y. Cui, W. Liu, *Adv. Mater. Weinheim* **2015**, *27*, 3566.

[81] H. Wang, S. C. Heilshorn, *Adv Mater* **2015**, *27*, 3717.

[82] J. Zhang, N. Wang, W. Liu, X. Zhao, W. Lu, *Soft Matter* **2013**, *9*, 6331.

[83] J. Shao, Z. Zhang, S. Zhao, S. Wang, Z. Guo, H. Xie, Y. Hu, *Starch - Stärke* **2019**, *71*, 1800281.

[84] Y. Deng, M. Huang, D. Sun, Y. Hou, Y. Li, T. Dong, X. Wang, L. Zhang, W. Yang, *ACS Appl. Mater. Interfaces* **2018**, *10*, 37544.

[85] R. Rodríguez-Rodríguez, Z. Y. García-Carvajal, I. Jiménez-Palomar, J. A. Jiménez-Avalos, H. Espinosa-Andrews, *Journal of Applied Polymer Science* **2019**, *136*, 47149.

[86] S. Baghaie, M. T. Khorasani, A. Zarrabi, J. Moshtaghian, *Journal of Biomaterials Science, Polymer Edition* **2017**, *28*, 2220.

[87] A. Joshi, G. Fussell, J. Thomas, A. Hsuan, A. Lowman, A. Karduna, E. Vresilovic, M. Marcolongo, *Biomaterials* **2006**, *27*, 176.

[88] T. Liu, X. Peng, Y.-N. Chen, Q.-W. Bai, C. Shang, L. Zhang, H. Wang, *Macromol Rapid Commun* **2018**, *39*, e1800050.

[89] Y.-N. Chen, L. Peng, T. Liu, Y. Wang, S. Shi, H. Wang, *ACS Appl. Mater. Interfaces* **2016**, *8*, 27199.

[90] L. E. Millon, C. J. Oates, W. Wan, *J. Biomed. Mater. Res. Part B Appl. Biomater.* **2009**, *90*, 922.

[91] J. T. Kaplan, C. P. Neu, H. Drissi, N. C. Emery, D. M. Pierce, *J Mech Behav Biomed Mater* **2017**, *65*, 734.

[92] S. Gu, L. Duan, X. Ren, G. H. Gao, *Journal of Colloid and Interface Science* **2017**, *492*, 119.

[93] X.-H. Wang, F. Song, J. Xue, D. Qian, X.-L. Wang, Y.-Z. Wang, *Polymer* **2018**, *153*, 637.

[94] Q. Chen, L. Zhu, H. Chen, H. Yan, L. Huang, J. Yang, J. Zheng, *Advanced Functional Materials* **2015**, *25*, 1598.

[95] J. Hou, X. Ren, S. Guan, L. Duan, G. Hui Gao, Y. Kuai, H. Zhang, *Soft Matter* **2017**, *13*, 1357.

[96] R. Bai, Q. Yang, J. Tang, X. P. Morelle, J. Vlassak, Z. Suo, *Extreme Mechanics Letters* **2017**, *15*, 91.

[97] R. Bai, J. Yang, X. P. Morelle, C. Yang, Z. Suo, *ACS Macro Lett.* **2018**, *7*, 312.

[98] E. Zhang, R. Bai, X. P. Morelle, Z. Suo, *Soft Matter* **2018**, *14*, 3563.

[99] J. Tang, J. Li, J. J. Vlassak, Z. Suo, *Extreme Mechanics Letters* **2017**, *10*, 24.

[100] W. Zhang, X. Liu, J. Wang, J. Tang, J. Hu, T. Lu, Z. Suo, *Engineering Fracture Mechanics* **2018**, *187*, 74.

[101] X. Hu, R. Liang, J. Li, Z. Liu, G. Sun, *Materials & Design* **2019**, *163*, 107547.

[102] M. Kasra, M. Parnianpour, A. Shirazi-Adl, J. L. Wang, M. D. Grynpas, *Technology and Health Care* **2004**, *12*, 333.

[103] R. E. Webber, C. Creton, H. R. Brown, J. P. Gong, *Macromolecules* **2007**, *40*, 2919.

[104] K. L. Spiller, S. A. Maher, A. M. Lowman, *Tissue Eng Part B Rev* **2011**, *17*, 281.

[105] S. L. Vega, M. Y. Kwon, J. A. Burdick, *Eur Cell Mater* **2017**, *33*, 59.

[106] T. Xia, W. Liu, L. Yang, *Journal of Biomedical Materials Research Part A* **2017**, *105*, 1799.

[107] I. Gadjanski, *F1000Research* **2018**, *6*, 2158.

[108] B. Weightman, *Journal of Biomechanics* **1976**, *9*, 193.

[109] B. Weightman, D. J. Chappell, E. A. Jenkins, *Annals of the Rheumatic Diseases* **1978**, *37*, 58.

[110] G. Bellucci, B. B. Seedhom, *Rheumatology (Oxford)* **2001**, *40*, 1337.

[111] S. R. Stauffer, N. A. Peppast, *Polymer* **1992**, *33*, 3932.

[112] K. Ou, X. Dong, C. Qin, X. Ji, J. He, *Materials Science and Engineering: C* **2017**, *77*, 1017.

[113] H. Bodugoz-Senturk, C. E. Macias, J. H. Kung, O. K. Muratoglu, *Biomaterials* **2009**, *30*, 589.

[114] Z. Gong, G. Zhang, X. Zeng, J. Li, G. Li, W. Huang, R. Sun, C. Wong, *ACS Appl. Mater. Interfaces* **2016**, *8*, 24030.

[115] H. Fan, J. Wang, Z. Jin, *Macromolecules* **2018**, *51*, 1696.

[116] T. Chen, Y. Chen, H. U. Rehman, Z. Chen, Z. Yang, M. Wang, H. Li, H. Liu, *ACS Appl. Mater. Interfaces* **2018**, *10*, 33523.

[117] M. T. Haseeb, M. A. Hussain, S. H. Yuk, S. Bashir, M. Nauman, *Carbohydrate Polymers* **2016**, *136*, 750.

[118] N. D. Broom, A. Oloyede, *Biomaterials* **1998**, *19*, 1179.

[119] Y. Shi, D. Xiong, Y. Liu, N. Wang, X. Zhao, *Materials Science and Engineering: C* **2016**, *65*, 172.

[120] R. Ricciardi, F. Auriemma, C. De Rosa, F. Lauprêtre, *Macromolecules* **2004**, *37*, 1921.

[121] R. Ricciardi, F. Auriemma, C. Gaillet, C. De Rosa, F. Lauprêtre, *Macromolecules* **2004**, *37*, 9510.

[122] R. C. Simoni, G. F. Lemes, S. Fialho, O. H. Gonçalves, A. M. Gozzo, V. Chiaradia, C. Sayer, M. A. Shirai, F. V. Leimann, *Anais da Academia Brasileira de Ciências* **2017**, *89*, 745.

[123] V. R. Patel, M. M. Amiji, *Pharm Res* **1996**, *13*, 588.

[124] A. Suzuki, S. Sasaki, *Proc Inst Mech Eng H* **2015**, *229*, 828.

[125] P. Guo, J. Liang, Y. Li, X. Lu, H. Fu, H. Jing, S. Guan, D. Han, L. Niu, *Colloids and Surfaces A: Physicochemical and Engineering Aspects* **2019**, *571*, 64.

[126] J. L. Holloway, A. M. Lowman, G. R. Palmese, *Soft Matter* **2012**, *9*, 826.

[127] S. J. Kerber, T. L. Barr, G. P. Mann, W. A. Brantley, E. Papazoglou, J. C. Mitchell, *J. of Materi Eng and Perform* **1998**, *7*, 329.

[128] T. Puspitasari, K. M. L. Raja, D. S. Pangerteni, A. Patriati, E. G. R. Putra, *Procedia Chemistry* **2012**, *4*, 186.

[129] T. Hatakeyema, J. Uno, C. Yamada, A. Kishi, H. Hatakeyama, *Thermochimica Acta* **2005**, *431*, 144.

[130] V. I. Lozinsky, L. G. Damshkaln, I. N. Kurochkin, I. I. Kurochkin, *Colloid J* **2008**, *70*, 189.

[131] C.-M. Tang, Y.-H. Tian, S.-H. Hsu, *Materials (Basel)* **2015**, *8*, 4895.

[132] L. M. Sanchez, V. A. Alvarez, R. P. Ollier, *Journal of Applied Polymer Science* **2019**, *136*, 47663.

[133] M. Huang, Y. Hou, Y. Li, D. Wang, L. Zhang, *Des Monomers Polym* **2017**, *20*, 505.

[134] M. Gong, L. Zhang, Y. Zuo, Q. Zou, Y. Wang, L. Wang, Y. Li, *Journal of Applied Polymer Science* **2012**, *125*, 2799.

[135] Y. Wang, J. Wu, Z. Cao, C. Ma, Q. Tong, J. Li, H. Liu, J. Zheng, G. Huang, *Polymer* **2019**, *179*, 121661.

[136] A. T. Miller, D. L. Safranski, K. E. Smith, D. G. Sycks, R. E. Guldberg, K. Gall, *Polymer* **2017**, *108*, 121.

[137] J. Móczó, B. Pukánszky, *Journal of Industrial and Engineering Chemistry* **2008**, *14*, 535.

[138] I. Srivastava, N. Koratkar, *JOM* **2010**, *62*, 50.

[139] B. M. J. Martens, W. J. J. Gerrits, E. M. A. M. Bruininx, H. A. Schols, *Journal of Animal Science and Biotechnology* **2018**, *9*, 91.

[140] J. A. M. Ferreira, L. P. Borrego, J. D. M. Costa, C. Capela, *Composites Part B: Engineering* **2013**, *52*, 286.

[141] ASTM D638-14, *Standard Test Method for Tensile Properties of Plastics*, ASTM International, West Conshohocken, PA, **2014**.

[142] T. Minas, A. H. Gomoll, R. Rosenberger, R. O. Royce, T. Bryant, *Am J Sports Med* **2009**, *37*, 902.

[143] J. D. Harris, R. A. Siston, R. H. Brophy, C. Lattermann, J. L. Carey, D. C. Flanigan, *Osteoarthritis and Cartilage* **2011**, *19*, 779.

[144] L. Cipollaro, M. C. Ciardulli, G. D. Porta, G. M. Peretti, N. Maffulli, *Br Med Bull* **2019**, *132*, 53.

[145] E. V. Medvedeva, E. A. Grebenik, S. N. Gornostaeva, V. I. Telpuhov, A. V. Lychagin, P. S. Timashev, A. S. Chagin, *Int J Mol Sci* **2018**, *19*, DOI 10.3390/ijms19082366.

[146] B. M. Devitt, S. W. Bell, K. E. Webster, J. A. Feller, T. S. Whitehead, *The Knee* **2017**, *24*, 508.

[147] G. Knutsen, J. O. Drogset, L. Engebretsen, T. Grøntvedt, T. C. Ludvigsen, S. Løken, E. Solheim, T. Strand, O. Johansen, *JBJS* **2016**, *98*, 1332.

[148] P. Bowland, E. Ingham, L. Jennings, J. Fisher, *Proc Inst Mech Eng H* **2015**, *229*, 879.

[149] L. Kunčická, R. Kocich, T. C. Lowe, *Progress in Materials Science* **2017**, *88*, 232.

[150] M. C. Chapter, J. H. Garfinkel, T. Cabe, S. Ellis, M. Roberts, M. O'Malley, A. Elliot, D. S. Levine, J. Deland, C. Demetracopoulos, M. Drakos, *Foot & Ankle Orthopaedics* **2019**, *4*, 2473011419S00137.

[151] M. G. Cisternas, L. Murphy, J. J. Sacks, D. H. Solomon, D. J. Pasta, C. G. Helmick, *Arthritis Care Res (Hoboken)* **2016**, *68*, 574.

[152] J. M. Hootman, C. G. Helmick, K. E. Barbour, K. A. Theis, M. A. Boring, *Arthritis Rheumatol* **2016**, *68*, 1582.

[153] G. E. Kempson, H. Muir, C. Pollard, M. Tuke, *Biochimica et Biophysica Acta (BBA) - General Subjects* **1973**, *297*, 456.

[154] G. E. Kempson, *Ann Rheum Dis* **1982**, *41*, 508.

[155] A. J. Kerin, M. R. Wisnom, M. A. Adams, *Proc Inst Mech Eng H* **1998**, *212*, 273.

[156] H. A. C. Jacob, *Clinical Biomechanics* **2001**, *16*, 783.

[157] A. Clifford, M. O'Connell, S. Gabriel, L. E. Miller, J. E. Block, *Journal of Medical Engineering & Technology* **2011**, *35*, 65.

[158] W. K. Wan, A. D. Bannerman, L. F. Yang, H. Mak, *Polymeric Cryogels: Macroporous Gels with Remarkable Properties*, Springer International Publishing, **2014**.

[159] M. I. Baker, S. P. Walsh, Z. Schwartz, B. D. Boyan, *Journal of Biomedical Materials Research Part B: Applied Biomaterials* **2012**, *100B*, 1451.

[160] R. K. Korhonen, M. S. Laasanen, J. Töyräs, J. Rieppo, J. Hirvonen, H. J. Helminen, J. S. Jurvelin, *Journal of Biomechanics* **2002**, *35*, 903.

[161] Y. Hagiwara, A. Putra, A. Kakugo, H. Furukawa, J. P. Gong, *Cellulose* **2010**, *17*, 93.

[162] A. Nakayama, A. Kakugo, J. P. Gong, Y. Osada, M. Takai, T. Erata, S. Kawano, *Advanced Functional Materials* **2004**, *14*, 1124.

[163] Q. Wang, R. Hou, Y. Cheng, J. Fu, *Soft Matter* **2012**, *8*, 6048.

[164] Y. Chen, K. Zheng, L. Niu, Y. Zhang, Y. Liu, C. Wang, F. Chu, *International Journal of Biological Macromolecules* **2019**, *128*, 414.

[165] F. Yang, V. Tadepalli, B. J. Wiley, *ACS Biomater. Sci. Eng.* **2017**, *3*, 863.

[166] G. E. Kempson, *Biochimica et Biophysica Acta (BBA) - General Subjects* **1991**, *1075*, 223.

[167] K. Yasuda, J. Ping Gong, Y. Katsuyama, A. Nakayama, Y. Tanabe, E. Kondo, M. Ueno, Y. Osada, *Biomaterials* **2005**, *26*, 4468.

[168] T. Nakajima, N. Takedomi, T. Kurokawa, H. Furukawa, J. P. Gong, *Polym. Chem.* **2010**, *1*, 693.

[169] Q. Chen, L. Zhu, C. Zhao, Q. Wang, J. Zheng, *Advanced Materials* **2013**, *25*, 4171.

[170] L. Xu, X. Zhao, C. Xu, N. A. Kotov, *Advanced Materials* **2018**, *30*, 1703343.

[171] S. Li, X. Bu, L. Wu, X. Ma, W. Diao, Z. Zhuang, Y. Zhou, *Polymer Engineering & Science* **2019**, *59*, 1657.

[172] Y. Zhao, M. Li, B. Liu, J. Xiang, Z. Cui, X. Qu, D. Qiu, Y. Tian, Z. Yang, *J. Mater. Chem. B* **2018**, *6*, 1351.

[173] K. Chen, G. Chen, S. Wei, X. Yang, D. Zhang, L. Xu, *Materials Science and Engineering: C* **2018**, *91*, 579.

[174] K. Fujii, H. Asai, T. Ueki, T. Sakai, S. Imaizumi, U. Chung, M. Watanabe, M. Shibayama, *Soft Matter* **2012**, *8*, 1756.

[175] L. Xu, C. Wang, Y. Cui, A. Li, Y. Qiao, D. Qiu, *Science Advances* **2019**, *5*, eaau3442.

[176] Z. Zhang, R. Liu, H. Zepeda, L. Zeng, J. Qiu, S. Wang, *ACS Appl. Polym. Mater.* **2019**, *1*, 2023.

[177] S. Gan, W. Lin, Y. Zou, B. Xu, X. Zhang, J. Zhao, J. Rong, *Carbohydrate Polymers* **2020**, *229*, 115523.

[178] W. Sun, B. Xue, Q. Fan, R. Tao, C. Wang, X. Wang, Y. Li, M. Qin, W. Wang, B. Chen, Y. Cao, *Science Advances* **2020**, *6*, eaaz9531.

[179] Y. Jiang, Y. Yang, X. Zheng, Y. Yi, X. Chen, Y. Li, D. Sun, L. Zhang, *NPG Asia Materials* **2020**, *12*, 1.

[180] X. Xiang, G. Chen, K. Chen, X. Jiang, L. Hou, *International Journal of Biological Macromolecules* **2020**, *142*, 574.

[181] L. Zhou, X. Pei, K. Fang, R. Zhang, J. Fu, *Polymer* **2020**, *192*, 122319.

[182] A. J. Sophia Fox, A. Bedi, S. A. Rodeo, *Sports Health* **2009**, *1*, 461.

[183] X. L. Lu, V. C. Mow, *Medicine & Science in Sports & Exercise* **2008**, *40*, 193.

[184] V. C. Mow, R. Huiskes, *Basic Orthopaedic Biomechanics & Mechano-Biology*, Lippincott Williams & Wilkins, **2005**.

[185] P. L. Chandran, F. Horkay, *Acta Biomaterialia* **2012**, *8*, 3.

[186] C. Kiani, L. Chen, Y. J. Wu, A. J. Yee, B. B. Yang, *Cell Research* **2002**, *12*, 19.

[187] T. Minas, *The Journal of Bone and Joint Surgery. British volume* **2012**, *94-B*, 141.

[188] X. Lux Lu, C. Miller, F. H. Chen, X. Edward Guo, V. C. Mow, *Journal of Biomechanics* **2007**, *40*, 2434.

[189] P. J. Basser, R. Schneiderman, R. A. Bank, E. Wachtel, A. Maroudas, *Archives of Biochemistry and Biophysics* **1998**, *351*, 207.

[190] D. Huster, L. Naji, J. Schiller, K. Arnold, *Appl. Magn. Reson.* **2004**, *27*, 471.

[191] A. Maroudas, C. Bannon, *Biorheology* **1981**, *18*, 619.

[192] A. Maroudas, E. Wachtel, G. Grushko, E. P. Katz, P. Weinberg, *Biochimica et Biophysica Acta (BBA) - General Subjects* **1991**, *1073*, 285.

[193] A. Maroudas, *Orthopaedic Proceedings* **2002**, *84-B*, 309.

[194] V. C. Mow, S. C. Kuei, W. M. Lai, C. G. Armstrong, *J Biomech Eng* **1980**, *102*, 73.

[195] J. Farr, G. C. Gracitelli, N. Shah, E. Y. Chang, A. H. Gomoll, *Am J Sports Med* **2016**, *44*, 2015.

[196] G. Helenius, H. Bäckdahl, A. Bodin, U. Nannmark, P. Gatenholm, B. Risberg, *Journal of Biomedical Materials Research Part A* **2006**, *76A*, 431.

[197] G. Guhados, W. Wan, J. L. Hutter, *Langmuir* **2005**, *21*, 6642.

[198] A. N. Nakagaito, S. Iwamoto, H. Yano, *Appl. Phys. A* **2005**, *80*, 93.

[199] W. K. Czaja, D. J. Young, M. Kawecki, R. M. Brown, *Biomacromolecules* **2007**, *8*, 1.

[200] A. Svensson, E. Nicklasson, T. Harrah, B. Panilaitis, D. L. Kaplan, M. Brittberg, P. Gatenholm, *Biomaterials* **2005**, *26*, 419.

[201] C. Grant, P. Twigg, A. Egan, A. Moody, A. Smith, D. Eagland, N. Crowther, S. Britland, *Biotechnology Progress* **2006**, *22*, 1400.

[202] H. Kosukegawa, K. Mamada, K. Kuroki, L. Liu, K. Inoue, T. Hayase, M. Ohta, *Journal of Fluid Science and Technology* **2008**, *3*, 533.

[203] U. Fumio, Y. Hiroshi, N. Kumiko, N. Sachihiko, S. Kenji, M. Yasunori, *International Journal of Pharmaceutics* **1990**, *58*, 135.

[204] D. N. Ku, L. G. Braddon, D. M. Wootton, *Poly(Vinyl Alcohol) Cryogel*, **1999**, US5981826A.

[205] Y. Sasazaki, R. Shore, B. B. Seedhom, *Journal of Anatomy* **2006**, *208*, 681.

[206] S. Wang, F. Jiang, X. Xu, Y. Kuang, K. Fu, E. Hitz, L. Hu, *Advanced Materials* **2017**, *29*, 1702498.

[207] R. Xue, X. Xin, L. Wang, J. Shen, F. Ji, W. Li, C. Jia, G. Xu, *Phys. Chem. Chem. Phys.* **2015**, *17*, 5431.

[208] F. Yang, J. Zhao, W. J. Koshut, J. Watt, J. C. Riboh, K. Gall, B. J. Wiley, *Advanced Functional Materials* **2020**, 2003451.

[209] W. J. Koshut, D. Smoot, C. Rummel, A. Kirillova, K. Gall, *Macromolecular Materials and Engineering* **2020**, *305*, 1900784.

[210] M. J. Askew, V. C. Mow, *J Biomech Eng* **1978**, *100*, 105.

[211] B. B. Seedhom, *Rheumatology (Oxford)* **2006**, *45*, 146.

[212] M. A. R. Freeman, *Adult Articular Cartilage*, Pitman Medical, **1979**.

[213] R. D. Jamison, Y.-L. Shen, *Journal of Composite Materials* **2016**, *50*, 507.

[214] C. N. Kelly, J. Francovich, S. Julmi, D. Safranski, R. E. Guldberg, H. J. Maier, K. Gall, *Acta Biomaterialia* **2019**, *94*, 610.

[215] J. P. Gong, Y. Katsuyama, T. Kurokawa, Y. Osada, *Advanced Materials* **2003**, *15*, 1155.

[216] K. Yasuda, N. Kitamura, J. P. Gong, K. Arakaki, H. J. Kwon, S. Onodera, Y. M. Chen, T. Kurokawa, F. Kanaya, Y. Ohmiya, Y. Osada, *Macromolecular Bioscience* **2009**, *9*, 307.

[217] W. Wang, R. Narain, H. Zeng, *Front Chem* **2018**, *6*, DOI 10.3389/fchem.2018.00497.

[218] F. Pizzocolo, J. M. Huyghe, K. Ito, *Engineering Fracture Mechanics* **2013**, *97*, 72.

[219] T. van Vliet, P. Walstra, *Faraday Discussions* **1995**, *101*, 359.

[220] J. Tong, J. R. Yates, M. W. Brown, *Engineering Fracture Mechanics* **1997**, *56*, 213.

[221] E. Rocha-Rangel, *Nanocomposites with Unique Properties and Applications in Medicine and Industry* **2011**, DOI 10.5772/18127.

[222] F. Luo, T. L. Sun, T. Nakajima, T. Kurokawa, Y. Zhao, A. B. Ihsan, H. L. Guo, X. F. Li, J. P. Gong, *Macromolecules* **2014**, *47*, 6037.

[223] Y. Yang, X. Wang, F. Yang, H. Shen, D. Wu, *Advanced Materials* **2016**, *28*, 7178.

[224] F. Wang, R. A. Weiss, *Macromolecules* **2018**, *51*, 7386.

[225] M. Liu, J. Guo, Z. Li, C.-Y. Hui, A. T. Zehnder, *Mechanics of Materials* **2019**, *138*, 103158.

[226] T. Baumberger, O. Ronsin, *J. Chem. Phys.* **2009**, *130*, 061102.

[227] M. Liu, J. Guo, C.-Y. Hui, A. T. Zehnder, *Exp Mech* **2019**, *59*, 1021.

[228] P. Yusong, D. Jie, C. Yan, S. Qianqian, *Materials Technology* **2016**, *31*, 266.

[229] G. Tao, Y. Wang, R. Cai, H. Chang, K. Song, H. Zuo, P. Zhao, Q. Xia, H. He, *Materials Science and Engineering: C* **2019**, *101*, 341.

[230] A. S. Oliveira, S. Schweizer, P. Nolasco, I. Barahona, J. Saraiva, R. Colaço, A. P. Serro, *Lubricants* **2020**, *8*, 36.

[231] W. Li, D. Wang, W. Yang, Y. Song, *RSC Adv.* **2016**, *6*, 20166.

[232] Y. Jiang, A. Schädlich, E. Amado, C. Weis, E. Odermatt, K. Mäder, J. Kressler, *Journal of Biomedical Materials Research Part B: Applied Biomaterials* **2010**, *93B*, 275.

[233] Q. Su, Y. Wang, S. Guan, H. Zhang, G. H. Gao, X. Zhu, *RSC Adv.* **2016**, *6*, 30570.

[234] J. Ma, J. Lee, S. S. Han, K. H. Oh, K. T. Nam, J.-Y. Sun, *ACS Appl. Mater. Interfaces* **2016**, *8*, 29220.

[235] R. Zhang, L. Wang, Z. Shen, M. Li, X. Guo, Y. Yao, *Macromolecular Rapid Communications* **2017**, *38*, 1700455.

[236] G. Du, F. Wu, Y. Cong, L. Nie, S. Liu, G. Gao, J. Fu, *Chem. Commun.* **2015**, *51*, 15534.

[237] M. Sun, J. Qiu, C. Lu, S. Jin, G. Zhang, E. Sakai, *Polymers* **2020**, *12*, 2263.

[238] C. Chen, Z. Wang, Z. Suo, *Extreme Mechanics Letters* **2017**, *10*, 50.

[239] W. Zhang, J. Hu, J. Tang, Z. Wang, J. Wang, T. Lu, Z. Suo, *ACS Macro Lett.* **2019**, *8*, 17.

[240] R. Long, C.-Y. Hui, *Soft Matter* **2016**, *12*, 8069.

[241] T. Stegmaier, P. Schneider, A. Vohrer, H. Planck, R. Blum, H. Bögner-Balz, in *Textiles, Polymers and Composites for Buildings* (Ed.: G. Pohl), Woodhead Publishing, **2010**, pp. 129–191e.

[242] M. J. Hammond, S. A. Fawaz, *Engineering Fracture Mechanics* **2016**, *153*, 25.

[243] H. Zhi, X. Fei, J. Tian, L. Zhao, H. Zhang, M. Jing, L. Xu, Y. Wang, Y. Li, *Biomater. Sci.* **2018**, *6*, 2320.

[244] J. Tavakoli, J. Gascooke, N. Xie, B. Z. Tang, Y. Tang, *ACS Appl. Polym. Mater.* **2019**, *1*, 1390.

[245] Y. Pan, *Micro Nano Letters* **2010**, *5*, 237.

[246] F. Yokoyama, I. Masada, K. Shimamura, T. Ikawa, K. Monobe, *Colloid & Polymer Sci* **1986**, *264*, 595.

[247] A. Ajovalasit, M. A. Sabatino, S. Todaro, S. Alessi, D. Giacomazza, P. Picone, M. Di Carlo, C. Dispenza, *Carbohydrate Polymers* **2018**, *179*, 262.

[248] K. C. Wasalathilake, D. G. D. Galpaya, G. A. Ayoko, C. Yan, *Carbon* **2018**, *137*, 282.

[249] Z. Bao, C. Xian, Q. Yuan, G. Liu, J. Wu, *Advanced Healthcare Materials* **2019**, *8*, 1900670.

[250] K. A. Athanasiou, M. P. Rosenwasser, J. A. Buckwalter, T. I. Malinin, V. C. Mow, *Journal of Orthopaedic Research* **1991**, *9*, 330.

[251] S. A. O'Leary, J. M. Link, E. O. Klineberg, J. C. Hu, K. A. Athanasiou, *Acta Biomaterialia* **2017**, *54*, 367.

[252] A. Chevrier, A. S. M. Kouao, G. Picard, M. B. Hurtig, M. D. Buschmann, *Journal of Orthopaedic Research* **2015**, *33*, 63.

[253] L. L. Y. Chiu, R. Giardini-Rosa, J. F. Weber, S. L. Cushing, S. D. Waldman, *Ann Otol Rhinol Laryngol* **2017**, *126*, 819.

[254] W. J. Koshut, C. Rummel, D. Smoot, A. Kirillova, K. Gall, *Macromolecular Materials and Engineering* **2021**, *306*, 2000679.

[255] U. Hansen, P. Zioupos, R. Simpson, J. D. Currey, D. Hynd, *Journal of Biomechanical Engineering* **2008**, *130*, DOI 10.1115/1.2838032.

[256] I. E. Shkolnik, *Cement and Concrete Composites* **2008**, *30*, 1000.

[257] P. Apelgren, E. Karabulut, M. Amoroso, A. Mantas, H. Martínez Ávila, L. Kölby, T. Kondo, G. Toriz, P. Gatenholm, *ACS Biomater. Sci. Eng.* **2019**, *5*, 2482.

[258] H. Martínez Ávila, S. Schwarz, E.-M. Feldmann, A. Mantas, A. von Bomhard, P. Gatenholm, N. Rotter, *Appl Microbiol Biotechnol* **2014**, *98*, 7423.

[259] H. Martínez Ávila, E.-M. Feldmann, M. M. Pleumeekers, L. Nimeskern, W. Kuo, W. C. de Jong, S. Schwarz, R. Müller, J. Hendriks, N. Rotter, G. J. V. M. van Osch, K. S. Stok, P. Gatenholm, *Biomaterials* **2015**, *44*, 122.

[260] V. Horbert, P. Foehr, F. Kramer, U. Udhardt, M. Bungartz, O. Brinkmann, R. H. Burgkart, D. O. Klemm, R. W. Kinne, *Cellulose* **2019**, *26*, 631.

[261] C. J. Zhang, L. Wang, J. C. Zhao, P. Zhu, *Advanced Materials Research* **2011**, *239–242*, 2667.

[262] M. P. Illa, C. S. Sharma, M. Khandelwal, *J Mater Sci* **2019**, *54*, 12024.

[263] H. Chiang, T.-F. Kuo, C.-C. Tsai, M.-C. Lin, B.-R. She, Y.-Y. Huang, H.-S. Lee, C.-S. Shieh, M.-H. Chen, J. A. M. Ramshaw, J. A. Werkmeister, R. S. Tuan, C.-C. Jiang, *Journal of Orthopaedic Research* **2005**, *23*, 584.

[264] C.-C. Jiang, H. Chiang, C.-J. Liao, Y.-J. Lin, T.-F. Kuo, C.-S. Shieh, Y.-Y. Huang, R. S. Tuan, *Journal of Orthopaedic Research* **2007**, *25*, 1277.

[265] A. I. Vasara, M. M. Hyttinen, O. Pulliainen, M. J. Lammi, J. S. Jurvelin, L. Peterson, A. Lindahl, H. J. Helminen, I. Kiviranta, *Osteoarthritis and Cartilage* **2006**, *14*, 1066.

[266] S. A. O'Leary, J. M. Link, E. O. Klineberg, J. C. Hu, K. A. Athanasiou, *Acta Biomaterialia* **2017**, *54*, 367.

Biography

William Joseph Koshut graduated from Mount Gallitzin Academy in 2009 and Quigley Catholic High School in 2013. Before attending Duke University, he graduated from Carnegie Mellon University with a Bachelor of Science in Chemistry in May of 2017. He then began work on his PhD in Mechanical Engineering and Materials Science at Duke under the direction of Ken Gall, with his first two years of financial support coming from the Pratt-Gardner Fellowship. William graduated with his Master of Science in Mechanical Engineering and Materials Science from Duke in May of 2019. William is a member of the Society of Duke Fellows. A list of his publications can be seen below:

- W. J. Koshut, N. Kwon, J. Zhao, A. Amendola, B. J. Wiley, K. Gall, "Flaw Sensitivity and Tensile Fatigue of High-Strength Hydrogel and Porcine Cartilage", *Journal of the Mechanical Behavior of Biomedical Materials*, **2021**, Under Review.
- Koshut, W. J.; Rummel, C.; Smoot, D.; Kirillova, A.; Gall K. "Flaw Sensitivity and Tensile Fatigue of Poly(Vinyl Alcohol) Hydrogels", *Macromolecular Materials and Engineering*. **2021**, *306*, 2000679.
- Zhao, J., Kirillova, A., Kelly, C. N., Xu, H., Koshut, W. J., Yang, F., Gall, K., Wiley, B. J. "High-Strength Hydrogel Attachment through Nanofibrous Reinforcement", *Adv. Healthcare Mater*. **2020**, 202001119.
- Yang, F., Zhao, J., Koshut, W. J., Watt, J., Riboh, J. C., Gall, K., Wiley, B. J. "A Synthetic Hydrogel Composite with the Mechanical Behavior and Durability of Cartilage", *Adv. Funct. Mater*. **2020**, 2003451.

- Koshut, W. J.; Smoot, D.; Rummel, C.; Kirillova, A.; Gall K. "Tensile Fatigue of Poly(Vinyl Alcohol) Hydrogels with Bio-Friendly Toughening Agents", *Macromolecular Materials and Engineering*, **2020**, *305*, 1900784.
- Koshut, W. J.; Arnold, A. M.; Smith, Z. C.; Wright, Z. M.; Sydlik, S. A. "Teaching Polymer Theory through the Living Polymerization and Characterization of Poly(Methyl Methacrylate) and Poly(Butyl Methacrylate) Homo- and Copolymers", *J. Chem. Educ*. **2019**.
- Good, J.; Duchesne, P. N.; Zhang, P.; Koshut, W.; Zhou, M.; Jin, R. "On the functional role of the cerium oxide support in the $Au_{38}(SR)_{24}/CeO_2$ catalyst for CO oxidation", *Catal. Today*, **2017**, 280, Part 2, 239–245.